이학박사 학위논문

척수신경손상 마우스 모델에서 척수후근신경절 위성교세포를 통한 척수 소교세포 활성화 및 신경병증성 통증 기전 연구

Mechanisms of nerve injury-induced spinal cord microglia activation and neuropathic pain via dorsal root ganglia satellite glial cells

2017 년 2 월

서울대학교 대학원

협동과정 뇌과학 전공

임 형 섭

척수신경손상 마우스 모델에서 척수후근신경절 위성교세포를 통한 척수 소교세포 활성화 및 신경병증성 통증 기전 연구

지도교수 이 성 중

이 논문을 이학박사 학위논문으로 제출함

2016 년 12 월

서울대학교 대학원

협동과정 뇌과학 전공

임 형 섭

임형섭의 박사학위논문을 인준함

2016 년 12 월

위 원 장 姜奉均 (인)

부위원장 李成中 (인)

위 원 李昇馥 (인)

위 원 崔世泳 (인)

위 원 金炳坤

Abstract

Mechanisms of nerve injury-induced spinal cord microglia activation and neuropathic pain via dorsal root ganglia satellite glial cells

Hyoungsub Lim
Interdisciplinary Program in Neuroscience
The Graduate School
Seoul National University

Neuropathic pain is caused by damage to or dysfuction of the nervous system. It is a pathological symptom that transcends the beneficial function of pain to protect the body from harmful stimuli or environment and to help with healing. Neuropathic pain has the following clinical characteristics: pain sensitization following normally non-painful, often repetitive, stimulation (allodynia); exaggerated reaction to normally painful stimuli (hyperalgesia); and stimulus-independent uncommon sensations associated with tingling or burning (spontaneous pain). These symptoms produce severe pain, negatively affect social and economic activities, and cause the onset of mental illnesses such as depression. Classically, many studies have focused on the hyper-excitatory mechanism of sensory neurons and the central sensitization of pain nerve circuits to understand the pathogenesis of

neuropathic pain. Based on these classical perspectives, research on the mechanism of pain hypersensitivity and the development of analgesic drugs has progressed. However, due to a lack of understanding of the precise molecular mechanisms underlying this condition, there remains no cure or drug that effectively controls neuropathic pain.

It has been reported that microglia in the spinal cord dorsal horn and satellite glial cell (SGC) in the dorsal root ganglion are activated during the onset of neuropathic pain caused by peripheral nerve injury. The activation of these glial cells plays an important role in the development of pain hypersensitivity, and inhibiting the activation of glial cells in the spinal cord and ganglia using inhibitors such as minocycline and fluorocitrate alleviates neuropathic pain. However, the molecular mechanisms underlying spinal cord microglial and satellite glial activation in ganglia and the relationship between two glia after peripheral nerve injury remain unknown. Therefore, to study the mechanisms of activation of glial cells and to investigate the relationship between glial cells, I developed *Ikkβ* conditional knockout mice in which IKK/NF-κB-dependent proinflammatory satellite glial activation is abrogated.

I induced neuropathic pain in conditional knockout and wild-type control mice by cutting the L5 spinal nerve, and performed pain behavior tests, immunohistochemistry, and various molecular experimental

techniques to elucidate the activation mechanisms of spinal cord microglia and SGCs. Compared to control mice, nerve injury-induced SGC activation was markedly reduced and macrophage infiltration into nerve-injured ganglia was dramatically decreased in conditional knockout mice. In addition, the activation of spinal cord microglia was markedly reduced, and compared with control mice, allodynic and hyperalgesic symptoms were alleviated in conditional knockout mice. However, nerve-recruited macrophages did not affect spinal cord microglial activation and neuropathic pain, suggesting a causal effect of SGC activation on spinal cord microglia activation. In an effort to elucidate the molecular mechanism, I searched for genes that are differentially regulated in conditional knockout ganglia compared to control ganglia after nerve injury using microarray analysis and identified the *St3gal2* gene. This *St3gal2* gene encodes a protein that produces ganglioside GT1b and GD1a in neurons, and its expression is increased in injured sensory neurons of control mice but suppressed in conditional knockout mice. Following nerve injury, *St3gal2* expression increase accompanied aberrant GT1b and GD1a production in injured neuron; GT1b is transported to the spinal cord along the central axon of sensory neurons. In the spinal cord, GT1b acts as an endogenous ligand of toll-like receptor 2, which is specifically expressed on microglia, to activate microglial cells, resulting in pain hypersensitivity.

In conclusion, peripheral nerve injury primarily activates the SGC of ganglion through the IKK/NF-κB signaling pathway and induces aberrant GT1b expression in injured sensory neurons. GT1b produced by damaged sensory neurons may induce pain sensitization by secondarily activating spinal cord microglial cells. These findings suggest that the interaction between SGCs and sensory neurons precedes injured neurons through microglial communication in the spinal cord. Thus, inhibiting the activation of satellite glial cells or the production and action of ganglioside GT1b from damaged sensory neurons may serve as a new therapeutic strategy for neuropathic pain.

Key Words: neuropathic pain, microglia, satellite glia, IκB kinase, GT1b, S*t3gal2*

Student Number: 2012-30114

Contents

List of figures

Background

1. Pain

1.1. Nociceptive pain

Nociceptive pain serves as a warning to the body by signaling tissue damage and inflammation. This physiological pain is caused by noxious stimuli that activate high-threshold nociceptive neurons. Two types of nociceptors, the unmyelinated C fiber and thinly myelinated Aδ fiber, transmit pain signals to nociceptive pathways in the central nervous system. Pain information is transmitted through the pain circuit and is perceived in the brain (Todd, 2010). Nociceptors express specialized transducer ion channels such as transient receptor potential channels, acid-sensing ion channels, and purinergic receptors (P2X/P2Y) and these ion channels sense thermal, mechanical, and some chemical stimuli and transduce external stimuli into pain information at peripheral nerve terminals (Cook et al., 1997; Lewin and Moshourab, 2004; Numazaki and Tominaga, 2004). Immune cells are not involved in nociceptive pain responses to noxious stimuli. Nociceptive pain is usually transitory or lasts only until tissue damage has healed (Omenn, 1987) and can be managed with medications such as analgesics and local anesthetics.

1.2. Pathological pain

Chronic pain, both inflammatory and neuropathic, is an intractable disorder affecting tens of millions of people worldwide, and pain experience persists after the initial cause has been resolved. Pathological pain is maladaptive and is likely due to the dysregulation of the nervous system. A neuroimmune interaction between neurons and immunocompetent cells, including glial cells, has emerged as a key factor underlying pathological pain mechanisms (Grace et al., 2014).

Inflammatory pain is caused by peripheral tissue inflammation and involves the detection of active inflammation by nociceptors and sensitization of the nociceptive system (Kidd and Urban, 2001). Various immune cells participate in the inflammatory response following tissue damage. In an inflamed tissue, resident macrophages, mast cells, and recruited neutrophils are activated and release various immune mediators such as IL-1β, TNF-α, IL-6, bradykinin, prostaglandin E_2, nerve growth factors, and nitric oxide (Marchand et al., 2005). These factors might activate or sensitize nociceptors and the nociceptive pathway, thereby enhancing pain to noxious stimuli. Hypersensitivity occurs in the inflamed region as well as in the non-inflamed region as a result of abnormal plasticity in nociceptors and the nociceptive pathway. In general, inflammatory pain is relieved upon the resolution of the initial tissue damage.

Neuropathic pain is triggered by damage to or dysfunction of the nervous system. Traumatic nerve injuries, bacterial or viral infections, neurotoxic chemicals, tumor invasion, anti-cancer drugs, and metabolic diseases such as diabetes may alter the structure and function of the nervous system such that pain spontaneously occurs and responses to noxious and innocuous stimuli are aberrantly amplified (Costigan et al., 2009). Patients with neuropathic pain suffer from burning-, stabbing-, shooting-, aching-, or electric shock-like sensations (Harden, 2005). Neuropathic pain generally persists for a prolonged period of time, even after resolution of the initial cause. In neuropathic pain development, multiple alterations occur such as ectopic discharge from damaged sites and dorsal root ganglion neurons (Amir et al., 2005), facilitation of synaptic transmission of pain signals (Campbell and Meyer, 2006), disinhibition of inhibitory synaptic transmission (Torsney and MacDermott, 2006), formation of new synaptic connectivity, loss of inhibitory synaptic circuits (Costigan et al., 2009), and neuron−glia interactions (Scholz and Woolf, 2007).

2. Glia as modulators of pain

Glia have long been considered as supporting cells of the nervous system (Haydon, 2001). Glial cells encapsulate synapses to form tripartite synapse; express receptors for many neurotransmitters and neuromodulators

(Kommers et al., 1998; Palma et al., 1997); synthesize and release gliotransmitters; inflammatory mediators, and neurotrophic factors (Inoue et al., 1999; Lee et al., 2011; Malarkey and Parpura, 2008; Watkins et al., 2001); and produce transporters that take up transmitters from the synaptic space (Anderson and Swanson, 2000). Thus, glia may also regulate the synaptic transmission of pain.

2.1. Microglial response to nerve injury

From sensation to perception, pain modulation was classically believed to be solely mediated by neurons and central sensitization was mainly due to alterations in neurons or neural circuits at the spinal cord level (Woolf and Mannion, 1999). However, in the early 2000s, it was discovered that spinal cord microglia are activated and play a pivotal role in the development of central sensitization and subsequent neuropathic pain induction (Raghavendra et al., 2003; Scholz and Woolf, 2007). This novel finding has shifted the paradigm in pain research.

Microglia are resident macrophages located in the central nervous system during development and originate from primitive macrophages in the yolk sac (Ginhoux et al., 2010). Microglia are ubiquitously distributed throughout the central nervous system and play a role in monitoring the surrounding microenvironment. In their normal state, microglia have small

cell bodies with branched and motile processes (Nimmerjahn et al., 2005). Sensory signals from damaged nerve terminals can activate spinal cord microglia and can result in the proliferation of microglia. Following peripheral nerve injury, the number of spinal cord microglia increases, and these cells transform to reactive states through the expression of various genes such as, cell-surface receptors (purinergic receptors and toll-like receptors) (Kim et al., 2007; Tanga et al., 2005; Tsuda et al., 2003), proinflammatory cytokines (IL-1β, IL-6, and TNF-α) (Zhang and An, 2007), and neurotropic factors (BDNF and NGF) (Ro et al., 1999; Trang et al., 2011) that can modulate the synaptic transmission of pain signals in the dorsal horn neuron of the spinal cord.

Many studies have focused on mechanisms underlying nerve injury-induced spinal cord microglial activation. Tsuda et al. have reported that microglial P2X4R is involved in nerve injury-induced microglial activation (Tsuda et al., 2003), which might be stimulated by ATP released from dorsal horn neurons of the spinal cord (Masuda et al., 2016). Similarly, Biber et al. have shown that neuronal CCL21 upregulates P2X4R expression in spinal cord microglia after nerve injury (Biber et al., 2011). Masuda et al. have shown that interferon regulatory factor (IRF) 8 and IRF5 are key players in microglial transformation, driving P2X4R expression in reactive microglia (Masuda et al., 2014; Masuda et al., 2012). More recently, Guan et al. have

reported that injured sensory neuron-derived colony-stimulating factor 1 is transported to the spinal cord to activate spinal microglia (Guan et al., 2016). In these studies, nerve injury-induced upregulation/release of the above molecules from sensory neurons has been suggested to represent the mechanism underlying nerve injury-induced spinal cord microglial activation. Each of these studies has implied that the signaling of injured sensory neurons to microglia following peripheral nerve injury is the initial triggering event leading to central sensitization.

2.2. Astrocyte response to nerve injury

In the central nervous system, astrocytes form tripartite synapses with neurons and maintain homeostasis in extracellular environments (Perea et al., 2009). Astrocytes take up extra neurotransmitters released into the tripartite synapse (Anderson and Swanson, 2000), and release gliotransmitters (glutamate and GABA) to actively regulate the transmission of information through synapses (Harada et al., 2015). After peripheral nerve injury, astrocytes in the spinal cord are activated and play an important role in the maintenance of established neuropathic pain (Ji et al., 2006). Astrocytes in the spinal cord can respond to peripheral nerve damage through ATP released from damaged sensory neurons or cytokine signals produced from primarily activated microglia. Astrocytes form astroglial networks through

gap junctions (connexin-43) and communicate with each other through Ca^{2+} waves. Nerve damage increases connexin-43 expression, and a gap-junction blocker inhibits the spread of pain (Rohlmann et al., 1993; Spataro et al., 2004). Nerve injury also reduces the expression of GLT-1 and GLAST, and number of glutamate transporters, which can inhibit glutamate uptake and facilitate excitatory synaptic transmission to cause pain, in astrocytes (Sung et al., 2003). Unlike other cells, astrocytes express serine racemase, an enzyme that synthesizes D-serine; the expression of this enzyme is increased by nerve injury. D-serine produced from activated astrocytes acts as a co-agonist of NMDA receptors, leading to NMDA receptor-dependent long-term potentiation of the neural circuitry of pain signaling. In contrast, the administration of D-aminoacid oxidase, an enzyme that degrades D-serine, to the spinal cord alleviates pain symptoms (Lefevre et al., 2015).

2.3. Satellite glial response to nerve injury

Satellite glial cells (SGCs) are present in sensory ganglia (dorsal root and trigeminal ganglia) and sympathetic and parasympathetic ganglia and surround cell bodies of sensory neurons with cellular sheaths. SGC share many similarities with astrocytes, including GFAP, gap junction (connexin-43), glutamine synthetase, and neurotransmitter transporter expression (Hanani, 2012). Similar to astrocytes, SGCs are closely associated with each

other and to sensory neurons through a gap junction. The gap junction constitutes the extracellular space of neurons and allows satellite cells to regulate the neuronal microenvironment.

SGCs respond to nerve injury by upregulating GFAP expression and by undergoing proliferation (Humbertson et al., 1969). Peripheral nerve injury upregulates the formation of gap junctions (Zhang et al., 2009). The increased formation of gap junctions can contribute to pain by inducing spontaneous activity and hyperexcitability in sensory neurons (Huang et al., 2010). The release of paracrine glutamate occurs in the ganglion, and SGCs can take up the glutamate from the extracellular milieu through transporters (GLAST and GLT-1) (Carlton and Hargett, 2007). Glutamate is converted into glutamine by glutamine synthetase, and glutamine can be transported to neurons through glutamate−glutamine cycle. Nerve injury upregulates machineries for glutamate recycling, leading to the hyperexcitability of injured sensory neurons. In addition, purinergic signaling in the SGC to neuron interaction is critically important. Nerve injury induces ATP release from activated satellite glia, and ATP stimulates P2X3 receptors on sensory neurons to increase their excitability (Cook et al., 1997). ATP can also be released from sensory neurons and activates satellite glia through the P2X7

receptor, leading to TNF-α production in SGCs. In turn, TNF-α stimulates surrounding neurons to induce hyperexcitability (Sorkin et al., 1997).

3. Clinical therapies for neuropathic pain

Neuropathic pain interferes with the transmission of normal sensory and nociceptive pain, leading to severe discomfort. Neuropathic pain symptoms vary among patients, and there are no therapies or medications that can effectively control neuropathic pain.

Several medications are available to relieve neuropathic pain such as antidepressants (serotonin-norepinephrine reuptake inhibitors and tricyclic antidepressants) (Dworkin et al., 2010), anticonvulsants (pregabalin and gabapentin) (Moore et al., 2014), cannabinoids (cannabis, cannabinoid receptor agonists) (Grotenhermen and Muller-Vahl, 2012), dietary supplements (alpha lipoic acid, Vitamin B1) (Foster, 2007), botulinum toxin type A (Ranoux et al., 2008), and opioids (Smith, 2012). However, these medications have no beneficial effect in certain patients and may often results in serious side effects or pain aggravation because these drugs were not specifically developed to relieve neuropathic pain and are not based on neuropathic pain mechanisms (Attal, 2012; Jefferies, 2010).

In addition to medications, there are several treatments that can

alleviate neuropathic pain. Surgical procedure such as “nerve block” and “spinal cord stimulators” can help relieve pain. A nerve block (of peripheral and sympathetic nerves) is an injection of local anesthetics, steroids, or opioids directly in the area of the affected nerve to control pain. Nerve block therapy effectively alleviates pain by blocking pain transmission, but it does not consistently inhibit pain (Abram, 2000). Spinal cord stimulation is a procedure in which a low level of electrical stimulation is directly applied to the dorsal portion of the spinal cord to suppress pain transmission from the spinal cord to the brain. A stimulator for electrical stimulation is implanted during the surgical procedure. Pain relief from this procedure last for more than 20 years, but this procedure is not suitable for all patients with neuropathic pain (Kumar et al., 1996).

Purpose

For over five decades, it was believed that central sensitization was mainly due to alterations in neurons or neural circuits at the spinal cord level (Woolf and Mannion, 1999). After the discovery of the pivotal role of spinal cord microglial activation in neuropathic pain induction, spinal cord microglial activation is now considered to be the triggering event leading to pain central sensitization after nerve injury. However, the activation mechanism has not yet been clarified. In addition to microglia, SGC activation in the DRG is involved in the development of neuropathic pain after peripheral nerve injury. There is only circumstantial evidence for the role of SGC in pain sensitization; the exact *in vivo* contribution of SGC activation in pain sensitization and the relationship between these glial cell types (spinal cord microglia and SGCs) in the development of neuropathic pain remains unknown. In this respect, I tried to investigate *in vivo* role for SGC activation and molecular mechanisms of microglia activation in the development of neuropathic pain. To archive this goal, I performed sequential experiments with the following three aims:

1. To elucidate the exact *in vivo* role of SGC activation in pain sensitization using *cIkkβ*$^{-/-}$ mice

2. To investigate the molecular mechanisms underlying spinal cord microglial activation after nerve injury

3. To elucidate the relationship between microglial and SGC activation in nerve injury-induced neuropathic pain development

This thesis addressed the specific aims described above.

Abstract

Increasing evidence supports that both microglia and satellite glial cell (SGC) activation play a causal role in neuropathic pain development after peripheral nerve injury, yet the activation mechanisms and their contribution to neuropathic pain remain elusive. To address this issue, I used *Ikkβ* conditional knockout mice (*Cnp-Cre*$^{+/-}$*/Ikkβ*$^{f/f}$) in which IKK/NF-κB-dependent proinflammatory SGC activation is abrogated. In these mice, nerve injury-induced proinflammatory gene expression and macrophage infiltration into the DRG were severely compromised. Likewise, nerve injury-induced spinal cord microglia activation and pain hypersensitivity were significantly attenuated in these mice compared to control mice. However, macrophages recruited into the DRG *per se* have minimal effects on spinal cord microglia activation suggesting a causal effect of SGC activation on spinal cord microglia activation. In an effort to elucidate the molecular mechanisms, I found that SGC activation induces *St3gal2* expression in sensory neurons and subsequently leads to aberrant increase in ganglioside GT1b in afferent axons in the dorsal horn. Studies using *St3gal2* knockout mice indicated that the GT1b increase is required for the nerve injury-induced spinal cord microglia activation and pain hypersensitivity. In the spinal cord, GT1b functions as an endogenous agonist of toll-like

receptor 2 (TLR2) to activate microglia and thereby induces pain central sensitization. Taken together, I present a novel mechanism for spinal cord microglia activation in nerve injury-induced neuropathic pain that is dependent on SGC activation, GT1b increase in the dorsal horn, and activation of microglial TLR2.

Introduction

Neuropathic pain is chronic pathological pain due to an injury or dysfunction in the nervous system and is characterized by sensitization of the normal pain sensory system. This results in enhanced pain sensation due to noxious stimuli (hyperalgesia) and abnormal pain sensation due to non-noxious stimuli (allodynia) (Jensen and Finnerup, 2014). Pain sensitization can be caused by alterations in peripheral sensory nerves (peripheral sensitization) and pain-transmitting circuits in the spinal cord or brain (central sensitization) (Costigan et al., 2009). Studies on the underlying mechanisms of neuropathic pain over the last decade have demonstrated that microglia in the spinal cord play a critical role in central sensitization and contribute to neuropathic pain (Milligan and Watkins, 2009). Upon peripheral nerve injury, microglia in the spinal cord dorsal horn become activated and express pain-mediators such as IL-1β (Hunt et al., 2001) and BDNF (Ulmann et al., 2008). IL-1β and BDNF, in turn, induce pain hypersensitization by directly enhancing the excitability of pain-transmitting neurons (Kawasaki et al., 2008; Lu et al., 2009) or disinhibiting inhibitory synaptic transmission in the spinal cord pain circuits (Coull et al., 2005). Indeed, disrupting the activation of spinal cord microglia and action of microglia-derived pain mediators attenuates pain hypersensitivity following

peripheral nerve injury (Ledeboer et al., 2005; Wei et al., 2013; Yin et al., 2015). Based on these studies, it has long been believed that spinal cord microglia activation is the triggering event leading to central sensitization after nerve injury. However, the mechanism by which peripheral nerve injury induces spinal cord microglia activation has not been clearly elucidated.

More recently, another type of glial cell, the satellite glial cell (SGC) that tightly envelops the perikaryon of a sensory neuron in a ganglion, has been implicated in the development of neuropathic pain (Fu et al., 2010; Liu et al., 2012). SGCs, like spinal cord microglia, rapidly respond to peripheral nerve injury by changing cell morphology and characteristics (Jasmin et al., 2010; Takeda et al., 2011). For instance, SGCs upregulate glial fibrillary acidic protein (GFAP), a glial cell activation marker, upon peripheral nerve injury (Stephenson and Byers, 1995). Decreases in the potassium-buffering capacity of SGCs are observed in such conditions (Vit et al., 2008). These activated SGCs express pain-related inflammatory mediators such as TNF-α (Miyagi et al., 2006) and NGF (Cheng et al., 2014). Inhibiting the expression or blocking the effects of these inflammatory mediators using neutralizing antibodies exerts an anti-allodynic effect in an animal model of neuropathic pain (Bohren et al., 2013; Cheng et al., 2014). These previous

studies suggest a putative role of SGC activation after nerve injury in the development of neuropathic pain, which is comparable to spinal cord microglia activation. This circumstantial evidence of SGC involvement in pain sensitization, however, does not elucidate the exact *in vivo* role of SGC activation in pain sensitization, and the relationship between these two glial cell types (spinal cord microglia and SGCs) in the development of neuropathic pain has not been addressed.

Most inflammatory mediators, such as TNF-α and NGF, produced by activated SGCs and implicated in pain sensitization are under the transcriptional control of NF-κB transcription factors (O'Neill and Kaltschmidt, 1997). To explore the cell type-specific *in vivo* roles of SGCs in the development of nerve injury-induced neuropathic pain, I used *Ikkβ* conditional knockout mice in which IKKβ-dependent NF-κB activation was abrogated selectively in SGCs among cells in the dorsal root ganglia (DRG). In the present study, using these mice, I uncovered a novel mechanism of neuropathic pain in which SGC activation in a nerve-injured ganglion is the initial triggering event that leads to remote spinal cord microglia activation and subsequent pain central sensitization.

Materials and methods

Animals

All mice were housed in a specific pathogen free vivarium under a 12-h light-dark cycle. Mice were allowed to access food and water *ad libitum*. *Ikkβ* conditional knockout (*cIkkβ*$^{-/-}$) mice were generated by breeding floxed-*Ikkβ* (*Ikkβ*$^{f/f}$) (Li et al., 2003) mice and *Cnp-Cre* knockin (*Cnp-Cre*$^{+/-}$) mice expressing Cre recombinase under the control of endogenous *Cnp* promoter as previously described (Lappe-Siefke et al., 2003). Genotypes of mouse offspring was determined by PCR with the following primers: 5'-GTC ATT TCC ACA GCC CTG TGA-3' and 5'-CCT TGT CCT ATA GAA GCA CAA C-3', which amplify both the *Ikkβ* (223 bp) and *Ikkβ*^{f} (310 bp) alleles. 5'-GCC TTC AAA CTG TCC ATC TC-3' and 5'-CCC AGC CCT TTT ATT ACC AC-3' to detect the normal *Cnp* allele, 5'-CAT AGC CTG AAG AAC GAG A-3' and 5'-CCC AGC CCT TTT ATT ACC AC-3' to detect the *Cnp-Cre* allele. *Ikkβ*$^{f/f}$ mice were used as controls. *Tlr2*$^{-/-}$/*Cx3cr1*$^{+/GFP}$ mice were generated by crossing *Tlr2*$^{-/-}$ mice with knockin mice that express EGFP under control of the endogenous *Cx3cr1* locus. PCR genotyping was performed using the following primers: 5'-TTG GAT AAG TCT GAT AGC CTT GCC TCC-3' and 5'-ATC GCC TTC TAT CGC CTT CTT GAC GAG-3' to detect the mutant *Tlr2* allele, 5'-TTG

GAT AAG TCT GAT AGC CTT GCC TCC-3' and 5'-GTT TAG TGC CTG TAT CCA GTC AGT GCG-3' to detect normal *Tlr2* allele. 5'-GGT TCC TAG TGG AGC TAG GG-3' and 5'-GAT CAC TCT CGG CAT GGA CG-3' to detect $Cx3cr1^{GFP}$ allele, 5'-GGT TCC TAG TGG AGC TAG GG-3' and 5'-TTC ACG TTC GGT CTG GTG GG-3' to detect the normal *Cx3cr1* allele. After weaning (P21), mice were group-housed (4-6 per cage). WT mice with C57BL/6 background and Sprague-Dawley rats were purchased from Daehan Biolink (Eumsung, Korea). Transgenic $Cx3cr1^{+/GFP}$ mice were purchased from the Jackson Laboratory (Bar Harbor, ME, USA). $Tlr2^{-/-}$ and $St3gal2^{-/-}$ mice were kindly provided by Dr. S. Akira (Osaka University, Japan) and Dr. Ronald L. Schnaar (Johns Hopkins University, USA), respectively (Ellies et al., 2002; Takeuchi et al., 1999). All male genotypes aged 8-10 weeks and weighing 21-25 g were used for experimentation.

Neuropathic pain model

All surgical and experimental procedures were reviewed and approved by the Institutional Animal Care and Use Committee at Seoul National University. The animal treatments were performed in accordance with the guidelines of the International Association for the Study of Pain. All

animals were used at 8-10 weeks old. To establish a persistent pain model with L5 SNT, mice were anesthetized with pentobarbital sodium (50 mg/kg, i.p.) as previously described (Lim et al., 2013). Briefly, an incision was made in the skin from the spinal processes at L4 to S2 levels. The paraspinal muscles were separated and the L6 transverse process was partially removed. The right L5 spinal nerve was exposed and carefully transected with small scissors. Then, 10% povidone-iodine topical solution was applied surrounding the site of incision and the surgical site was closed in two layers with surgical staples. Sham-operated mice were subjected to removal of the L6 transverse process. L5 spinal nerve ligation (SNL) was performed using rats as previously described (Kim and Chung, 1992). Briefly, under enflurane inhaled anesthesia (0.5-2%), the L5 and L6 vertebra were surgically exposed. The L6 transverse process was removed and the L5 spinal nerve was tightly ligated with 6-0 silk thread. Then L5 laminectomy was carried out, the dura opened and the L5 dorsal root ipsilateral to the nerve injury tightly ligated with 6-0 silk thread and transected. Sterile procedures were used throughout the surgery to prevent infection and to minimize the influence of inflammation. Animals that had been operated on were monitored on a warm pad during recovery.

Behavioral test

Pain test – Animals were daily habituated to the testing environment for 3 days. Pain was deemed to be present if the animal starts to exhibit the flight or struggle response. To measure mechanical allodynia, mice were placed in clear plastic chambers on an elevated table and allowed to acclimate for approximately 30 min. The 50% withdrawal threshold was determined using the up-down method (Chaplan et al., 1994) with a set of von Frey filaments (0.02-2 g, North Coast Medical, Morgan Hill, CA, USA). Thermal hyperalgesia was assessed by measuring the latency of paw withdrawal in response to a radiant heat source (Hargreaves et al., 1988) by using the plantar test (IITC Life Science, Woodland Hills, CA, USA). A light beam was applied from underneath the glass floor, which was heated at 30°C to exclude the possibility of delayed response time to the applied heat source. The bulb voltage (active intensity: 30, idle intensity: 5) was adjusted to obtain a baseline withdrawal latency (6-8 s) in naive animals and the cutoff time was set at 15 sec to avoid tissue damage to the hind paw. Paw withdrawal latency was measured for three trials with 1 min interval between each trial. The means of the trials were calculated. For the tail-immersion test (Ramabadran et al., 1989), mice were immobilized in a tube restrainer and the water bath was maintained at 48 or 52°C. The terminal 3-

5 cm of tail was immersed in the water bath. I measured tail reflex time with a stopwatch in response to hot water. Fifteen sec of the cutoff time was used to prevent tissue damage.

Open field test (OFT) - The open field apparatus consisted of a four-sided 52 × 52 × 50 cm (L × W × H) acrylic box. A mouse was placed in the center of the test chamber and allowed to explore freely for 60 min. During the test period, the numbers of grooming, rearing, and total distance movement behaviors in the chamber were measured (Gould, 2009). Total distance movement was recorded automatically with a video tracking system, and both grooming and rearing behaviors were monitored manually. After each test, the test apparatus was cleaned with a 70% ethanol and dried for 5 min to remove any olfactory cues.

Elevated plus maze (EPM) - The elevated plus maze consisted of an enclosure with 2 open arms 30 × 5 cm in size (L × W) and 2 enclosed arms of the same size with transparent walls 20 cm high. The arms were made up of black acrylic plates radiating from a central platform (5 × 5 cm) to form a “plus” sign. The entire apparatus was elevated to a height of 70 cm above floor level. Each mouse was placed in the central platform facing one of the open arms. The time spent and the number of entries on the open, closed arms and the central platform was recorded for 5 min (Walf and Frye, 2007).

Forced swimming test (FST) – One day prior to the test, a mouse was placed for conditioning in a 10 × 30 cm clear acrylic cylinder (diameter × height) containing 15 cm of water (22 ± 1°C) for 15 min (pretest session). Then, 24 hours later, the mouse was tested under the same condition for 5 min (test session). Following each session, the mouse was removed from the water, dried with a towel, placed in a warm cage for 15 min, and then returned to the home cage. Each test session was recorded automatically with a video tracking system. The total duration of immobility (non-swimming) within a 5 min session was recorded as immobility time in seconds and compared among groups (Slattery and Cryan, 2012). In the behavioral experiments the open field test was performed first, and then the elevated plus maze and forced swimming test were conducted together to minimize any stress effects on mouse behavior. In the test room, the temperature was 23 ± 3°C and the light intensity was 390 lux. All sessions were performed blinded to group assignment and took place between 12:00 and 17:00 h. Data are represented as mean ± SEM.

Real-time RT-PCR

Total RNA was isolated from each tissue and cell culture using TRIzol reagent (Life Technologies, Grand Island, NY, USA) and 1-2 μg of total

RNA was used to synthesize cDNA. I added 4 μl of diluted cDNA (1/20), 1 μl of 10 pmol primer, and 5 μl of 2× SYBR Green PCR Master mixture (Applied Biosystems, Foster City, CA, USA) in a tube and each gene was amplified in duplicate using ABI Prism 7500 sequence detection system (Applied Biosystems). The mRNA level of the each gene was normalized to the corresponding level of GAPDH and represented as the fold induction, which was calculated using the $2^{-\Delta\Delta CT}$ method as previously described (Livak and Schmittgen, 2001). All real-time RT-PCR experiments were performed at least three times, and the mean ± SEM values are presented unless otherwise noted. The following PCR primer sequences were used: GAPDH forward, 5'-AGG TCA TCC CAG AGC TGA ACG-3'; GAPDH reverse, 5'-CAC CCT GTT GCT GTA GCC GTA-3'; IL-1β forward, 5'-GTG CTG TCG GAC CCA TAT GA-3'; IL-1β reverse, 5'-TTG TCG TTG CTT GGT TCT CC-3'; TNF-α forward, 5'-AGC AAA CCA CCA AGT GGA GGA-3'; TNF-α reverse, 5'-GCT GGC ACC ACT AGT TGG TTG T-3'; IL-6 forward, 5'-TCC ATC CAG TTG CCT TCT TGG-3'; IL-6 reverse, 5'-CCA CGA TTT CCC AGA GAA CAT G-3'; ST3Gal-II forward, 5'-ATG GCT ACC TTG CCC TAC CT-3'; ST3Gal-II reverse, 5'-GTC CAG ACG GGT GAG ATG TT-3'; iNOS forward, 5'-GGC AAA CCC AAG GTC TAC GTT-3'; iNOS reverse, 5'-TCG CTC AAG TTC AGC TTG GT-3'; BDNF forward, 5'-TGC AGG GGC ATA GAC AAA AGG-3';

BDNF reverse, 5'-CTT ATG AAT CGC CAG CCA ATT CTC-3'; Nox2 forward, 5'-GAC CCA GAT GCA GGA AAG GAA-3'; Nox2 reverse, 5'-TCA TGG TGC ACA GCA AAG TGA T-3'.

Immunohistochemistry and live cell imaging

Animals were deeply anesthetized with pentobarbital sodium (80 mg/kg, i.p.) and transcardially perfused with saline solution followed by 4% paraformaldehyde in 0.1 M phosphate buffer (pH 7.4). The L4-5 spinal cord, L5 DRG, L5 dorsal root, and spleen were removed, postfixed in 4% paraformaldehyde at 4°C overnight, and transferred to a 30% sucrose phosphate buffer for 48 h. For ganglioside immunostaining in DRG and dorsal root, the animals were perfused through the heart with saline solution followed by 10% sucrose. The L5 DRG and dorsal root were collected and snap-frozen at -80°C. Tissue transverse sections (14-18 μm-thick) were prepared on a gelatin-coated slide glass using a cryocut microtome. The sections were blocked in a solution containing 5% normal donkey serum (Jackson Immuno-Research, Bar Harbor, ME, USA), 2% BSA (Sigma, St. Louis, MO, USA), and 0.1% Triton X-100 (Sigma) for 1 h at room temperature. The sections were then incubated overnight at 4°C with primary antibody in the blocking solution for mouse anti-CNPase (1:200,

Sigma), rabbit anti-p-p65 (1:100, Santa Cruz Biotechnology, Santa Cruz, CA, USA), rabbit anti-GFAP (1:5000, DAKO, Glostrup, Denmark), goat anti-IL-1β (1:100, Santa Cruz Biotechnology), rabbit anti-Iba-1 (1:1000, Wako, Osaka, Japan), rat anti-CD11b (1:200, AbD Serotec, Kidlington, UK), rat anti-CD68 (1:500, Serotec, Oxford, UK), rabbit anti-ST3Gal-II (1:250, Santa Cruz Biotechnology), mouse anti-GT1b (1:1500, Millipore, Temecula, CA, USA), mouse anti-GD1a (1:1500, Millipore), rabbit anti-CGRP (1:1000, Peninsula Laboratories, San Carlos, CA, USA), rat anti-CD31 (1:100, eBioscience, San Diego, CA, USA), goat anti-ASPA (1:200, Santa Cruz Biotechnology), mouse anti-NeuN (1:200, Millipore), and rat anti-Ki-67 (1:100, eBioscience). After rinsing in 0.1 M PBS, the sections were incubated for 1 h at room temperature with a mixture of FITC-conjugated, Cy3-conjugated secondary antibodies (1:200, Jackson Immuno-Research) or FITC-conjugated isolectin B4 (IB4, 10 μg/ml, Sigma). Upon rinsing in 0.1 M PBS, the sections were mounted with Vectashield mounting medium (Vector Laboratories, Burlingame, CA, USA). For ganglioside immunostaining, the detergent was omitted from the entire process. For live cell imaging, primary microglia were prepared from WT, *Cx3cr1*$^{+/GFP}$, and *Tlr2*$^{-/-}$*/Cx3cr1*$^{+/GFP}$ mice. To measure intracellular ROS level, primary microglia cultured from WT mice were treated with 4.5 μM of GT1b for 5.5 h. Then, 10 μM of CM-H_2DCFDA (Life Technologies) was loaded in the

microglia and incubated for 30 min at 37°C. Upon rinsing the microglia with PBS, the fluorescence intensity was measured. To test the direct interaction between TLR2 and GT1b, primary microglia were incubated with 5 μg/ml of GT1b-rhodamine for 1 h in the presence or absence of LTA (sigma) at 37°C in a 5% CO_2 incubator. LTA was pretreated for 30 min prior to the GT1b-rhodamine treatment. After incubation, cells were rinsed with glial cell culture medium three times. The fluorescent images were obtained with a confocal microscope (LSM700, Carl Zeiss, Germany) and the fluorescent signal intensity was quantified using ZEN software (version ZEN 2010B SP1) of Carl Zeiss.

Microarray

Total RNA was isolated from 5 pooled L5 DRGs of sham-operated or L5 SNT-injured *Ikkβ*$^{f/f}$ and *cIkkβ*$^{-/-}$ mice and 300 ng of total RNA from each sample was converted to double-stranded cDNA using a random hexamer incorporating a T7 promoter. cRNA was generated from the double-stranded cDNA template though an *in vitro* transcription reaction and purified with the Affymetrix sample cleanup module. cDNA was regenerated from cRNA through a random-primed reverse transcription. The cDNA was then fragmented by UDG and APE 1 restriction endonucleases and end-labeled by terminal transferase reaction incorporating a biotinylated

dideoxynucleotide. Fragmented end-labeled cDNA was hybridized to Mouse Gene 2.0 ST arrays (Affymetrix, Santa Clara, CA USA) for 17 h at 45°C and 60 rpm as described in the Gene Chip Whole Transcript Sense Target Labeling Assay Manual (Affymetrix). After hybridization, the chips were stained and washed in a Genechip Fluidics Station 450 (Affymetrix) and scanned by using a Genechip Array scanner 3000 7G (Affymetrix). The scanned raw files were imported into the statistical programming environment R (version 2.3) for further analysis with tools available from the Bioconductor Project. Expression data were normalized and log2 transformed using the robust multichip average method implemented in the Bioconductor package RMA. To reduce noise for the significance analysis, probe sets that did not show detection call rate at least 50% of the samples in the comparison were filtered out. Highly expressed genes that showed a 1.5-fold change in expression were selected. The results were classified using hierarchical clustering algorithms (Eisen et al., 1998) implemented in TMEV software 4.0.

Primary cell culture

Primary glial cell and DRG neuron cultures were prepared according to previously established procedures with minor modificaton (Kim et al., 2011b; Lim et al., 2013). In brief, brain glial cells were cultured from

postnatal day 1-3 WT, *Tlr2*$^{-/-}$, *Cx3cr1*$^{+/GFP}$, and *Tlr2*$^{-/-}$/*Cx3cr1*$^{+/GFP}$ mice. After the animals were anesthetized, brain tissues were extirpated and the meninges were removed from the cerebral hemispheres. The tissue was dissociated into single cells by trituration and incubated in glial cell culture medium (DMEM supplemented with 10 mM HEPES, 10% FBS, 2 mM L-glutamine, 1× non-essential amino acids and 1× antibiotic-antimycotic) in a 75-cm^2 flask at 37°C in a 5% CO_2 incubator. The medium was changed every five days thereafter. After two weeks, the glial cells were trypsinized and seeded in six-well plates for subsequent use. Primary microglia were harvested from brain mixed glial cell cultures. The sides of 75-cm^2 flasks containing 14 day-old cultures of mixed glial cells were tapped against the palm of the hand several times, and the supernatants from the cultures were collected and centrifuged at 800 rpm for 5 min. Microglia were plated in glial culture media. After 15 min, the dishes were washed with medium three times to remove any unattached astrocytes. The purity of the microglia was routinely monitored and determined to be >98% after immunostaining with Iba-1 antibody (1:1000, Wako).

DRG neurons obtained from 8-week old mice were prepared. Animals were anesthetized with overdose of isoflurane, decapitated, and DRGs from all spinal levels were rapidly collected under aseptic conditions and placed in HBSS. 35-40 DRGs were digested in 1 mg/ml collagenase A

(Roche) and 2.4 U/ml dispase II (Roche) in HBSS for 60 min, respectively, followed by 8 min in 0.25% trypsin (Sigma), all at 37°C. The DRGs were then washed in DMEM three times and resuspended in DMEM medium supplemented with 10% FBS and 1% penicillin/streptomycin. DRGs were then mechanically dissociated using fire-polished glass pipettes, centrifuged (800 rpm, 5 min), resuspended in DMEM/F12 medium supplemented with 10% FBS and 1% penicillin/streptomycin, and plated on 0.5 mg/ml poly D-lysine-coated 35-mm dish. To suppress glial cell proliferation at 2 days *in vitro*, 1 μM cytosine arabinoside was added to the medium for 1 day. Cells were maintained at 37°C in a 5% CO2 incubator.

Western blot analysis

Protein lysates were prepared by lysing glial cells in RIPA buffer containing 50 mM Tris-HCl (pH 7.5), 150 mM NaCl, 1% NP-40, 0.5% deoxycholic acid, 0.1% SDS, 1 mM PMSF, and phosphatase inhibitor mixture set IV (Millipore). A total of 20 μg of the cell lysate was separated on a 10% SDS-PAGE by electrophoresis and electrotransferred to a nitrocellulose membrane. Membranes were blocked with 5% BSA in Tris-buffered saline containing Tween 20 (20 mM Tris, pH 7.4, 150 mM NaCl, and 0.1% Tween 20) and probed overnight with primary antibody against p-p38 (Thr180/Tyr182) (1:1000, Cell Signaling Technology, Danvers MA, USA)

at 4°C, followed by incubation with horseradish peroxidase-conjugated secondary antibody at room temperature for 1 h prior to ECL treatment. For normalization, the membranes were stripped and reprobed with p38 antibody (1:1000, Cell Signaling Technology). Immunoreactivity signals were visualized by MicroChemi (DNR Bio-imaging Systems, Jerusalem, Israel).

Enzyme-linked immunosorbent assay (ELISA)

Primary microglia were plated in 96-well plates at a density of 50,000 cells per well and allowed to adhere overnight. Cells were incubated for 6 h in serum-free glial cell culture medium prior to stimulation. For IL-1β release, microglia were primed by pre-treatment of 10 μg/ml GT1b for 2 h prior to stimulation with 5 mM ATP for 1 h. Neither the GT1b nor ATP affected cell viability. For BDNF release, microglia were stimulated with 10 μg/ml GT1b for 2 h followed by 50 μM ATP for 1 h. Cell supernatants and lysates were collected and stored at -20°C until the day of assay. IL-1β and BDNF release were analyzed using an IL-1β ELISA kit (Komabiotech, Seoul, Korea) and BDNF ELISA kit (Boster Biological Technology, Pleasanton, CA, USA) according to the manufacturer's instructions, respectively. Total protein concentrations from each cell lysate were measured using a BCA

protein assay kit (Thermo Scientific, Rockford, IL, USA) and used for normalization.

Nitric oxide (NO) assay

NO production was determined by measuring nitrite level with Griess reagents (Sigma) according to the manufacturer's instructions. In brief, equal volumes of the culture supernatants and the Griess reagents were mixed and then incubated for 15 min at room temperature. Absorbance was measured at 540 nm. The nitrite concentration was calculated using a standard curve and data are presented as a mean ± SEM values.

Macrophage depletion

To deplete macrophages, a dose of 200 μl liposome-encapsulated clodronate (Cl_2MDP, www.clodronateliposomes.com, 1098 XH Amsterdam, Netherlands) was injected intraperitoneally 2 days prior to L5 SNT (Van Rooijen and Sanders, 1994). Spleens were harvested on day 2 post Cl_2MDP injection. Immunohistochemistry using CD68 antibody was performed on the spleen sections to verify the depletion of peripheral macrophages.

Intrathecal injection

Mice were anesthetized with pentobarbital sodium (25 mg/kg, i.p.) and GT1b (25 μg/5 μl) in saline solution or vehicle alone was administrated by

direct lumbar puncture between the L5 and L6 vertebrae of the spine of WT and *Tlr2*$^{-/-}$ mice, using a 10 μl Hamilton syringe (Hamilton Company, Reno, NV, USA) with a 30-gauge one-half-inch needle as previously described (Hylden and Wilcox, 1980). Polymyxin B (10 μg/ml, Sigma) was used to prevent LPS contamination 30 min before GT1b administration. PDMP (Matreya LLC, State College, PA, USA) was dissolved in 5% Tween 80 (Sigma) in saline and diluted with sterile saline immediately before intrathecal injection. The success of the intrathecal injection was assessed by monitoring the tail-flick response when the needle penetrated the subarachnoid space.

LC-MRM-mass spectrometry (MS) analysis for gangliosides

All organic solvents of high-performance liquid chromatography (HPLC) grade were purchased from J.T. Baker (Philipsburg, NJ, USA). Gangliosides were extracted from 10 mg of pooled ipsilateral L4-5 spinal cord tissues of *Ikkβ*$^{f/f}$ and *cIkkβ*$^{-/-}$ mice. Ganglioside isolation was performed in accordance with established methods (Takamizawa et al., 1986) with minor modifications. Briefly, the tissue samples were pulverized in 400 μl methanol. Then, 10 μg of d18:1-18:0 GM3-*d*3 (Matreya LLC) was added to the samples for internal standard and then were immediately mixed with 200

μl chloroform-methanol/chloroform (2:1 v/v). After vigorous mixing, the samples were placed on ice and incubated for 10 min. After incubation, the suspensions were mixed with equal volume of chloroform and 1.3 volume of water. After mixing for 30 sec, the suspensions were incubated at room temperature for 30 min. The samples were centrifuged at 2,500 × *g* for 10 min and the upper phase was transferred into a new microtube and dried. For enrichment of gangliosdies, 100 μl of binding buffer (1 mM $MnCl_2$, 1 mM $CaCl_2$, 0.5 M NaCl, and 20 mM Tri-HCl, pH 7.3) and 100 μg of SNA lectin (VECTOR, Burlingame, CA, USA) were added sequentially in the microtube. To promote the binding of the SNA lectin to gangliosides, the samples were incubated at 25°C for 1 h in a Thermomixer (Eppendorf, Hamburg, Germany). Then, 200 μl of washing solution (1 mM $MnCl_2$, 1 mM $CaCl_2$, 0.5 M NaCl, 20 mM Tris-HCl, pH 7.3, and 40 mM NH_5CO_3) was applied to the filters with 14,000 × *g* centrifugal force at 25°C for 10 min. This clean-up step was performed twice to remove nonglycolipids from the filter. For the elution of gangliosides, 100 μl of an acidic hydrophobic solution (80% acetonitrile, 0.1% formic acid in water) was added twice at 25°C and 14,000 × *g* for 20 min; the eluents were removed completely by drying and the pellets were resuspended in 10 μl solvent A (20 mM ammonium formate, 0.1% formic acid in acetonitrile/methanol/water mixture (19:19:2)) for further mass spectrometry analysis. Quantification of

gangliosides in samples was performed by a 6490 Accurate-Mass Triple Quadrupole LC-MS instrument connected to a 1200 series HPLC system with an SB-C18 2.1 × 50 mm, 1.8 μm column (Agilent Technologies, Wilmington, DE, USA). The mobile phase was pumped at 0.1 ml/min of the flow rate and the 3.5 μl was injected for each run. To determine MRM paris for all ganglioside subclasses, I used data on parent and daughter ions from a previous study (Sturgill et al., 2012). For ganglioside analysis, I optimized MRM parameters with GM3-*d*3 internal standard. The collision energies for GT1 species were set as 32 V and 38 V for GM3-*d*3 internal standard (optimized condition). The collision gas and sheath gas temperatures were adjusted to 250°C and 350°C, respectively. Finally, I performed a validation study using an internal standard, GM3-*d*3. Peak intensity of GT1 species in each sample was normalized to the corresponding level of internal standard and presented as percent of corresponding controls. Data are expressed as mean ± SEM values.

Fluorescent dye-labeled GT1b

Three mg of GT1b (Matreya LLC) was dissolved in chloroform/ methanol/distilled water (2:1:0.2). 5(6)-Carboxy-X-rhodamine (16.6 mg) in anhydrous dimethylformamide (DMF, Sigma) was added dropwise to the GT1b solution. A mixture of GT1b and two equivalents of N-

hydroxybenzotriazole (HOBt, Anaspec Inc., San Jose, CA, USA), 2-(1H-benzotriazole-1-yl)-1,1,3,3-tetramethyluronium (HBTU, Anaspec Inc.), and four equivalents of N,N-diisopropylethylamine (DIPEA, Sigma) per surface hydroxyl group of the GT1b in anhydrous DMF was stirred for 24 h at room temperature. The crude product was eluted onto a Sephadex®LH-20 (lipophilic sephadex, Sigma) column (DMF only) to separate the unreacted excess rhodamine, HOBt, and HBTU. The sample solution was dialyzed (MWCO 1000, Sigma) against pure water for 4 h. After filtration with a 0.22 μm filter, the sample solution was freeze-dried. All steps were performed in the absence of light. The synthesis of the GT1b-rhodamine was confirmed from proton NMR spectra (Avance DPX-300, Bruker, Billerica, MA, USA) with the conjugation ester bond.

Statistics

The statistical significances of differences were assessed using SigmaPlot software (version 11.0, Systat Software, Inc., San Jose, CA, USA). Statistical analyses were performed using one-way ANOVA followed by Bonferroni's post test for multiple comparisons or Student's *t*-test. All data are presented as the mean ± SEM, and differences were considered statistically significant when the *p*-value was smaller than 0.05.

Results

Nerve injury-induced IKK/NF-κB activation is inhibited in SGCs of *cIkkβ*$^{-/-}$ mice.

To investigate the *in vivo* role of SGC activation in nerve injury-induced neuropathic pain, I used *Ikkβ* conditional knockout mice (*Cnp-Cre*$^{+/-}$*/Ikkβ*$^{f/f}$; *cIkkβ*$^{-/-}$) by breeding floxed-*Ikkβ* (*Ikkβ*$^{f/f}$) mice with *Cnp*-Cre transgenic mice, in which Cre expression is restricted to SGCs, oligodendrocytes, and Schwann cells (Braun et al., 1988; Toma et al., 2007; Yoshino et al., 1985). To verify SGC-specific inactivation of IKK/NF-κB signaling pathways in the DRG, I stained L5 DRG tissues from sham-operated or nerve-injured *Ikkβ*$^{f/f}$ and *cIkkβ*$^{-/-}$ mice 1 day post injury (dpi) with CNPase and p-p65 antibodies. To induce neuropathic pain, I applied L5 spinal nerve transection (SNT) to the mice, a well-known method for creating a mouse neuropathic pain model. To quantify the number of NF-κB-activated cells in DRG tissues after nerve injury, I counted p-p65 immunoreactivity (IR) cells and distinguished between SGC and neuron in cell size criterion; SGC body diameter is <10 μm, and the glial sheath envelops the sensory neuronal cell bodies (>10 μm). I observed an increase of phospho-p65-IR in SGCs (3.9% vs. 30.5%) and DRG neurons (14.1% vs. 60%) of *Ikkβ*$^{f/f}$ mice after peripheral nerve injury (Figs. 1a, b) indicating that nerve injury induces NF-

κB activation both in damaged neurons and SGCs. In *cIkkβ*$^{-/-}$ mice, the percentages of phospho-p65-immunoreactive neurons were comparable to those in *Ikkβ*$^{f/f}$ mice. However, p65 activation was severely compromised in SGCs (30.5% in *Ikkβ*$^{f/f}$ mice vs. 7.4% in *cIkkβ*$^{-/-}$ mice) indicating SGC-specific inactivation of IKK/NF-κB pathways in the DRG.

In addition to SGCs, CNPase is expressed in oligodendrocytes (Braun et al., 1988) and Schwann cells (Yoshino et al., 1985). Therefore, I tested whether NF-κB activation in oligodendrocytes was also affected after nerve injury. I stained L4-5 spinal cord sections from sham-operated or nerve-injured *Ikkβ*$^{f/f}$ and *cIkkβ*$^{-/-}$ mice 3 dpi with antibodies against p-p65 and cell type-specific marker for microglia (CD11b), astrocyte (GFAP), neuron (NeuN), and oligodendrocyte (ASPA). To quantify the NF-κB-activated cells in the ipsilateral dorsal horn of the spinal cord, I counted the number of p-p65-IR cells of each cell type. A significant increase in phospho-p65-IR cells was detected in the ipsilateral side compared with the contralateral spinal cord of SNT-injured *Ikkβ*$^{f/f}$ mice (Fig. 2a). Immunostaining with cell type-specific markers presents that these phospho-p65-IR cells in the spinal cord were mostly CD11b-IR microglia, NeuN-IR neurons, or GFAP-IR astrocytes (Fig. 2b). However, NF-κB activation was barely detected in the ASPA-IR oligodendrocytes (Fig. 2b).

In the *cIkkβ*$^{-/-}$ mice, nerve injury-induced NF-κB activation in the ipsilateral spinal cord was severely compromised (Fig. 2a). Of interest, nerve injury-induced NF-κB activation was compromised in the spinal cord microglia, but not in neurons or astrocytes in the *cIkkβ*$^{-/-}$ mice (Fig. 2c). To test if NF-κB activation in Schwann cells was affected after nerve injury, I stained tissue sections of proximal stump of L5 spinal nerve from sham-operated or nerve-injured *Ikkβ*$^{f/f}$ mice 1 dpi with antibodies against p-p65 and CNPase. To assess the number of NF-κB-activated Schwann cells in the proximal stump of L5 spinal nerve, I counted the number of p-p65-IR cells. In the spinal nerve, only a few phospho-p65-IR Schwann cells were detected in the *Ikkβ*$^{f/f}$ mice in the absence of nerve injury (Figs. 3a, b). However, NF-κB activation was not further significantly induced in Schwann cells after SNT injury 1 dpi. Taken together, these data indicate that nerve injury-induced NF-κB activation is inhibited in the SGCs of *cIkkβ*$^{-/-}$ mice, but not in Schwann cells or oligodendrocytes.

IKK/NF-κB-dependent SGC activation after nerve injury is inhibited in *cIkkβ*$^{-/-}$ mice.

In order to study if the IKK/NF-κB pathway is critical for nerve injury-induced SGC activation, I immunostained L5 DRG sections of *Ikkβ*$^{f/f}$ and

cIkkβ$^{-/-}$ mice with or without L5 SNT using GFAP antibody since its expression was upregulated in activated SGC (Woodham et al., 1989). SGC activation was observed following L5 SNT, as a marked upregulation of GFAP-IR was detected in the DRGs of *Ikkβ*$^{f/f}$ mice (Fig. 4a). To quantify the GFAP expression level, I measured GFAP-IR using ZEN software (version ZEN 2010B SP1), which was increased more than 5-fold at 3dpi compared to sham control (Fig. 4b). In *cIkkβ*$^{-/-}$ mice, however, nerve injury-induced SGC activation was significantly reduced by 60-78% compared to control mice (Figs. 4a, b).

To investigate the functional inhibition in SGC of *cIkkβ*$^{-/-}$ mice, I measured the expression of NF-κB-dependent proinflammatory cytokines in DRG tissues that were implicated in the modulation of pain hypersensitivity (O'Neill and Kaltschmidt, 1997; Schafers et al., 2001). I isolated total RNA from 3-5 pooled L5 DRG tissues of sham-operated or SNT-injured *Ikkβ*$^{f/f}$ and *cIkkβ*$^{-/-}$ mice and synthesized cDNA to measure proinflammatory cytokines level. Following L5 SNT, transcript levels of IL-1β, IL-6, and TNF-α were upregulated 13-, 23-, and 12-fold, respectively, in L5 DRG tissues (Fig. 5). By contrast, expression of these genes was significantly decreased by 40-75% in *cIkkβ*$^{-/-}$ mice compared to control mice. To measure IL-1β protein level after nerve injury, I immunostained L5 DRG sections of

Ikkβ$^{f/f}$ and *cIkkβ*$^{-/-}$ mice using IL-1β antibody. Similarly, L5 SNT upregulated IL-1β protein expression in the DRG of *Ikkβ*$^{f/f}$ mice, but not in the DRG of *cIkkβ*$^{-/-}$ mice (Fig. 6a). To quantify IL-1β protein expression, I measured IL-1β-IR in DRG tissues. IL-1β fluorescent intensity increased by more than 2.7-fold in control mice following L5 SNT, but IL-1β-IR was decreased by 82% in *cIkkβ*$^{-/-}$ mice (Fig. 6b). It has been reported that IL-6 and TNF-α are expressed in SGCs after nerve injury (Bohren et al., 2013; Dubovy et al., 2010). However, the IL-1β-expressing cell type in the DRG after nerve injury has not been identified. Therefore, I tested and found that IL-1β expression was detected mainly in CNPase-IR SGCs (Fig. 6c). Taken together, these data indicate that IKK/NF-κB-dependent SGC activation is abrogated in *cIkkβ*$^{-/-}$ mice.

IKKβ-mediated SGC activation is required for nerve injury-induced neuropathic pain.

To examine whether the blockade of NF-κB-dependent SGC activation attenuates neuropathic pain, I induced L5 SNT injury in *Ikkβ*$^{f/f}$ and *cIkkβ*$^{-/-}$ mice and measured pain sensitization by assessing mechanical allodynia and thermal hyperalgesia using Von Frey test and Hargreaves test, respectively. First of all, I investigated acute pain perception to test whether the pain

transmission pathway in *cIkkβ*$^{-/-}$ mice is intact. There was no difference in acute physiological pain perception between *Ikkβ*$^{f/f}$ and *cIkkβ*$^{-/-}$ mice, as measured by the tail immersion test (Fig. 7a). Moreover, in physiological conditions without nerve injury, basal mechanical and thermal sensitivity of *cIkkβ*$^{-/-}$ mice were comparable to those in control mice (Figs. 7b, c). Peripheral nerve injury produced a robust and sustained reduction in the paw withdrawal threshold to mechanical and thermal stimuli. The paw withdrawal threshold to mechanical stimuli on 1 dpi decreased from 1.07 ± 0.09 g to 0.34 ± 0.07 g after L5 SNT and remained below 0.2 g for up to 14 days (Fig. 7b). However, the paw withdrawal threshold of *cIkkβ*$^{-/-}$ mice was reduced to only 0.60 ± 0.08 g on 1 dpi and did not further decrease until the end of the procedure. Likewise, the paw withdrawal threshold to thermal stimuli in *Ikkβ*$^{f/f}$ mice at 7 dpi decreased by more than 60%, and the effect lasted up to 14 days (Fig. 7c). In contrast, in *cIkkβ*$^{-/-}$ mice, the threshold was gradually reduced by only 30% at 7 dpi. These data suggest that satellite glial cell activation is required for the maximum induction of pain hypersensitivity following peripheral nerve injury.

To exclude the possibility that the attenuated pain behavior observed in *cIkkβ*$^{-/-}$ mice was due to congenital defects in other physiological functions (Burke et al., 2013; Shi et al., 2010; Zeng et al.,

2008), I performed a battery of behavior tests assessing locomotor activity, anxiety, and depression-like phenotype on *cIkkβ*$^{-/-}$ mice (Fig. 8). *cIkkβ*$^{-/-}$ mice showed no abnormalities in locomotor activity, grooming, or rearing behavior in open field tests (Fig. 8a) and did not display anxiety or depression-like behavior in the elevated plus maze or forced swim tests compared to control mice (Figs. 8b, c).

SGC activation is required for nerve injury-induced spinal cord microglia activation.

Spinal cord microglia activation and subsequent proinflammatory cytokine production play causal roles in the development of neuropathic pain due to peripheral nerve injury (Watkins et al., 2001). To investigate the relationship between SGC activation in the DRG and spinal cord microglia activation after nerve injury, I compared spinal cord microglia activation of *Ikkβ*$^{f/f}$ and *cIkkβ*$^{-/-}$ mice by immunostaining L4-5 spinal cord sections with Iba-1 antibody. After L5 SNT, I detected marked microglia activation, which was measured by ionized calcium-binding adapter molecule 1 (Iba-1) upregulation and an increase of Iba-1-IR cells, in the ipsilateral dorsal horn of *Ikkβ*$^{f/f}$ mice (Fig. 9a). Iba-1-IR in ipsilateral dorsal horn of spinal cord increased more than 7-fold at 7 dpi in control mice (Fig. 9b). Nerve injury-

induced microglia activation was greatly attenuated by 70% in *cIkkβ*$^{-/-}$ mice at all time points tested (Figs. 9a, b). To further explore the increase of microglia cell in spinal dorsal horn, I immunostained L4-5 spinal cord sections of nerve-injured *Ikkβ*$^{f/f}$ and *cIkkβ*$^{-/-}$ mice with antibodies against Ki-67, a cell proliferation marker, and Iba-1. I found that SNT induced an increase of Ki-67-IR microglia in the ipsilateral dorsal horn of *Ikkβ*$^{f/f}$ mice, which was compromised in *cIkkβ*$^{-/-}$ mice (Figs. 10a, b). This indicates that microglia proliferation after SNT was reduced in *cIkkβ*$^{-/-}$ mice compared to *Ikkβ*$^{f/f}$ mice (Figs. 10a, b).

To measure transcripts level of IL-1β and TNF-α in L4-5 ipsilateral spinal cord tissues, I isolated total RNA from spinal cord tissues and synthesized cDNA for real-time RT-PCR. In addition, nerve injury-induced pain-mediating gene expression was similarly decreased in the spinal cords of *cIkkβ*$^{-/-}$ mice (Fig. 11). Transcripts of IL-1β and TNF-α were upregulated by 4.5- and 3.2-fold, respectively, after nerve injury in the spinal cords of control mice. However, expression of these genes was reduced by 30-75% in *cIkkβ*$^{-/-}$ mice. These results show that SGC activation is required for nerve injury-induced spinal cord microglia activation and pain-mediating gene expression *in vivo*.

Macrophage recruitment into DRG does not affect nerve injury-induced spinal cord microglia activation or pain hypersensitivity.

In addition to spinal cord microglia activation, peripheral nerve injury induces macrophage infiltration into injured DRG tissue (Hu and McLachlan, 2002). To investigate macrophage recruitment in DRG after L5 SNT, I stained nerve-damaged L5 DRG sections with Iba-1 antibody, a specific marker for macrophages in DRG, to detect resident and infiltrated macrophages (Imai et al., 1996). On day 3 after L5 SNT, Iba-1-IR was greatly increased in the ipsilateral L5 DRG of *Ikkβ$^{f/f}$* mice (Fig. 12a). However, in *cIkkβ$^{-/-}$* mice, Iba-1-IR upregulation was significantly reduced compare to control mice. Quantitatively, the number of macrophages per 0.04 mm^2 of DRG sections in control mice following nerve injury increased more than 5-fold; however, only a 2-fold increase was observed in *cIkkβ$^{-/-}$* mice (Fig. 12b). To test if the increase of macrophages is due to cell proliferation, I immunostained L5 DRG sections with Ki-67 and Iba-1 antibodies. The number of Ki-67-IR macrophages in the SNT-injured DRG was not significantly attenuated in *cIkkβ$^{-/-}$* mice (Figs. 13a, b), indicating that the macrophage increase in the injured DRG can be attributed to macrophage infiltration rather than proliferation of resident macrophages.

These data suggested that DRG-infiltrating macrophages may affect spinal cord microglia activation and pain hypersensitivity.

To test this possibility, I investigated whether the depletion of peripheral macrophages using clodronate liposome (Cl_2MDP) inhibits spinal cord microglia activation and pain sensitization following L5 SNT. Two days after Cl_2MDP administration, I stained spleen sections with CD68 antibody to verify peripheral monocytes/macrophages depletion. I observed that intraperitoneal injection of Cl_2MDP nearly completely depleted monocytes/macrophages in spleen tissues (Fig. 14) and reduced the number of macrophages infiltrating into the injured DRG by more than 90% (Fig. 15). To study the nerve injury-induced spinal cord microglia activation in these macrophage-depleted mice, I immunostained L4-5 spinal cord sections with Iba-1 antibody. I observed that L5 SNT-induced spinal cord microglia activation in macrophage-depleted mice is comparable to that of control mice (Figs. 16a, b). In addition, nerve injury induced mechanical allodynia in the absence of macrophage infiltration at a comparable level with that of control mice (Fig. 17). These data suggest that macrophages infiltrating into DRG have minimal effects on spinal cord microglia activation or development of neuropathic pain.

Satellite glial activation induces gangliosides upregulation in DRG neurons and spinal cord dorsal horn.

To investigate the mechanisms underlying the causal role of SGC activation in spinal cord microglia activation and pain hypersensitivity, I searched for genes that are differentially regulated in *cIkkβ*$^{-/-}$ DRG compared to *Ikkβ*$^{f/f}$ DRG after nerve injury by microarray analysis. Among genes induced in the nerve-injured *Ikkβ*$^{f/f}$ DRG but not in *cIkkβ*$^{-/-}$ DRG, I identified *St3gal2* gene, which encodes an enzyme converting gangliosides GM1 and GD1b into GD1a and GT1b, respectively (Sturgill et al., 2012). I focused on this gene based on previous studies implicating ganglioside in neuropathic pain, in which increased gangliosides GD1a and GT1b were documented in lumber spinal cord after peripheral nerve injury (Pavic et al., 2011) and in the cerebrospinal fluid of neuropathy patients (Trbojevic-Cepe et al., 1991).

To validate differential regulation of *St3gal2* gene in *cIkkβ*$^{-/-}$ mice after nerve injury, I measured *St3gal2* mRNA expression by real-time RT-PCR in the 3-5 pooled L5 DRG tissues of sham-operated and L5 SNT-injured mice. Peripheral nerve injury increased *St3gal2* mRNA expression 80% in L5 DRG tissues of *Ikkβ*$^{f/f}$ mice, which was completely abrogated in *cIkkβ*$^{-/-}$ mice (Fig. 18). To identify the cell type expressing *St3gal2* gene in DRG after L5 SNT, I immunostained L5 DRG sections with ST3Gal-II

antibody. Likewise, I found that ST3Gal-II protein is upregulated more than 2.8-fold in the DRG of *Ikkβ*$^{f/f}$ mice at 1 dpi (Fig. 19a, b). In DRG, ST3Gal-II-IR was mainly localized in cells morphologically identifiable as DRG neurons. In contrast, the nerve injury-induced ST3Gal-II protein expression was almost completely blocked in *cIkkβ*$^{-/-}$ mice. In order to confirm ST3Gal-II antibody specificity, I immunostained L5 DRG section of *St3gal2*$^{-/-}$ mice with the ST3Gal-II antibody. I could not detect ST3Gal-II-IR in *St3gal2*$^{-/-}$ mice, confirming the specificity of ST3Gal-II antibody (Fig. 20).

St3gal2 gene encodes ST3 beta-galactoside alpha-2,3-sialyltransferase 2 which is a type II membrane protein that catalyzes the transfer of sialic acid from CMP-sialic acid to galactose-containing substrates such as GM1 and GD1b. ST3Gal-II is expressed in the Golgi body but can be proteolytically processed to a soluble form that is responsible for production of ganglioside GT1b and GD1a (Sturgill et al., 2012). To measure ganglioside GT1b and GD1a expression level after L5 SNT, I immunostained L5 DRG and L4-5 spinal cord sections of sham-operated or SNT-injured *Ikkβ*$^{f/f}$ and *cIkkβ*$^{-/-}$ mice with GT1b or GD1a antibody. I found that the increase in *St3gal2* expression in the nerve-injured *Ikkβ*$^{f/f}$ DRG accompanied an aberrant increase in GT1b levels in DRG neuronal soma (Fig. 21a) and spinal cord dorsal horn that the central axon terminal of DRG neurons innervates (Fig. 22a). GD1a was also upregulated

in DRG soma (Fig. 21b) and spinal cord dorsal horn (Fig. 22b) of nerve-injured *Ikkβ*$^{f/f}$ mice, although the increase was less than that of GT1b. The upregulation of GT1b and GD1a in the DRG and dorsal horn after nerve injury were almost completely abrogated in *cIkkβ*$^{-/-}$ mice, demonstrating that the increase of GT1b and GD1a is dependent on *St3gal2* upregulation in DRG. To investigate whether the ganglioside GT1b and GD1a expression in central afferent axon in spinal cord is increased, I performed a double-immunohistochemistry in L4-5 spinal cord section with antibodies against gangliosides and a cell type specific marker for afferent nerve (CGRP and IB4), microglia (Iba-1), astrocytes (GFAP), oligodendrocytes (ASPA), and endothelial cells (CD31). In the ipsilateral dorsal horn of the spinal cord, enhanced GT1b- and GD1a-IR mainly co-localized with CGRP-positive and IB4-positive afferent axons, but not with Iba-1-positive microglia, GFAP-positive astrocytes, ASPA-positive oligodendrocytes, or CD31-positive endothelial cells (Fig. 23), indicating that the GT1b and GD1a increases I observed are likely originated from injured DRG neurons.

I further confirmed the nerve injury-induced ganglioside increase in the spinal cord by LC/MS analysis. For the LC/MS analysis of ganglioside GT1 species, I extracted gangliosides from pooled L4-5 ipsilateral spinal cord tissues of *Ikkβ*$^{f/f}$ and *cIkkβ*$^{-/-}$ mice at 3 dpi. During the enrichment process of gangliosides using Sambucus nigra (SNA) lectin column, I added

GM3-*d*3 to the concentrated ganglioside sample to serve the internal standard for normalization of LC/MS analysis. I could detect that the peak intensity of GT1 species (d18:1-18:0) increased by more than 2-fold in spinal cord tissues of *Ikkβ*$^{f/f}$ mice but not in *cIkkβ*$^{-/-}$ mice at 3 dpi (Fig. 24). Taken together, these data show that nerve injury-induced SGC activation leads to *St3gal2* upregulation in DRG neurons and subsequently aberrant increases of GT1b and GD1a in DRG neuron soma and in central axons in the spinal cord dorsal horn.

The role of GT1b in nerve injury-induced spinal cord microglia activation and pain hypersensitivity.

To test if there is a temporal correlation between the ganglioside increase and microglia activation by nerve injury in ipsilateral dorsal horn of spinal cord, I immunostained L4-5 spinal cord sections with GT1b and Iba-1 antibodies. I found that nerve injuries induced ganglioside increases, which was peaked at 3 dpi, in ipsilateral dorsal horn areas where spinal cord microglia are activated after nerve injury (Fig. 25a). In addition, the kinetics of ganglioside increase in the dorsal horn was correlated with nerve injury-induced microglia activation slightly preceding microglia activation (Fig. 25b).

Based on these findings, I explored the possibility that gangliosides are involved in nerve injury-induced spinal cord microglia activation. To begin with, I cultured primary glial cells from neonatal (P1) mouse brain and tested the potential of gangliosides to activate glial cells *in vitro*. I treated primary glial cells with GT1b or GD1a for 3 h and isolated total RNA from the glial cells to analyze pain-mediating gene expression level with real-time RT-PCR. In cultured primary glial cells, GT1b induced expressions of pain-mediating genes such as IL-1β, TNF-α, BDNF, iNOS, and Nox2 by 198-, 43-, 1.4-, and 16-, 1.8-fold, respectively (Fig. 26), while GD1a had no effect on the induction of these genes. A sub-optimal concentration of GT1b (4.5 μM) was selected based on dose-dependent experiments (1-45 μM) and uses for further studies. Within the concentrations tested, I could not observe microglia-activating effects of GD1a and any cytotoxic effects of GT1b. The protein expressions of IL-1β and BDNF, NO production, and intracellular reactive oxygen species (ROS) production by GT1b stimulation were confirmed by ELISA, Griess assay, and CM-H_2DCFDA dye, respectively (Figs. 27a-c). For the analysis of IL-1β, BDNF, and ROS production, I prepared pure primary microglia culture from mixed glial cells. For IL-1β and BDNF ELISA, I primed the primary microglia by pre-treating with GT1b for 2 h followed by an hour of ATP treatment. I measured IL-1β and BDNF protein expression level using cell

supernatants. GT1b stimulation induced IL-1β and BDNF production in microglia culture and these were released from microglia after ATP treatment (Fig. 27a). Interestingly, I also found that BDNF could be released by only GT1b stimulation. I measured nitrite level with Griess reagent to determine NO production in glial cells after GT1b treatment. GT1b stimulation significantly produced NO in glial cells (Fig. 27b). I determined intracellular ROS production in primary microglia using cell-permeant CM-H_2DCFDA dye. GT1b stimulation increased intracellular ROS production in microglia by 6.2-fold (Fig. 27c).

It has been reported that p38 MAP kinase activation is important for above pain-mediating gene expression in microglia (Ji and Suter, 2007). Therefore, I tested whether GT1b stimulation activates p38 MAP kinase pathway in glial cells with western blot analysis. GT1b stimulation induced p38 MAP kinase phosphorylation in glial cells (Fig. 28a). This activation peaked as early as 30 min post GT1b treatment and lasted as long as 60 min. To quantify the p38 MAP kinase activation, I measured p-p38 band intensity and presented as the fold increase compared to the control, which was normalized to the intensity of p38 (Fig. 28b). These data indicates that ganglioside GT1b has a potential to activate microglia *in vitro*, whereas GD1a does not.

To assess whether GT1b activates spinal cord microglia *in vivo*, I directly administrated GT1b into mouse spinal cord. One day after intrathecal GT1b injection, I immunostained spinal cord sections with Iba-1 antibody to determine microglia activation and found that Iba-1-IR was robustly upregulated in L4-5 spinal cord segments (Fig. 29). To measure pain-mediating gene level produced from activated spinal cord microglia, I removed L4-5 spinal cord tissues after intrathecal injection of GT1b and isolated total RNA from the tissues for real-time RT-PCR analysis. I found that GT1b administration upregulated pain-mediating gene expressions of IL-1β, TNF-α, and BDNF by 25-, 6-, and 1.6-fold, respectively (Fig. 30). These data demonstrate that GT1b induces spinal cord microglia activation *in vivo*.

To test whether the GT1b-activated microglia leads to pain central sensitization, I assessed pain behaviors to mechanical and thermal stimuli in these mice. I observed significant decreases in thresholds to mechanical and thermal stimuli in GT1b-injected mice but not in vehicle-injected mice (Figs. 31a, b). In allodynia test, the paw withdrawal threshold to mechanical stimuli on 1 day after GT1b injection was reduced from 0.96 ± 0.06 g to 0.23 ± 0.05 g and the decreased threshold was maintained for 7 days. Likewise, the paw withdrawal threshold to thermal stimuli in GT1b-injected mice on 3 d decreased by 48%, and the effect lasted until the end of the

procedure. The decreases of thresholds on 1 day post GT1b injection were comparable to the levels found in nerve-injured mice. These data suggest that aberrant upregulation of GT1b in the spinal cord may induce spinal cord microglia activation and pain hypersensitivity.

To further explore this possibility, I assessed nerve injury-induced spinal cord microglia activation and pain sensitization in *St3gal2*$^{-/-}$ mice. To determine whether SNT-induced GT1b increase in spinal cord is inhibited in *St3gal2*$^{-/-}$ mice, I prepared L4-5 spinal cord sections from sham-operated or SNT-injured *St3gal2*$^{-/-}$ mice and performed immunohistochemistry using GT1b antibody. I found that the nerve injury-induced GT1b upregulation at the spinal cord dorsal horn of *St3gal2*$^{-/-}$ mice was attenuated more than 85% compared to control mice (Figs. 32a, b). In *St3gal2*$^{-/-}$ mice, half the normal amount of GT1b is expressed by *St3gal3* gene, however, GT1b upregulation was blocked following L5 SNT (Sturgill et al., 2012). I also found that the nerve injury-induced spinal cord microglia activation measured by Iba-1-IR was reduced at a similar level in *St3gal2*$^{-/-}$ mice compared to control mice at 3 dpi (Figs. 33a, b). Quantitatively, Iba-1-IR in spinal cord dorsal horn increased more than 5.4-fold 3 dpi in WT mice but only a 1.8-fold increase was observed in *St3gal2*$^{-/-}$ mice. To evaluate pain sensitivity in *St3gal2*$^{-/-}$ mice, I measured responses to mechanical and thermal stimuli. Accordingly, nerve injury-induced mechanical allodynia and thermal hyperalgesia were

relieved in *St3gal2*$^{-/-}$ mice compared to wild-type mice (Figs. 34a, b), demonstrating that *St3gal2* is required for optimal spinal cord microglia activation and pain sensitization after nerve injury.

To exclude the possibility of *St3gal2* and GT1b effects in other cell types, I attempted to inhibit GT1b only in the spinal cord and DRG by intrathecally administrating D-*threo*-1-phenyl-2-decanoylamino-3-morpholino-1-propanol·HCl (PDMP), a pharmacological inhibitor of ganglioside synthesis (Vunnam and Radin, 1980). I directly injected PDMP in mouse spinal cord once daily for 7 days prior to L5 SNT. To confirm that PDMP administration inhibits GT1b upregulation by SNT, I immunostained L5 DRG and L4-5 spinal cord sections with GT1b antibody. I could find that intrathecal PDMP administration decreased basal GT1b level in DRG neuron and significantly reduced nerve injury-induced GT1b expression in sensory neurons (Figs. 35a, b) and afferent nerves in the spinal cord (Figs. 36a, b). In addition, PDMP injection attenuated nerve injury-induced spinal cord microglia activation (Figs. 37a, b). Quantitatively, spinal cord microglia activation, measured by Iba-1 immunohistochemistry, was reduced by 60% in PDMP-injected mice compared to control. In mechanical allodynia test, the paw withdrawal threshold to mechanical stimuli on 1 dpi decreased from 0.86 ± 0.13 g to 0.21 ± 0.04 g after L5 SNT and remained below 0.1 g for up to 7 days. However, the paw withdrawal threshold of

PDMP-injected mice was reduced to only 0.56 ± 0.09 g on 1 dpi and gradually decreased until the end of the procedure (Fig. 38). Taken together, these data suggest that L5 SNT induces GT1b upregulation at the afferent nerve of L4-5 dorsal horn that activates nearby microglia and induces pain central sensitization.

GT1b is transported to the spinal cord after nerve injury.

To examine whether sensory neuron-derived *de novo* GT1b is transported to the spinal cord, I ligated and transected the L5 dorsal root (rhizotomy) after L5 spinal nerve ligation (SNL) in rats. Three days after surgery, I prepared L5 DRG, L5 dorsal root, and L4-5 spinal cord sections from nerve-injured rats and immunostained the sections with GT1b or Iba-1 antibody. Similar to mouse SNT injury, I found that GT1b was upregulated in ipsilateral L5 DRG neurons (Fig. 39) and the ipsilateral dorsal horn of spinal cord (Fig. 40) after L5 SNL. Upon dorsal root rhizotomy followed by L5 SNL, GT1b was accumulated at the transection site of the dorsal root (Fig. 41), indicating that GT1b was transported from the DRG to the spinal cord via the dorsal root. In addition, L5 dorsal root rhizotomy completely inhibited L5 SNL-induced GT1b upregulation in the ipsilateral spinal cord (Fig. 42). Likewise, L5 rhizotomy inhibited L5 SNL-induced spinal cord microglia activation (Fig. 43). These data support that GT1b produced in the sensory neuron

after nerve injury is transported to the spinal cord via the dorsal root of the spinal nerve, which is responsible for aberrant GT1b upregulation and microglia activation in the spinal cord after nerve injury.

GT1b activates spinal cord microglia via toll-like receptor 2 activation.

It was previously reported that toll-like receptor 2 (TLR2) is required for nerve injury-induced spinal cord microglia activation (Kim et al., 2007). To test whether TLR2 is involved in ganglioside GT1b-mediated spinal cord microglia activation, I prepared glial cells from WT and *Tlr2*$^{-/-}$ mice. I stimulated the glial cells with GT1b for 3 h and isolated total RNA from the cell for real-time RT-PCR analysis. Notably, I found that GT1b-induced pain-mediating gene expression (IL-1β, TNF-α, and BDNF) was almost completely abrogated in glial cells from *Tlr2*$^{-/-}$ mice (Fig. 44). To assess spinal cord microglia activation by GT1b injection, I prepared spinal cord sections from vehicle or GT1b-injected WT and *Tlr2*$^{-/-}$ mice and immunostained the sections with Iba-1 antibody. Similarly, spinal cord microglia activation after intrathecal GT1b injection was almost entirely abolished (Figs. 45a, b). In addition, GT1b-induced pain-mediating gene expression in the spinal cord *in vivo* was blocked in *Tlr2*$^{-/-}$ mice (Fig. 46). I then tested the susceptibility of *Tlr2*$^{-/-}$ mice to GT1b-induced pain

hypersensitivity. Intrathecal GT1b administration produced hypersensitivity to both mechanical and thermal stimuli in control mice (Figs. 47a, b). The paw withdrawal threshold to mechanical stimuli on 1 day after GT1b injection was reduced from 0.92 ± 0.05 g to 0.32 ± 0.11 g and the decreased threshold was maintained for 7 days and the paw withdrawal threshold to thermal stimuli in GT1b-injected mice on 3 d decreased by 46%, and the effect was lasted until the end of the procedure. In *Tlr2*$^{-/-}$ mice, however, GT1b failed to decrease the thresholds in either mechanical allodynia or thermal hyperalgesia. These data indicate that the effects of GT1b were mediated by the TLR2, expressed mainly on spinal cord microglia *in vivo* (Lim et al., 2013).

Based on the functional significance of TLR2 in GT1b-induced microglia activation, I explored whether TLR2 acts as the receptor for ganglioside GT1b. I assessed the direct interaction between GT1b and TLR2 by using rhodamine-conjugated GT1b and primary microglia cultured from *Cx3cr1*$^{+/GFP}$ and *Tlr2*$^{-/-}$*/Cx3cr1*$^{+/GFP}$ mice. Upon GT1b-rhodamine treatment, I could observe that the GFP-positive microglia showed robust binding of GT1b-rhodamine on the cell surface (Fig. 48). However, the obvious fluorescent signal of rhodamine was not detected in microglia from *Tlr2*$^{-/-}$*/Cx3cr1*$^{+/GFP}$ mice. To further explore the direct interaction between GT1b and TLR2 on microglia, I performed competitive binding assays using

lipoteichoic acid (LTA), a TLR2 agonist. Likewise, in competitive binding assays between GT1b and LTA, LTA pretreatment inhibited GT1b-rhodamine binding on microglia at a dose-dependent manner (Figs. 49a, b). These results suggest that GT1b directly binds to the TLR2, and thereby serves as an endogenous agonist of TLR2 to activate spinal cord microglia during nerve injury-induced neuropathic pain.

Discussion

Spinal cord microglia are activated after peripheral nerve injury, and this activation plays a causal role in the development of neuropathic pain. However, the mechanisms for spinal cord microglia activation are not fully understood. In this study, I present evidence suggesting that spinal cord microglia activation detected in nerve injury-induced neuropathic pain is secondary to the activation of DRG SGCs. IKK/NF-κB-dependent SGC activation after nerve injury leads to *St3gal2* upregulation and subsequent GT1b production in sensory neurons. GT1b transported to the spinal dorsal horn via the dorsal root in turn activates spinal cord microglia through TLR2 activation (Fig. 51).

Previously, studies indicated pivotal role of the TLR2 signaling pathway in nerve injury-induced spinal cord microglia activation and subsequent neuropathic pain (Kim et al., 2007; Kim et al., 2010; Lim et al., 2013). However, how microglial TLR2 is activated during peripheral nerve injury remained elusive. I propose that GT1b that is upregulated after nerve injury may serve as an endogenous agonist to activate TLR2 on microglia in the dorsal horn. First, nerve injury induces GT1b increase in spinal cord dorsal horn that is temporally and spatially correlated with nerve injury-induced microglia activation. Second, GT1b induces pain-mediating gene expression such as IL-1β and BDNF in microglia *in vitro*, which is

dependent on TLR2. Third, GT1b injection induces spinal cord microglia activation and pain central sensitization *in vivo*, and the ablation of GT1b increase by knocking out *St3gal2* or intrathecal PDMP injection diminishes spinal cord microglia activation and pain sensitization. Finally, *in vitro* data using rhodamine-conjugated GT1b clearly demonstrate that GT1b directly binds to TLR2. Taken together, these data support the hypothesis that GT1b is the long-sought endogenous agonist of TLR2 in nerve injury-induced neuropathic pain.

GT1b is a major ganglioside that is abundant in the brain (Tettamanti et al., 1973). Studies have shown that GT1b on the axonal membrane interacts with myelin-associated glycoprotein on Schwann cells or oligodendrocytes, and contributes to long-term axon-myelin stability (Sheikh et al., 1999; Yang et al., 1996). In this regard, sensory neurons may upregulate this ganglioside in an effort to maintain axon-myelin integrity after nerve injury. My data indicate that, once aberrantly upregulated, GT1b in the spinal cord induces microglia activation. Considering that the basal level of GT1b in the absence of nerve injury does not activate microglia, upregulated GT1b may be released in the spinal cord dorsal horn after nerve injury, which in turn activates microglia nearby. Although I demonstrated that GT1b is upregulated in the sensory neurons and then transported to the spinal dorsal horn after peripheral nerve injury using immunohistochemistry

after rhizotomy, I did not formally assess GT1b release in the spinal cord dorsal horn in this study. I attempted an experiment to detect GT1b increase in the interstitial fluid of lumbar dorsal horn by microdialysis combined with LC/MS approach but I did not successfully detect ganglioside, most likely due to technical limitations making it difficult to obtain enough highly concentrated spinal cord interstitial fluid and the detection limits of LS/MS. However, a previous documentation of the increase of GT1b in the cerebrospinal fluid of neuropathy patients supports the possibility that GT1b is released during nerve injury-induced neuropathic pain (Trbojevic-Cepe et al., 1991). This mechanism should be explored in future studies.

Due to its clinical importance, great efforts have been made to understand the mechanisms of spinal cord microglia activation in neuropathic pain. Thus far, it has been proposed that ATP released from the spinal cord dorsal horn neuron activates microglia in the spinal dorsal horn via P2X4 receptor (Masuda et al., 2016; Tsuda et al., 2003). P2X4 activation of microglia, in turn, induces release of BDNF that may induce pain central sensitization by disinhibiting inhibitory synaptic transmission (Coull et al., 2005). However, P2X4 receptor is hardly detected in spinal cord microglia *in vivo* without peripheral nerve injury (Biber et al., 2011). This suggests that neuronal ATP might not be a primary or sole activator of microglia after nerve injury, and that other microglia-activating signals are required

during nerve injury-induced neuropathic pain. In this regard, my identification of GT1b as a novel microglia activator in nerve injury-induced neuropathic pain may fill the missing gap in this mechanism of neuropathic pain.

TLR2 is a pattern-recognition receptor that detects danger-associated and pathogen-associated molecular patterns and activates innate immune cells upon tissue damage and infection, respectively (Kirschning and Schumann, 2002). Besides neuropathic pain, TLR2 is implicated in glial cell activation and neuroinflammation in neurological conditions including spinal cord injury (Kigerl et al., 2007), stroke (Tang et al., 2007), and neurodegenerative diseases (Jana et al., 2008). Thus far, studies show that HMGB1 and misfolded-synuclein may function as endogenous TLR2 agonists (Kim et al., 2013; Park et al., 2004). My study found that GT1b is another TLR2 endogenous agonist that induces neuroinflammation. In addition to neuropathic pain, GT1b upregulation is detected in other neurological diseases including amyotrophic lateral sclerosis and epilepsy (Trbojevic-Cepe et al., 1991). Notably, in these diseases microglia activation and neuroinflammation are also observed (Beach et al., 1995; Henkel et al., 2009). Therefore, it may be worthwhile to investigate whether GT1b is also involved in microglia activation and neuroinflammation in these neurological disorders.

Several lines of evidence have demonstrated that peripheral macrophages infiltrate nerve-damaged DRG and contribute to pain hypersensitivity following peripheral nerve injury (Ma and Quirion, 2006a, b; Maeda et al., 2009; Vega-Avelaira et al., 2009). Macrophages are recruited in the L5 DRG, which is prominent on day 3, peaked on day 7, and then decreased on day 14 dpi (Kim et al., 2011a). However, in the present study, Cl_2MDP did not reduce mechanical allodynia for up to 7 days, indicating a limited role of macrophages in the onset of mechanical allodynia after L5 SNT. Rutkowski et al. utilized strategies to investigate the role of peripheral macrophages in the generation of mechanical allodynia in a rat model of neuropathy and found that the Cl_2MDP depletion of peripheral macrophages prior to nerve injury did not affect the resultant mechanical allodynia and spinal cord glial activation (Rutkowski et al., 2000). Moreover, the perineural administration of activated macrophages did not evoke mechanical allodynia in sham-operated rats, suggesting that peripheral glial cells or non-glial cells play a role in the inflammatory processes and generation of pain. From these data, it can be reasoned that macrophages that infiltrated into the DRG are implicated through the maintenance of established pain hypersensitivity rather than through oneset of neuropathy after peripheral nerve injury.

In the present study, I uncovered the role of SGC activation in nerve injury-induced microglia activation using *Cnp-Cre*$^{+/-}$*/Ikkβ*$^{f/f}$ mice. It should be noted that, in addition to SGCs, *Cnp* is also expressed in oligodendrocytes and Schwann cells. Therefore, it is possible that IKK/NF-κB activation of oligodendrocytes and Schwann cells is also blocked in *cIkkβ*$^{-/-}$ mice following nerve injury. However, in my immunohistochemistry analyses, I did not find evidence of NF-κB activation in spinal cord oligodendrocytes in *Ikkβ*$^{f/f}$ mice after L5 SNT (Fig. 2b). This finding is consistent with previous reports showing NF-κB activation only in microglia, astrocytes, and neurons, and not in oligodendrocytes, in the spinal cord following traumatic spinal cord injury or Freund's complete adjuvant injection (Bethea et al., 1998; Luo et al., 2014). Based on this information, it is unlikely that oligodendrocyte NF-κB activation affects spinal cord microglia activation in neuropathic pain. Meanwhile, I did detect a few NF-κB-activated Schwann cells in the L5 spinal nerve of *Ikkβ*$^{f/f}$ mice in the presence or absence of SNT (Fig. 3). However, Schwann cell NF-κB activation is unlikely to play a major role because: (i) The number of NF-κB-activated Schwann cells was very low compared to SGCs and there was no significant increase in the number of NF-κB-activated Schwann cells after SNT 1 dpi, when spinal cord microglia

begin to be activated, and (ii) the sensory neuron soma in which I observed *St3gal2* induction was in direct contact with SGCs, but not Schwann cells. Therefore, I reasoned that it is most likely that *St3gal2* induction in the SNT-injured sensory neurons is due to NF-κB activation in SGCs.

My *in vivo* data show that nerve injury-induced *St3gal2* induction in DRG neurons is blocked in *cIkkβ*$^{-/-}$ mice, indicating that IKK/NF-κB-dependent SGC activation somehow leads to *St3gal2* upregulation in sensory neurons. In this study, I observed IL-1β induction in SGCs upon peripheral nerve injury and found that recombinant IL-1β treatment upregulated *St3gal2* mRNA expression in DRG neurons *in vitro* (Fig. 50). Although I did not address the underlying mechanisms in this study, these data imply that the interplay between SGCs and DRG neurons via cytokine signaling may induce *St3gal2* upregulation in injured DRG neurons.

In summary, I demonstrate a novel mechanism for spinal cord microglia activation after peripheral nerve injury: nerve injury-induced SGC activation aberrantly leads to GT1b upregulation in DRG neurons and afferent axons in the spinal cord, which in turn activates spinal cord microglia through direct binding to microglial TLR2 to induce pain-mediating gene expression. Targeting SGC activation and subsequent GT1b induction is a potential novel therapeutic strategy in the treatment of neuropathic pain.

Figures

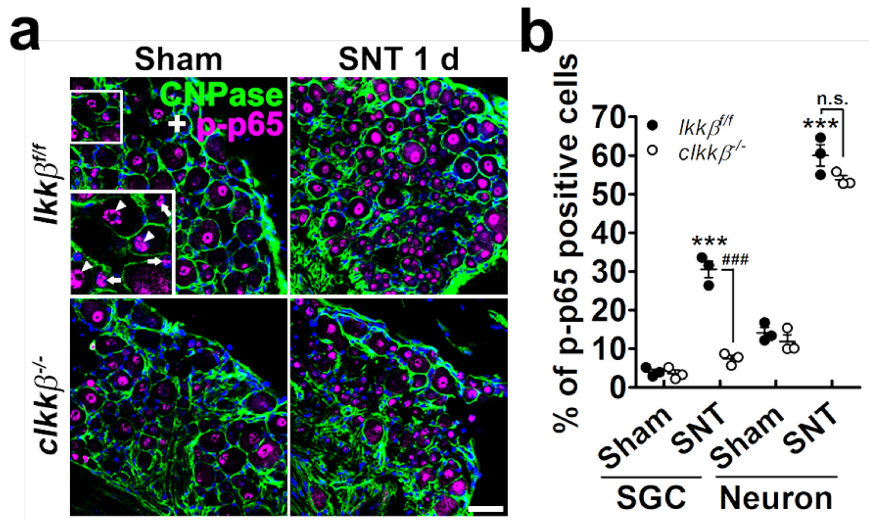

Fig. 1. Nerve injury-induced NF-κB activation is inhibited in SGC of *cIkkβ*$^{-/-}$ mice. (a) L5 DRG sections were prepared from *Ikkβ*$^{f/f}$ and *cIkkβ*$^{-/-}$ mice with or without L5 SNT, and then immunostained with CNPase and p-p65 antibodies. Nuclei were stained with DAPI (blue). Representative images are shown (n = 3/group; scale bar, 50 μm). Arrows and arrowheads indicate satellite glia and neurons in enlarged image, respectively. (b) The number of p-p65-IR cells was expressed as a percentage of total cells sampled (Student's t-test, ***$p < 0.001$, vs. sham control in *Ikkβ*$^{f/f}$ mice, $^{###}p < 0.001$, vs. *cIkkβ*$^{-/-}$ mice).

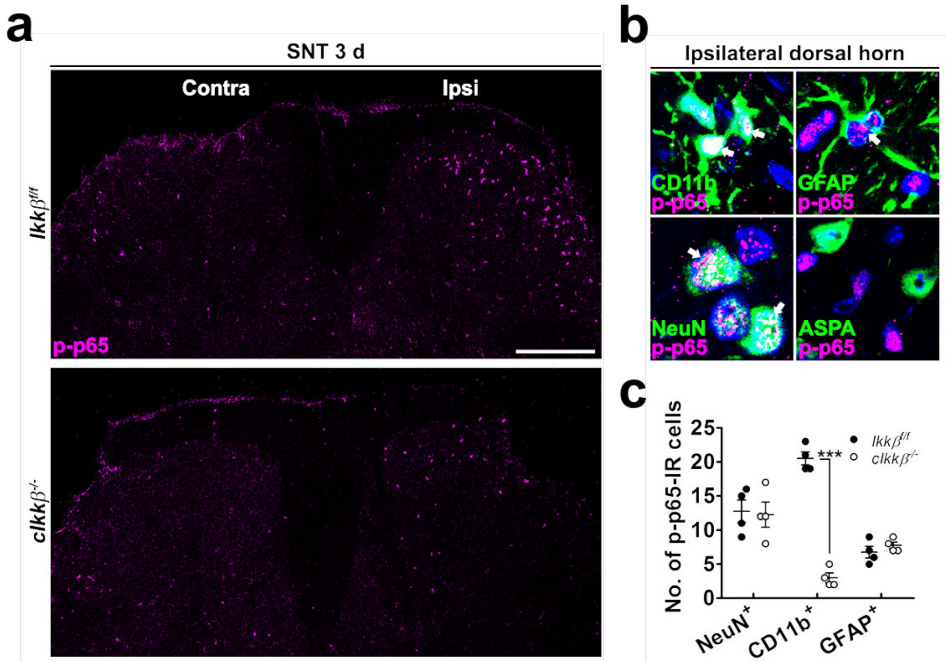

Fig. 2. NF-κB activation is barely detected in oligodendrocyte of spinal cord after nerve injury. (a) L5 spinal cord sections of L5 SNT-injured *Ikkβ$^{f/f}$* and *cIkkβ$^{-/-}$* mice (3 dpi) were immunostained with p-p65 antibody, and representative images are shown (n = 4; scale bar, 200 μm). (b) L5 spinal cord sections of L5 SNT-injured *Ikkβ$^{f/f}$* mice (3 dpi) were double-immunostained with antibodies against p-p65 and cell type-specific markers for microglia (CD11b), astrocytes (GFAP), neurons (NeuN), and oligodendrocytes (ASPA). Representative magnified images are shown. (c) The number of p-p65 immunoreactive (IR) cells of each cell type in the ipsilateral dorsal horn of the spinal cord was counted and presented as mean ± SEM (Student's t-test, ***$p < 0.001$).

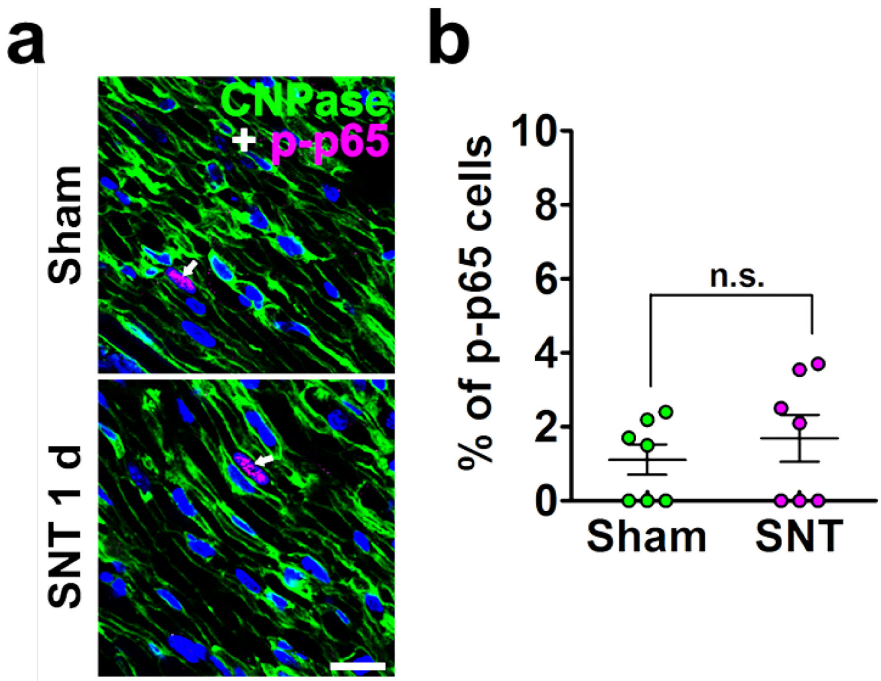

Fig. 3. NF-κB activation is not significantly induced in Schwann cell after nerve injury. (a) The tissue sections of the proximal stump of the injured L5 spinal nerve of *Ikkβ*$^{f/f}$ mice (1 dpi) were double-immunostained with CNPase and p-p65 antibodies. Representative images are shown (n = 7; scale bar, 20 μm). (b) The number of p-p65-IR cells was counted and expressed as a percentage of the total cells sampled. Nuclei were stained with DAPI (blue).

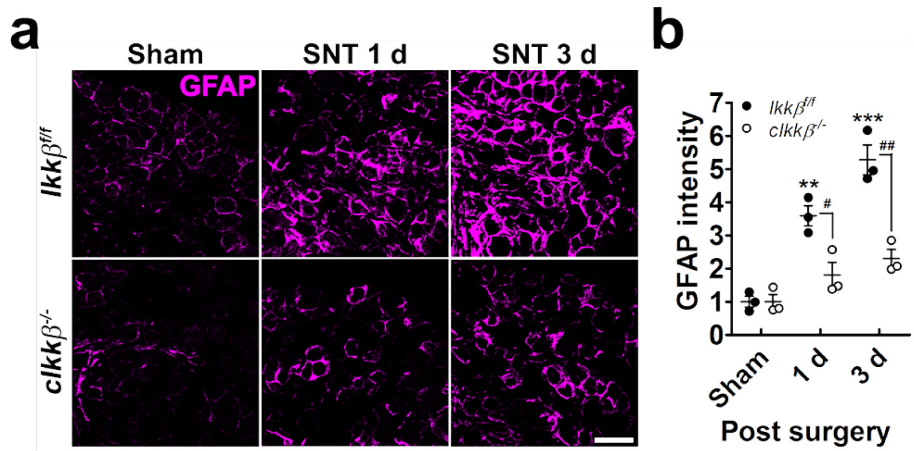

Fig. 4. Nerve injury-induced SGC activation is attenuated in *cIkkβ*$^{-/-}$ mice. (a) The L5 DRG sections were immunostained with GFAP antibody, and representative images are shown (n = 3/group; scale bar, 50 μm). (b) The fluorescent intensity of GFAP-IR signals was measured and presented as the fold induction compared to the corresponding level measured in sham-operated mice (Student's t-test, $^{**}p < 0.01$, $^{***}p < 0.001$ vs. sham controls in *Ikkβ*$^{f/f}$ mice; $^{\#}p < 0.05$, $^{\#\#}p < 0.01$ vs. *cIkkβ*$^{-/-}$ mice).

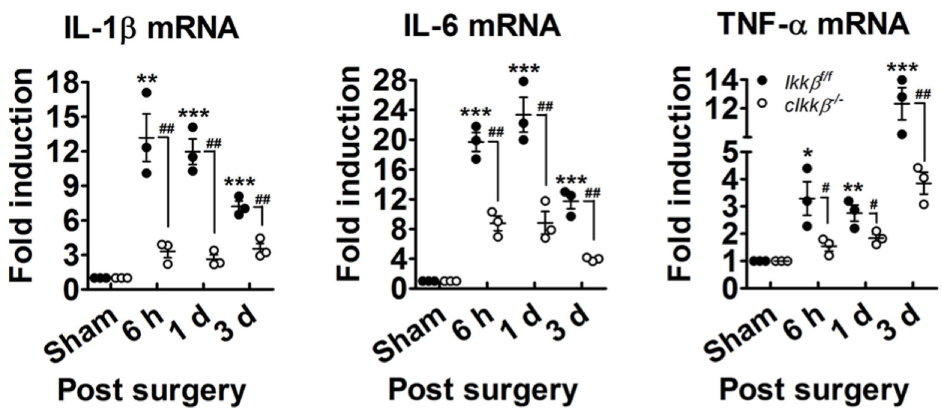

Fig. 5. NF-κB-dependent proinflammatory cytokines production due to nerve injury is reduced in *cIkkβ*$^{-/-}$ mice. Total RNA was isolated from 3-5 pooled L5 DRG and used to measure transcript levels of IL-1β, IL-6, and TNF-α at the indicated time points after L5 SNT (Student's *t*-test, *$p < 0.05$, **$p < 0.01$, ***$p < 0.001$ vs. sham controls in *Ikkβ*$^{f/f}$ mice; $^{\#}p < 0.05$, $^{\#\#}p < 0.01$ vs. *cIkkβ*$^{-/-}$ mice).

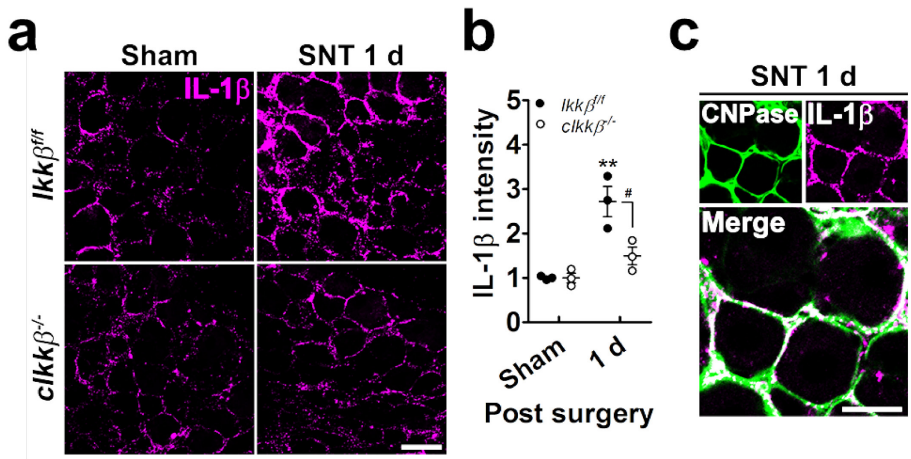

Fig. 6. Nerve injury-induced IL-1β protein expression is inhibited in SGC of *cIkkβ*$^{-/-}$ mice. (a) The L5 DRG sections were incubated with antibody against IL-1β (n = 3/group; scale bar, 50 μm). (b) The fluorescent intensity of IL-1β-IR signals was measured and presented as the fold induction compared to the corresponding level measured in sham-operated mice (Student's t-test, $^{**}p < 0.01$ vs. sham controls in *Ikkβ*$^{f/f}$ mice; $^{\#}p < 0.05$ vs. *cIkkβ*$^{-/-}$ mice). (c) L5 DRG sections of *Ikkβ*$^{f/f}$ mice 1 dpi were immunostained with CNPase and IL-1β antibodies, and representative images are shown (n = 3; scale bar, 25 μm).

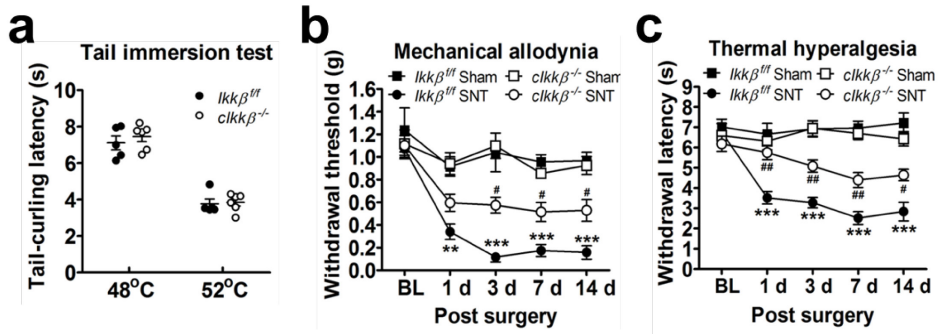

Fig. 7. Blockade of NF-κB-dependent SGC activation attenuates neuropathic pain without affecting acute pain sensation. (a) Tail withdrawal latency was measured by immersing tails of mice in hot water for an acute pain test (n = 5 for *Ikkβ*$^{f/f}$; n = 6 for *cIkkβ*$^{-/-}$). Mechanical allodynia (b) and thermal hyperalgesia (c) were evaluated for two weeks following L5 SNT (sham, n = 5; SNT, n = 5 for *Ikkβ*$^{f/f}$; sham, n = 6; SNT, n = 7 for *cIkkβ*$^{-/-}$; one-way ANOVA, $^{**}p < 0.01$, $^{***}p < 0.001$ vs. the sham-operated group in *Ikkβ*$^{f/f}$ mice; $^{\#}p < 0.05$, $^{\#\#}p < 0.01$ vs. the nerve-injured *Ikkβ*$^{f/f}$ group in each time point).

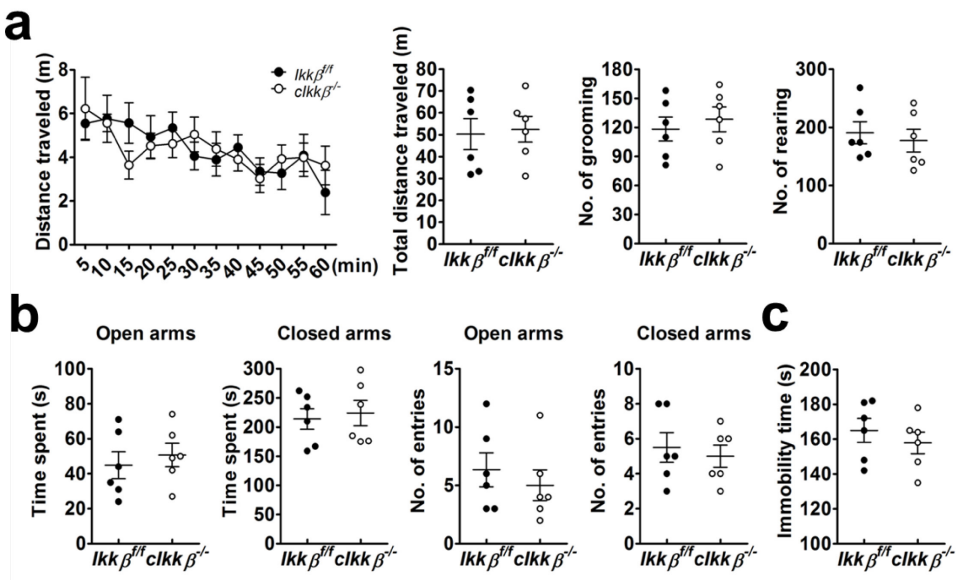

Fig. 8. *cIkkβ*$^{-/-}$ mice did not exhibit anxiety, depression-like behavior, or alteration in locomotion. (a) During 60 min of open field test sessions, no significant difference in distance traveled was observed between *Ikkβ*$^{f/f}$ (n = 6) and *cIkkβ*$^{-/-}$ mice (n = 6). The frequencies of grooming and rearing behaviors were not altered in *cIkkβ*$^{-/-}$ mice. (b) In the EPM test, compared to control mice, *cIkkβ*$^{-/-}$ mice did not exhibit any difference in the staying duration or the numbers of entries into the open and closed arms, respectively. (c) *cIkkβ*$^{-/-}$ mice show comparable immobility times in the FST.

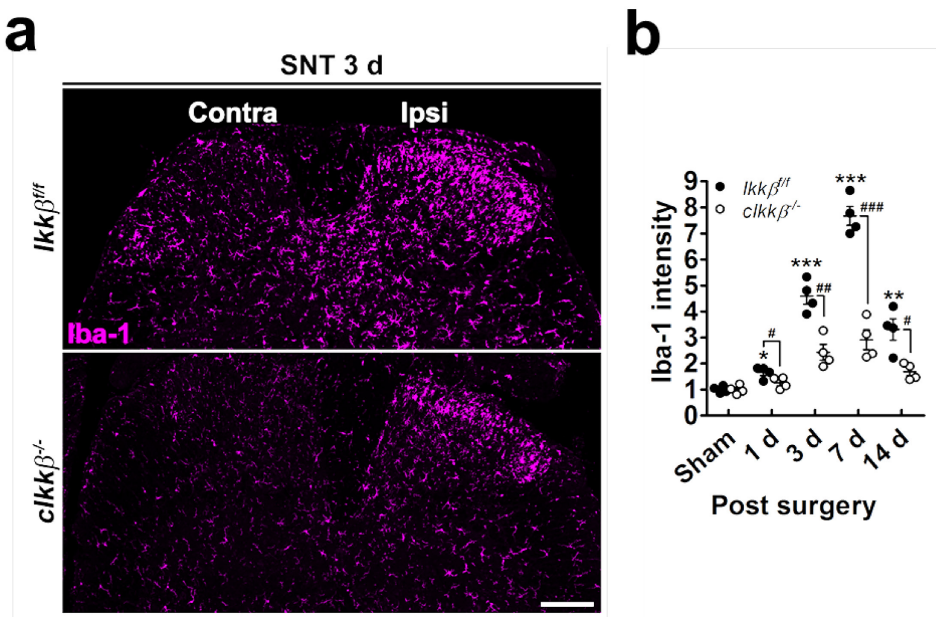

Fig. 9. NF-κB-dependent satellite glial cell activation is required for spinal cord microglia activation after nerve injury. (a) L4-5 spinal cord sections were prepared from sham-operated or nerve-injured *Ikkβ*$^{f/f}$ (n = 4/group) and *cIkkβ*$^{-/-}$ (n = 4/group) mice and immunostained with Iba-1 antibody. Representative images are shown (scale bar, 200 μm). (b) The fluorescent intensity of Iba-1-IR signals was measured and presented as the fold induction compared to the corresponding level measured in sham-operated mice (Student's t-test, *$p < 0.05$, **$p < 0.01$, ***$p < 0.001$ vs. sham controls in *Ikkβ*$^{f/f}$ mice; $^{\#}p < 0.05$, $^{\#\#}p < 0.01$, $^{\#\#\#}p < 0.001$ vs. *cIkkβ*$^{-/-}$ mice, n = 5/group).

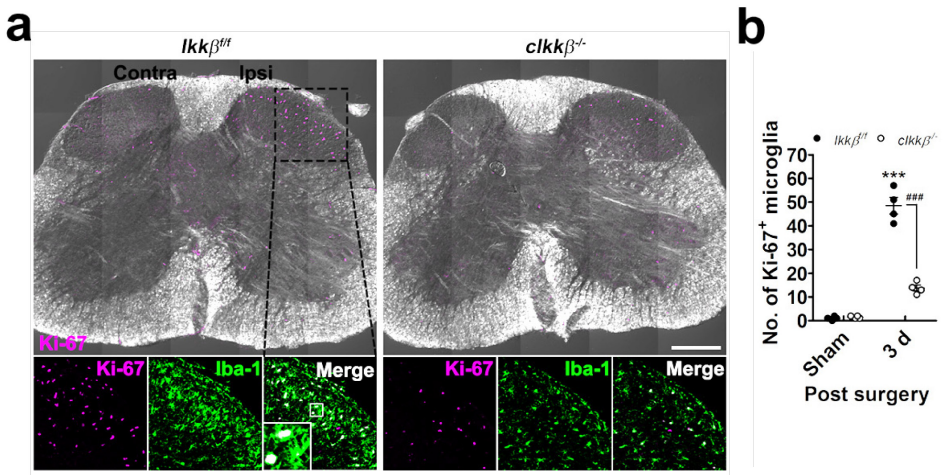

Fig. 10. Spinal cord microglia proliferation is reduced in *cIkkβ*$^{-/-}$ mice after nerve injury. (a) The spinal cord sections of SNT-injured *Ikkβ*$^{f/f}$ and *cIkkβ*$^{-/-}$ mice (3 dpi) were double-immunostained with Ki-67 and Iba-1 antibodies and representative images are shown (n = 4; scale bar, 200 μm). (b) The number of Ki-67-positive microglia in the ipsilateral dorsal horn of the spinal cord was counted and presented as mean ± SEM (Student's t-test, $^{***}p < 0.001$, vs. sham control in *Ikkβ*$^{f/f}$ mice, $^{\#\#\#}p < 0.001$, vs. *cIkkβ*$^{-/-}$ mice).

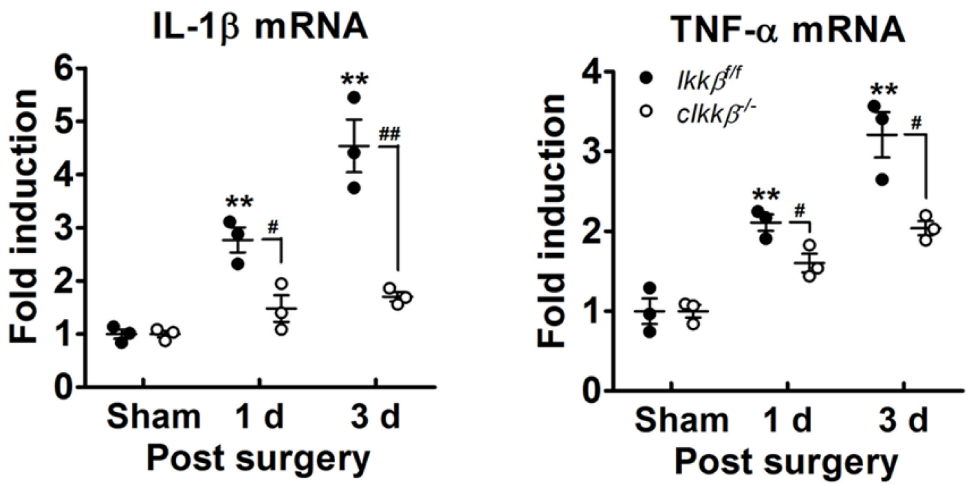

Fig. 11. Proinflammatory gene expression is inhibited in L4-5 spinal cord of *cIkkβ*$^{-/-}$ mice. IL-1β and TNF-α mRNA expression in L4-5 ipsilateral spinal cord tissues after L5 SNT were measured by real-time RT-PCR (Student's *t*-test, $^{**}p < 0.01$ vs. sham controls in *Ikkβ*$^{f/f}$ mice; $^{\#}p < 0.05$, $^{\#\#}p < 0.01$ vs. *cIkkβ*$^{-/-}$ mice, $n = 3$/group).

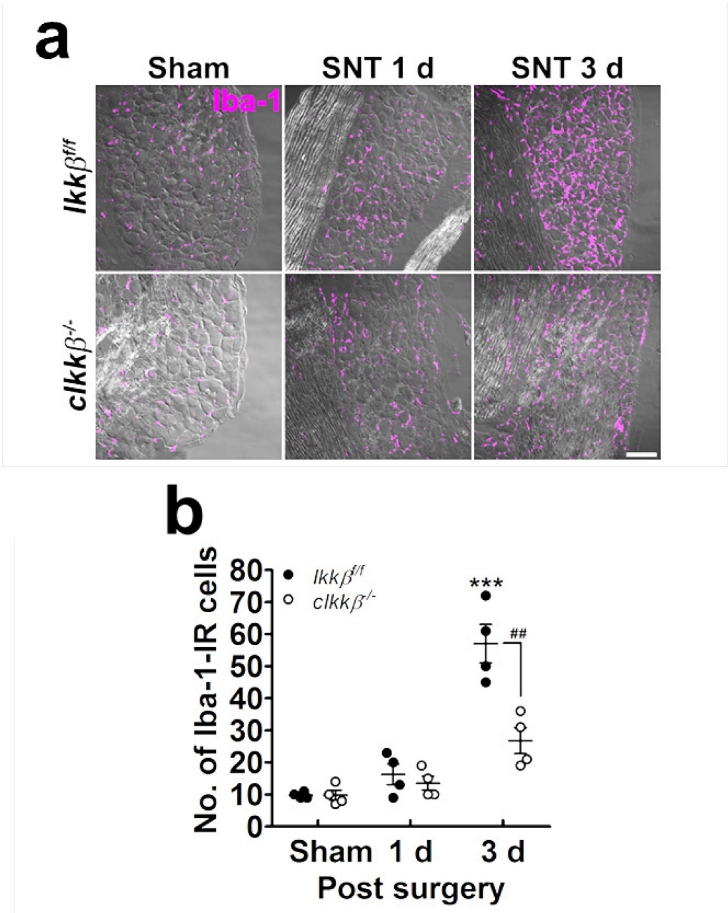

Fig. 12. Macrophage infiltration into DRG is reduced in *cIkkβ*$^{-/-}$ mice after nerve injury. (a) L5 DRG sections were prepared from *Ikkβ*$^{f/f}$ mice (n = 4/time point) and *cIkkβ*$^{-/-}$ mice (n = 4/time point) after L5 SNT and immunostained with Iba-1 antibody. Representative images are shown (scale bar, 100 μm). (b) The number of Iba-1-IR cells in the L5 DRG sections was counted in an area of 0.2 × 0.2 mm (Student's t-test, ***$p < 0.001$ vs. sham controls in *Ikkβ*$^{f/f}$ mice; $^{\#\#}p < 0.01$ vs. *cIkkβ*$^{-/-}$ mice).

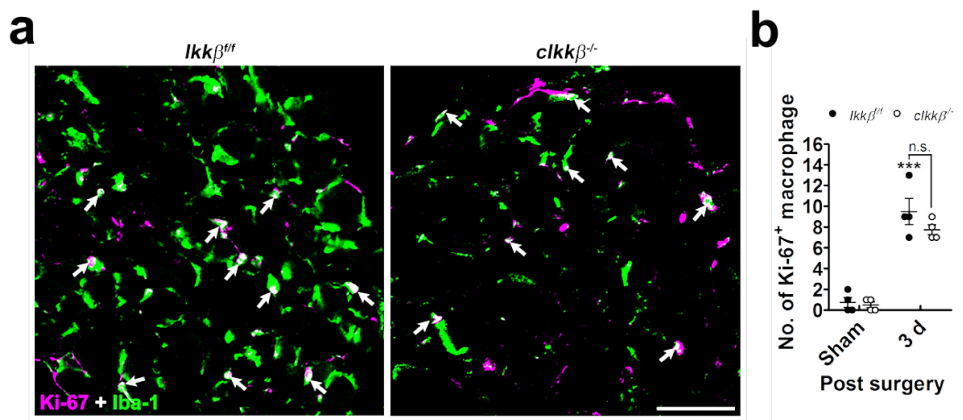

Fig. 13. Macrophage proliferation in DRG of *cIkkβ*$^{-/-}$ mice is comparable to control mice after nerve injury. (a) L5 DRG tissue sections of SNT-injured *Ikkβ*$^{f/f}$ and *cIkkβ*$^{-/-}$ mice (3 dpi) were double-immunostained with Ki-67 and Iba-1 antibodies and representative images are shown (n = 4; scale bar, 50 μm). (b) The number of Ki-67-positive macrophages in the ipsilateral DRG was counted and presented as mean ± SEM (Student's t-test, ***$p < 0.001$, vs. sham control in *Ikkβ*$^{f/f}$ mice).

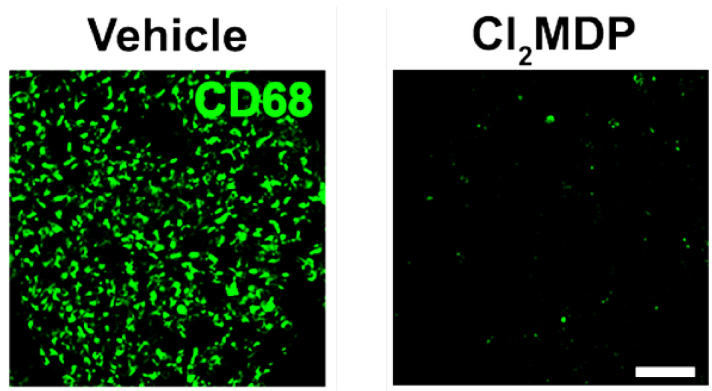

Fig. 14. Cl_2MDP injection depletes peripheral monocytes/macrophages. Spleen tissues were sampled from *Ikkβ*$^{f/f}$ mice 2 days after Cl_2MDP injection and immunostained with CD68 antibody to verify macrophage depletion. Saline was used as a vehicle (n = 3/group; scale bar, 100 μm).

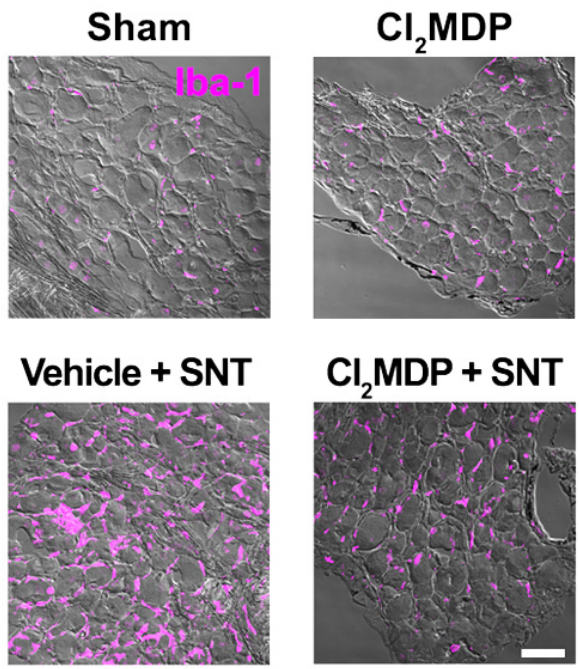

Fig. 15. Cl_2MDP injection reduces macrophage infiltration into L5 DRG after nerve injury. L5 DRG sections were prepared from sham-operated or L5 SNT-injured *Ikkβ*$^{f/f}$ mice (3 dpi) with or without Cl_2MDP injection and immunostained with Iba-1 antibody. Representative images are shown (*n* = 4/group; scale bar, 50 μm).

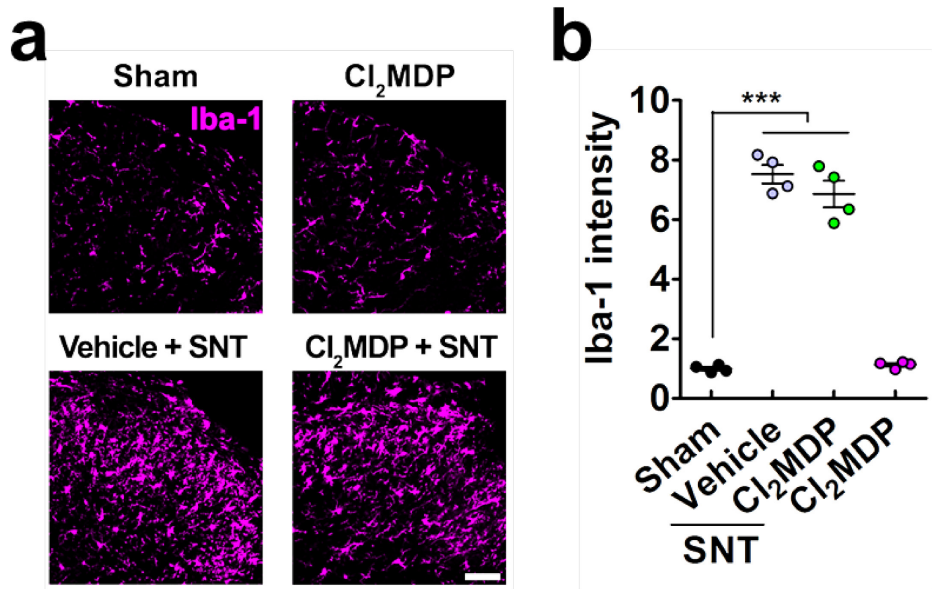

Fig. 16. Macrophage depletion does not affect nerve injury-induced spinal cord microglia activation. (a) L4-5 spinal cord sections were prepared from sham-operated or L5 SNT-injured *Ikkβ*$^{f/f}$ mice (3 dpi) with or without Cl_2MDP injection and immunostained with Iba-1 antibody. Representative images are shown (n = 4/group; scale bar, 50 μm). (b) The fluorescent intensity of Iba-1-IR signals was measured (Student's t-test, ***$p < 0.001$).

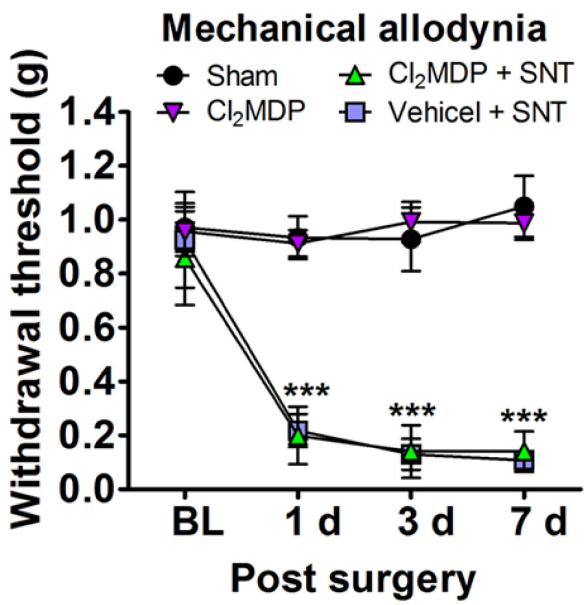

Fig. 17. Macrophage depletion does not affect nerve injury-induced pain hypersensitivity. The 50% withdrawal threshold of the ipsilateral hind paw in response to mechanical stimuli was assessed for 7 d in the sham controls (n = 5), L5 SNT-injured *Ikkβ*$^{f/f}$ mice with vehicle injection (n = 5), L5 SNT-injured *Ikkβ*$^{f/f}$ mice with Cl_2MDP injection (n = 5), and Cl_2MDP-injected *Ikkβ*$^{f/f}$ mice (n = 4, one-way ANOVA, ***$p < 0.001$ vs. sham controls).

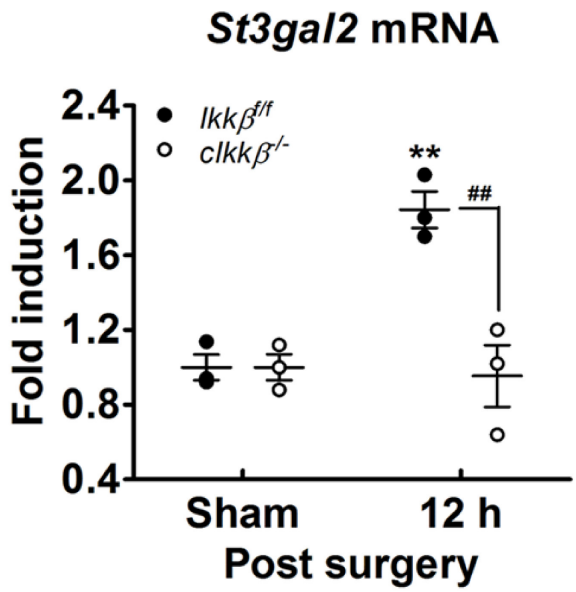

Fig. 18. Nerve injury-induced *St3gal2* mRNA expression is blocked in DRG tissue of *cIkkβ*$^{-/-}$ mice. *St3gal2* mRNA expression was measured by real-time RT-PCR in the pooled L5 DRG tissues of sham-operated and L5 SNT-injured mice (n = 3/group, Student's t-test, $^{**}p < 0.01$, vs. sham control in *Ikkβ*$^{f/f}$ mice, $^{\#\#}p < 0.01$, vs. *cIkkβ*$^{-/-}$ mice).

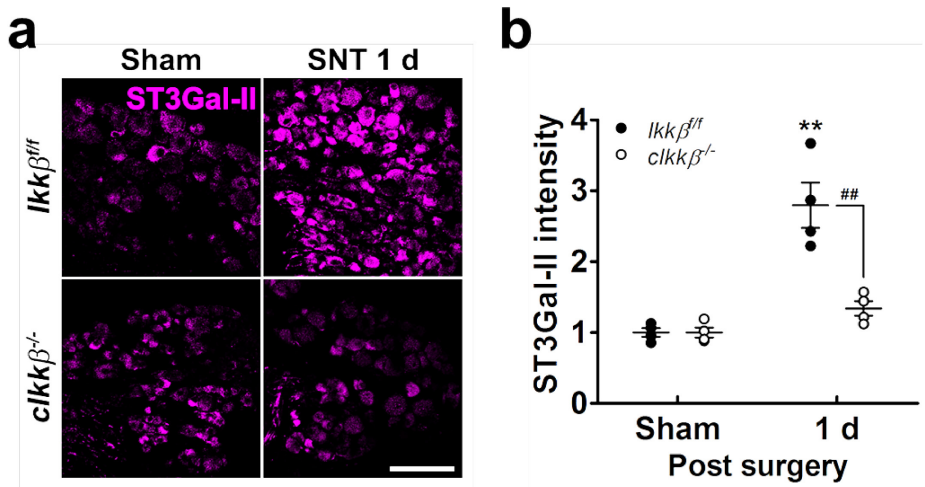

Fig. 19. Nerve injury-induced ST3Gal-II protein expression is inhibited in DRG neurons of *cIkkβ*$^{-/-}$ mice. (a) L5 DRG sections were prepared from *Ikkβ*$^{f/f}$ (n = 4/group) and *cIkkβ*$^{-/-}$ (n = 4/group) mice with or without L5 SNT (1 dpi) and immunostained with ST3Gal-II antibody. Representative images are shown (scale bar, 100 μm). (b) The fluorescent intensity of ST3Gal-II-IR was measured from each L5 DRG sections and presented as the fold induction compared to the corresponding level measured in sham control (Student's t-test, $^{**}p < 0.01$, vs. sham control in *Ikkβ*$^{f/f}$ mice, $^{\#\#}p < 0.01$, vs. *cIkkβ*$^{-/-}$ mice).

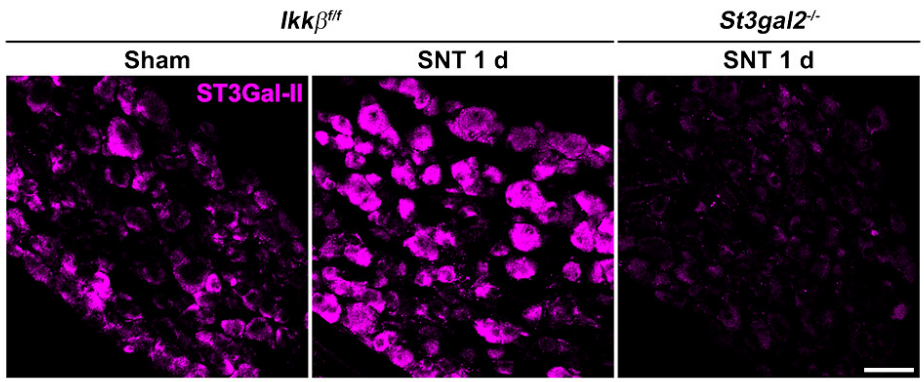

Fig. 20. ST3Gal-II immunohistochemistry in the L5 DRG. To confirm ST3Gal-II antibody specificity, L5 DRG sections of *Ikkβ*$^{f/f}$ and *St3gal2*$^{-/-}$ mice with or without L5 SNT (1 dpi) were immunostained with anti-ST3Gal-II antibody (scale bar, 50 μm).

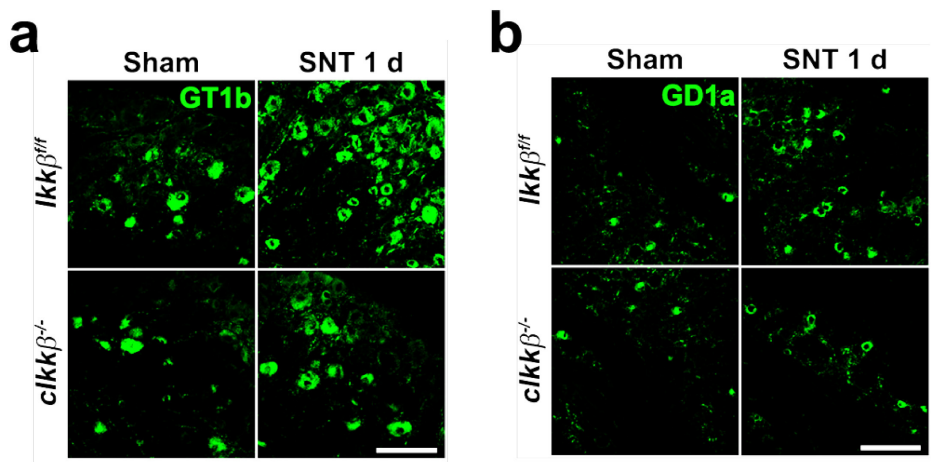

Fig. 21. Aberrant ganglioside GT1b and GD1a increase in DRG is inhibited in *cIkkβ*$^{-/-}$ mice upon nerve injury. L5 DRG sections were sampled from sham-operated (n = 5/group) and L5 SNT-injured (1 dpi) mice (n = 5/group) and immunostained with antibodies against GT1b (a) and GD1a (b), respectively. Representative images are shown (scale bar, 100 μm).

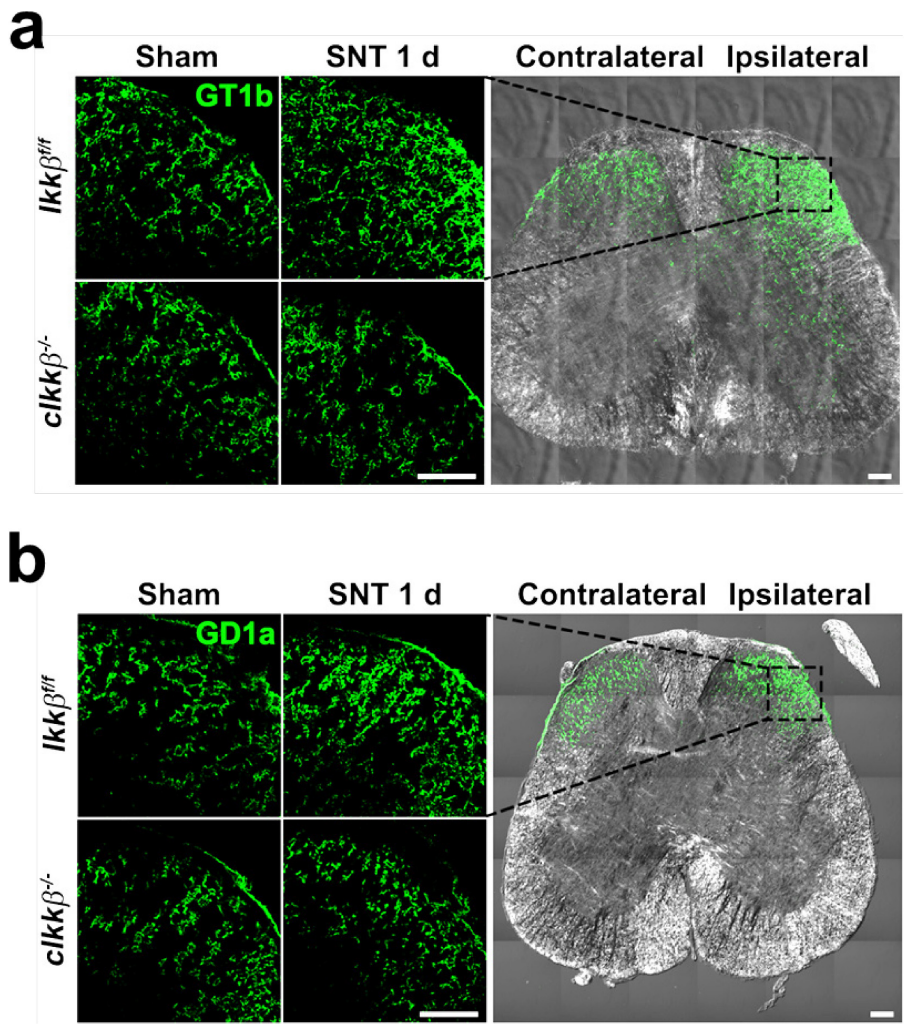

Fig. 22. Abnormal ganglioside GT1b and GD1a increase in spinal cord is inhibited in *cIkkβ*$^{-/-}$ mice after nerve injury. L4-5 spinal cord sections were sampled from sham-operated (n = 5/group) and L5 SNT-injured (1 dpi) mice (n = 5/group) and immunostained with antibodies against GT1b (a) and GD1a (b), respectively. Representative images are shown (scale bar, 100 μm).

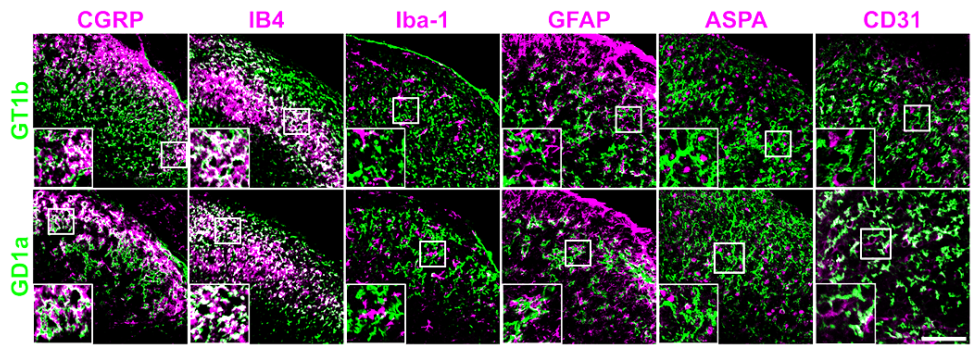

Fig. 23. Ganglioside GT1b and GD1a are upregulated in afferent axons in spinal cord dorsal horn after nerve injury. L4-5 spinal cord sections were double-immunostained with antibodies against gangliosides and a cell type specific marker for afferent nerve (CGRP and IB4), microglia (Iba-1), astrocytes (GFAP), oligodendrocytes (ASPA), and endothelial cells (CD31). Representative images are shown (scale bar, 100 μm).

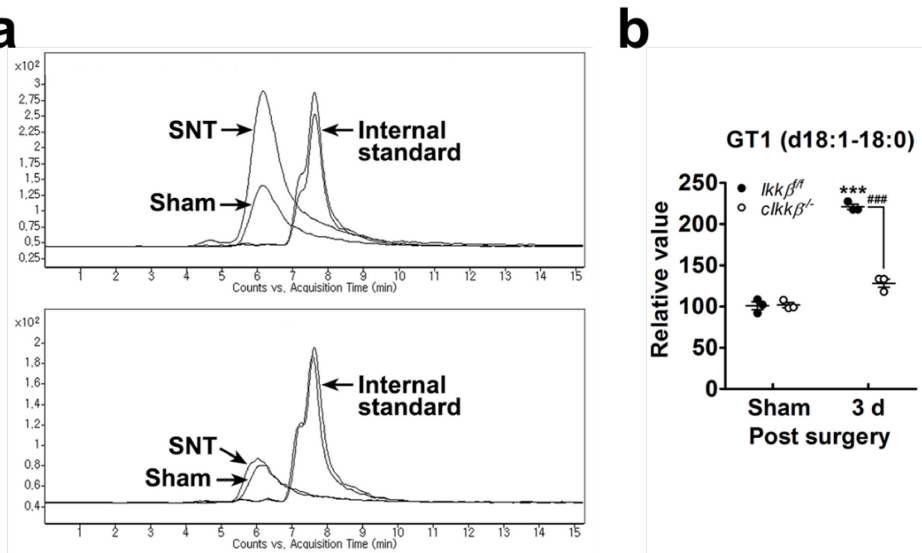

Fig. 24. Abnormal ganglioside GT1b upregulation in spinal cord following L5 SNT. (a) LC/MS analysis of ganglioside GT1 species in pooled spinal cord tissues of *Ikkβ*$^{f/f}$ (upper panel) and *cIkkβ*$^{-/-}$ (lower panel) mice at 3 dpi. Representative traces of GT1 species (d18:1-18:0) are shown. (b) The peak intensity of the GT1 species in each sample is presented as percent of corresponding control. Data are represented as mean ± SEM (Student's *t*-test, ***$p < 0.001$, vs. sham control in *Ikkβ*$^{f/f}$ mice, $^{###}p < 0.001$, vs. *cIkkβ*$^{-/-}$ mice).

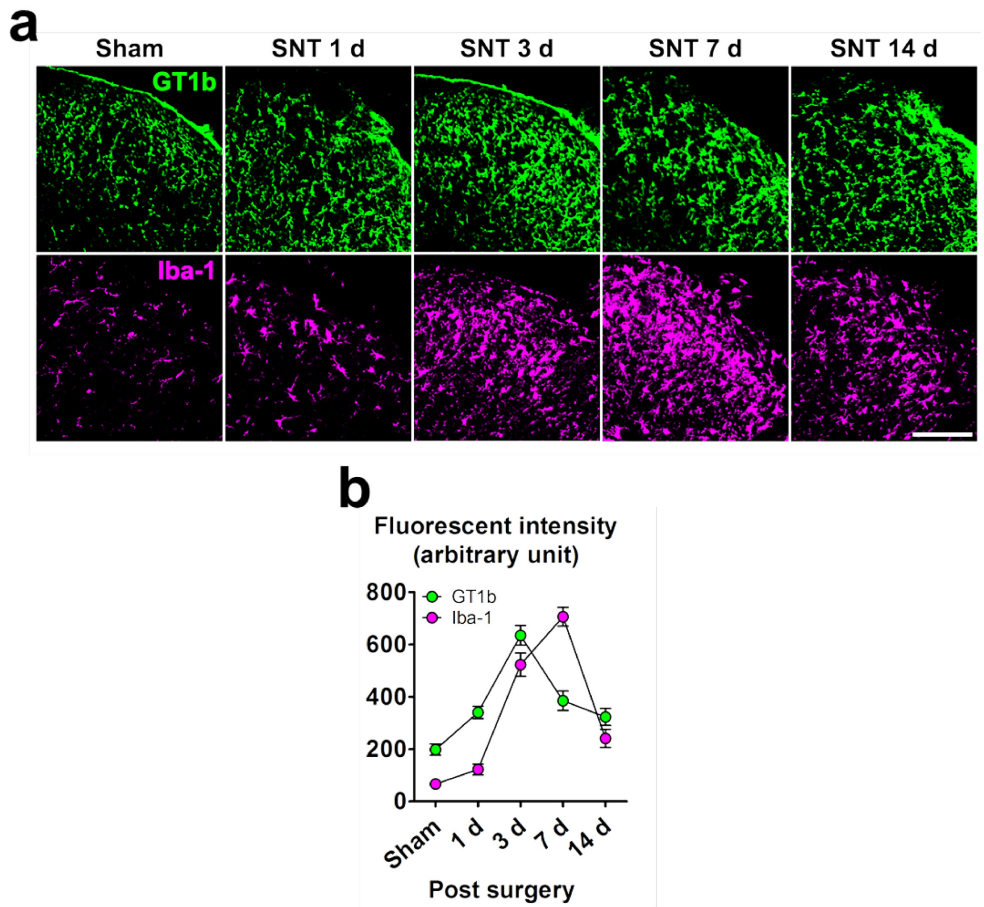

Fig. 25. Kinetics of ganglioside GT1b upregulation and microglia activation in spinal cord following nerve injury. (a) Double immunohistochemistry in L4-5 spinal cord tissues (n = 3/time point) after L5 SNT and representative images are shown (scale bar, 100 μm). (b) The fluorescent intensity of GT1b-IR and Iba-1-IR was measured and expressed as mean ± SEM.

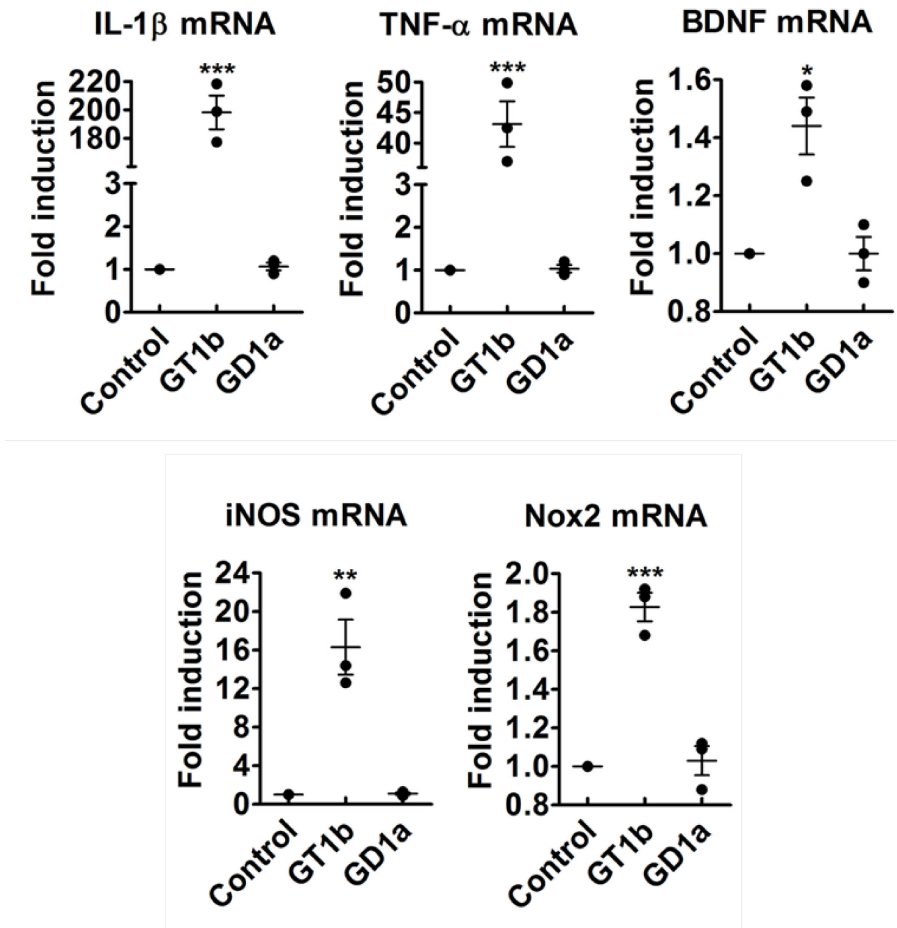

Fig. 26. Ganglioside GT1b induces pain-mediating gene expression in glial cells. Glial cells were stimulated with 4.5 μM of GT1b or GD1a for 3 h. Transcript levels of IL-1β, TNF-α, BDNF, iNOS, and Nox2 were measured by real-time RT-PCR (Student's *t*-test, *$p < 0.05$; **$p < 0.01$; ***$p < 0.001$).

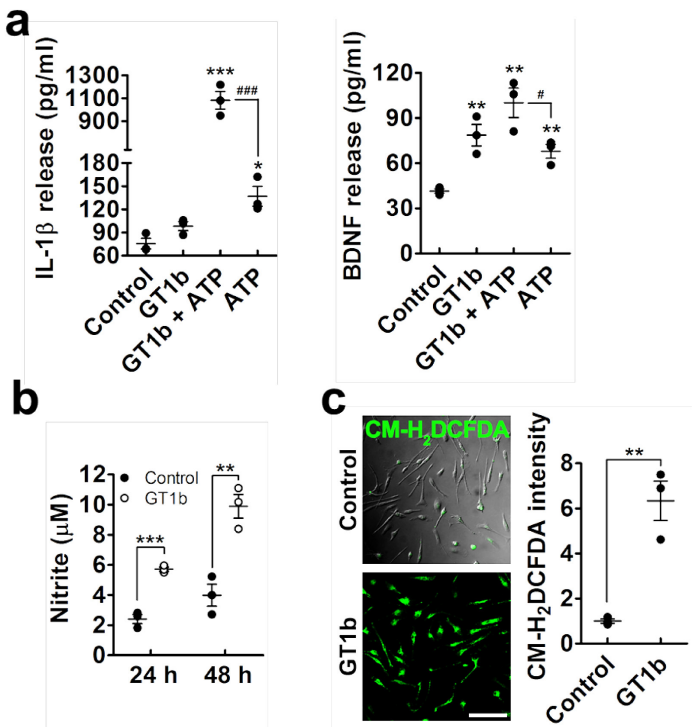

Fig. 27. Ganglioside GT1b induces production of proinflammatory cytokines, NO, and ROS in glial cells. (a) The culture media from primary microglia stimulated with GT1b followed by ATP were collected for IL-1β and BDNF ELISA analysis (Student's *t*-test, $*p < 0.05$; $**p < 0.01$; $***p < 0.001$, vs. control, $^{\#}p < 0.05$; $^{\#\#\#}p < 0.001$, vs. ATP condition). (b) Glial cells were treated with 4.5 μM of GT1b for 24 or 48 h and the culture media were analyzed for nitrite production using Griess reagent (Student's *t*-test, $**p < 0.01$; $***p < 0.001$). (c) Intracellular ROS production in primary microglia was measured using CM-H2DCFDA (10 μM) 6 h after GT1b (4.5 μM) treatment. Three experiments were independently performed and representative images are shown. The fluorescent intensity of CM-H2DCFDA was measured and presented as the fold induction (Student's *t*-test, $**p < 0.01$).

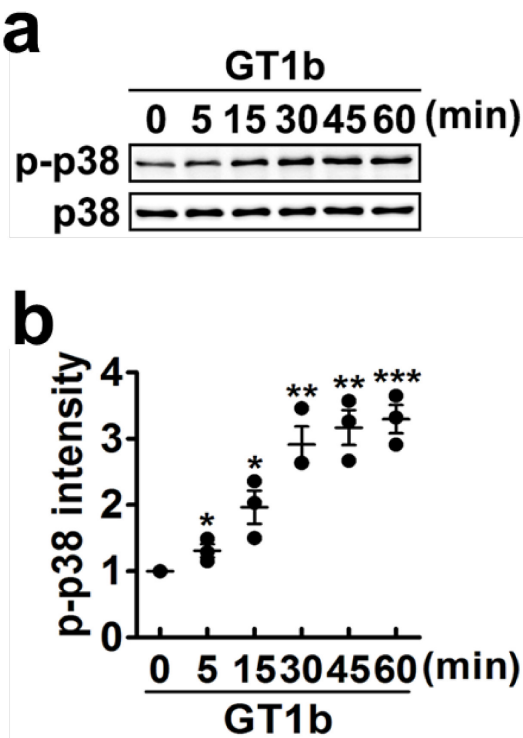

Fig. 28. Ganglioside GT1b activates p38 MAP kinase signaling in glial cells. (a) Glial cells were stimulated with GT1b (4.5 μM) at the indicated time points and cell lysates were prepared from each sample. p38 MAPK activation was determined by western blot analysis. Three independent experiments were performed and representative blot image is shown. (b) The band intensity of p-p38 was measured and presented as fold induction compared to the control (Student's *t*-test, **p* < 0.05; ***p* < 0.01; ****p* < 0.001, vs. control).

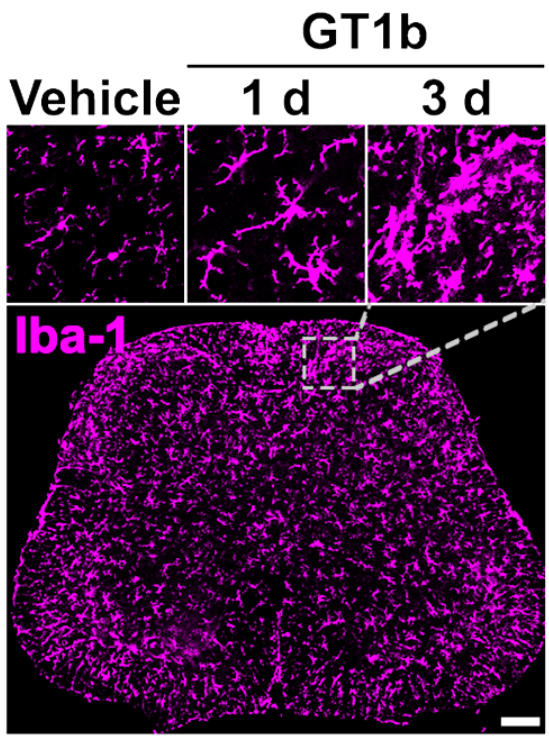

Fig. 29. Intrathecal GT1b injection induces spinal cord microglia activation. GT1b (25 μg/5 μl, *n* = 3/time point) or vehicle (saline, *n* = 3) was intrathecally administrated and L4-5 spinal cord sections were immunostained with Iba-1 antibody. Vehicle-injected mice served as controls and representative images are shown (scale bar, 100 μm).

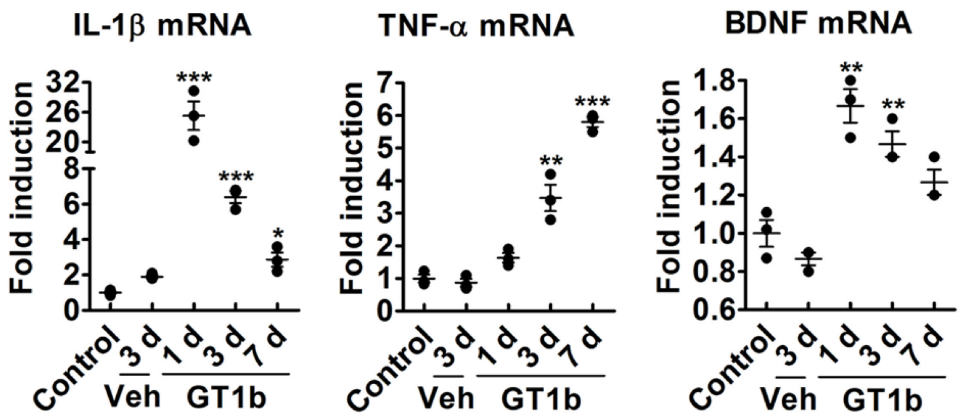

Fig. 30. Intrathecal GT1b administration induces pain-mediating gene expression in spinal cord. L4-5 spinal cord tissues were removed after intrathecal injection of GT1b (25 μg/5 μl, n = 3/time point) or vehicle (n = 3) injection and total RNA was isolated from the tissues. IL-1β, TNF-α, and BDNF mRNA level were measured by real-time RT-PCR (Student's t-test, *$p < 0.05$; **$p < 0.01$; ***$p < 0.001$, vs. control).

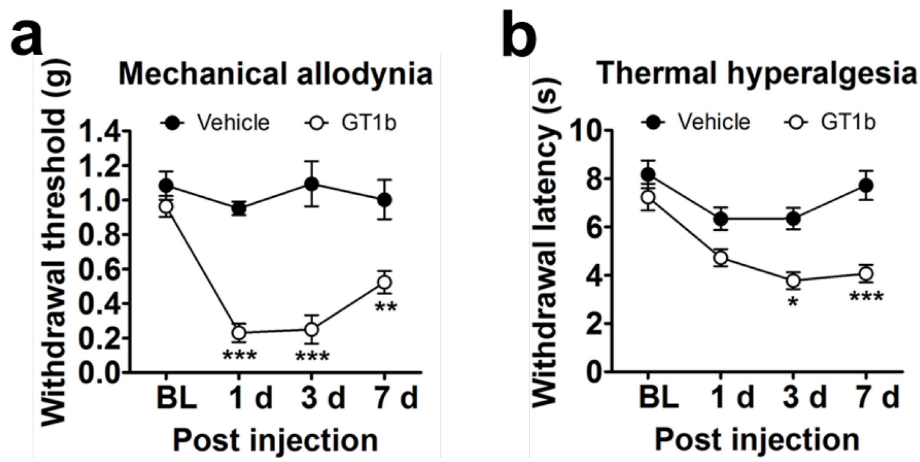

Fig. 31. Ganglioside GT1b induces pain hypersensitivity. Mechanical allodynia (a) and thermal hyperalgesia (b) were assessed after intrathecal injection of GT1b (25 μg/5 μl, $n = 6$) or vehicle ($n = 5$; one-way ANOVA, *$p < 0.05$; **$p < 0.01$; ***$p < 0.001$, vs. vehicle). Data are expressed as mean ± SEM.

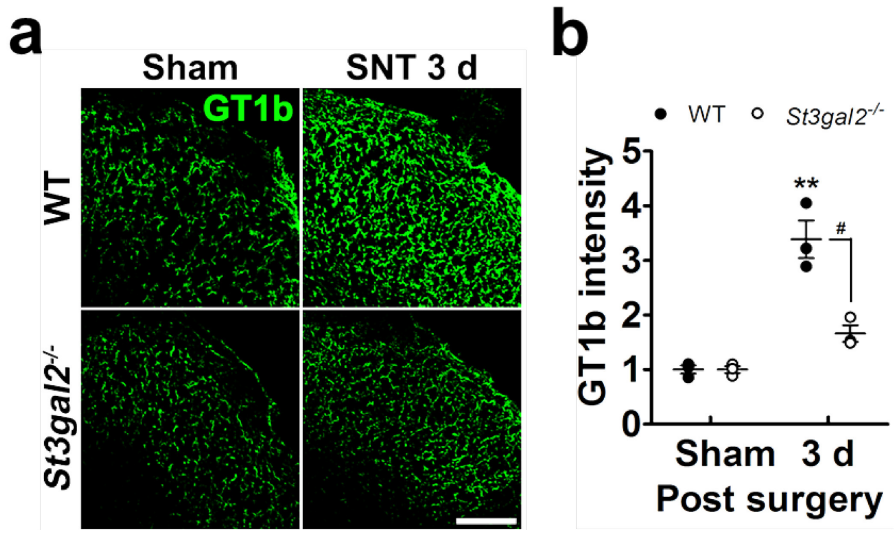

Fig. 32. Nerve injury-induced GT1b upregulation is attenuated in *St3gal2*$^{-/-}$ mice. (a) L4-5 spinal cord sections from WT (n = 3/group) and *St3gal2*$^{-/-}$ mice (n = 3/group) with or without L5 SNT at 3 dpi were immunostained with GT1b antibody and representative images are shown (scale bar, 100 μm). (b) The fluorescent intensity of GT1b-IR was measured and presented as the fold induction compared to the corresponding level of sham control (Student's t-test, $^{**}p < 0.01$, vs. sham control in WT, $^{\#}$, $p < 0.05$, vs. *St3gal2*$^{-/-}$ mice).

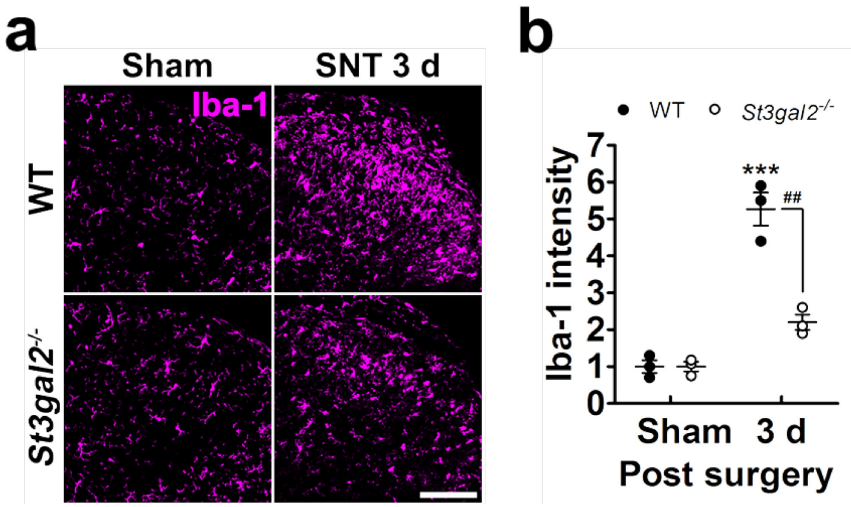

Fig. 33. Nerve injury-induced spinal cord microglia activation is reduced in *St3gal2*$^{-/-}$ mice. (a) L4-5 spinal cord sections from WT (n = 3/group) and *St3gal2*$^{-/-}$ mice (n = 3/group) with or without L5 SNT at 3 dpi were immunostained with Iba-1 antibody and representative images are shown (scale bar, 100 μm). (b) The fluorescent intensity of Iba-1-IR was measured and presented as the fold induction compared to the corresponding level of sham control (Student's t-test, ***$p < 0.001$, vs. sham control in WT, $^{\#\#}p < 0.01$, vs. *St3gal2*$^{-/-}$ mice).

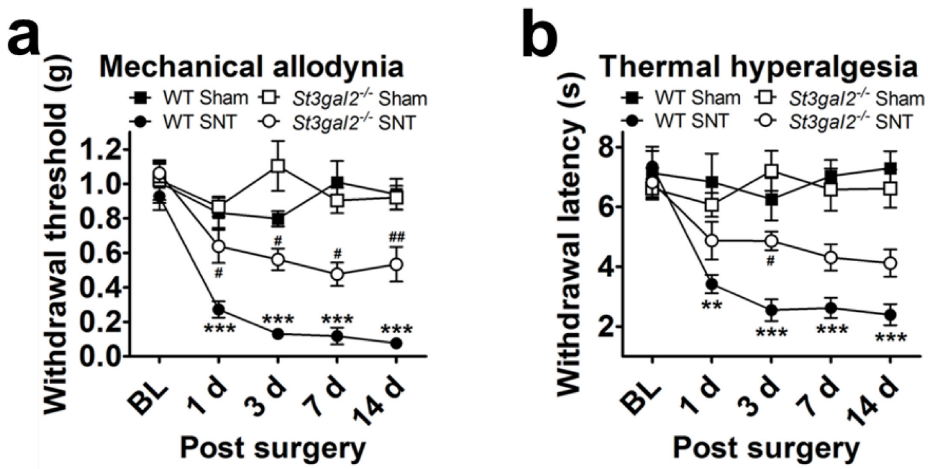

Fig. 34. Nerve injury-induced pain hypersensitivity is relieved in *St3gal2*$^{-/-}$ mice. Mechanical allodynia (a) and thermal hyperalgesia (b) were evaluated in sham-operated or L5 SNT-injured WT (sham, n = 5; SNT, n = 5) and *St3gal2*$^{-/-}$ (sham, n = 5; SNT, n = 5) mice (one-way ANOVA, **, p < 0.01; ***, p < 0.001, vs. sham control in WT, $^{\#}$, p < 0.05; $^{\#\#}$, p < 0.01, vs. nerve-injured WT in each time point).

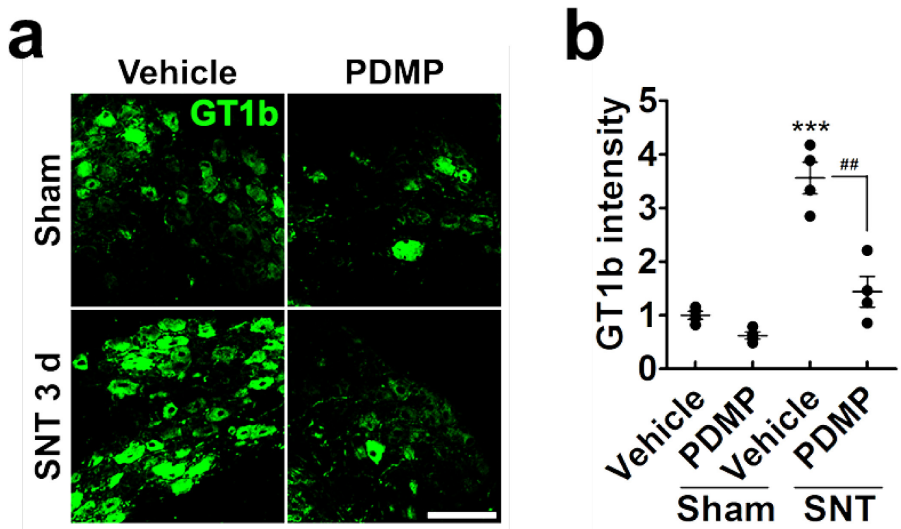

Fig. 35. Intrathecal PDMP injection inhibits nerve injury-induced ganglioside GT1b expression in DRG. PDMP (10 μg/5 μl) was intrathecally injected once daily for 7 days prior to L5 SNT. (a) L5 DRG sections of sham-operated or SNT-injured (3 dpi) WT mice were immunostained with GT1b antibody. Representative images are shown (n = 4/group; scale bar, 100 μm). The fluorescence intensity of GT1b-IR was measured and presented as the fold induction compared to that of the vehicle + sham control (Student's t-test, ***$p < 0.001$, vs. vehicle + sham group, $^{\#\#}p < 0.01$, vs. PDMP + SNT).

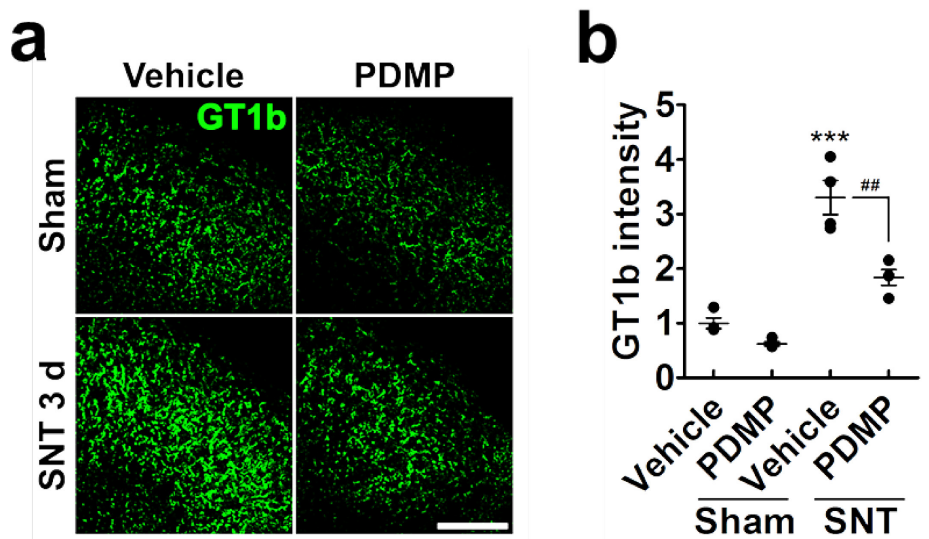

Fig. 36. Intrathecal PDMP injection inhibits nerve injury-induced ganglioside GT1b expression in afferent axon in spinal cord. PDMP (10 μg/5 μl) was intrathecally injected once daily for 7 days prior to L5 SNT. (a) L5 spinal cord tissue sections of sham-operated or SNT-injured (3 dpi) WT mice were immunostained with GT1b. Representative images are shown (n = 4/group; scale bar, 100 μm). (b) The fluorescence intensity of GT1b-IR was measured and presented as the fold induction compared to that of the vehicle + sham control (Student's t-test, ***$p < 0.001$, vs. vehicle + sham group, $^{\#\#}p < 0.01$, vs. PDMP + SNT).

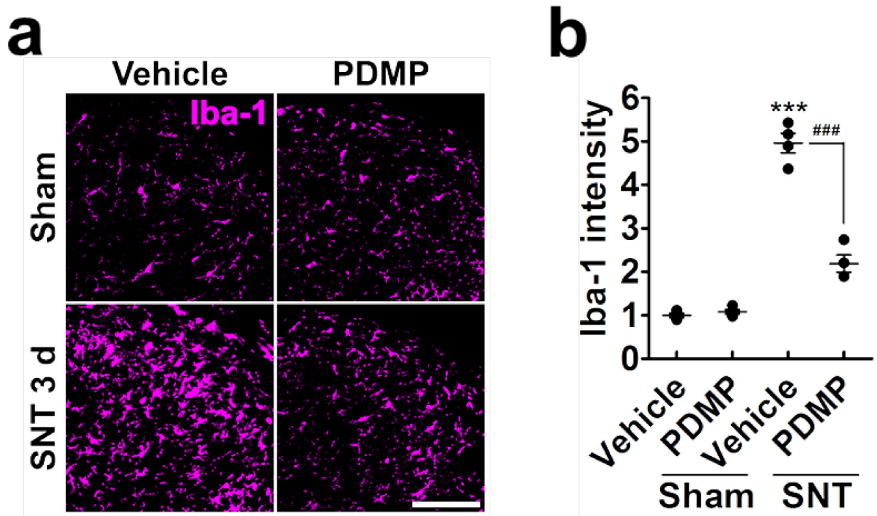

Fig. 37. Intrathecal PDMP injection inhibits nerve injury-induced spinal cord microglia activation. PDMP (10 μg/5 μl) was intrathecally injected once daily for 7 days prior to L5 SNT. L5 spinal cord tissue sections of sham-operated or SNT-injured (3 dpi) WT mice were immunostained with Iba-1 antibody. Representative images are shown (n = 4/group; scale bar, 100 μm). The fluorescence intensity of Iba-1-IR was measured and presented as the fold induction compared to that of the vehicle + sham control (Student's t-test, ***$p < 0.001$, vs. vehicle + sham group, $^{###}p < 0.001$, vs. PDMP + SNT).

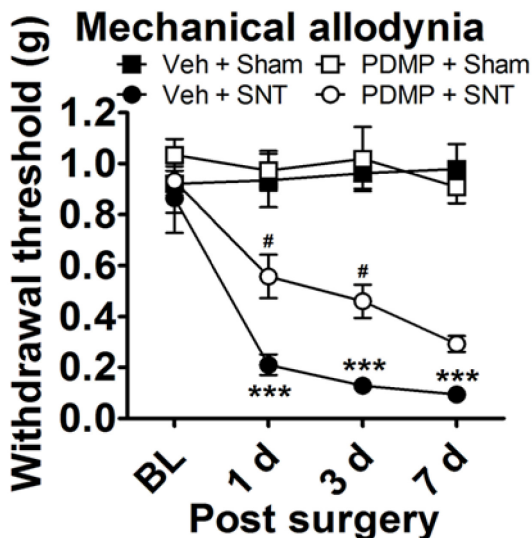

Fig. 38. Intrathecal PDMP injection attenuates nerve injury-induced pain hypersensitivity. Mechanical allodynia was assessed in sham-operated WT mice with or without PDMP injection (Veh + Sham, n = 5; PDMP + Sham, n = 5), and L5 SNT-injured WT mice with or without PDMP injection (Veh + SNT, n = 5; PDMP + SNT, n = 8; one-way ANOVA, ***p < 0.001, vs. Veh + sham group, $^{\#}p$ < 0.05, vs. Veh + SNT group at each time point). Data are presented as mean ± SEM.

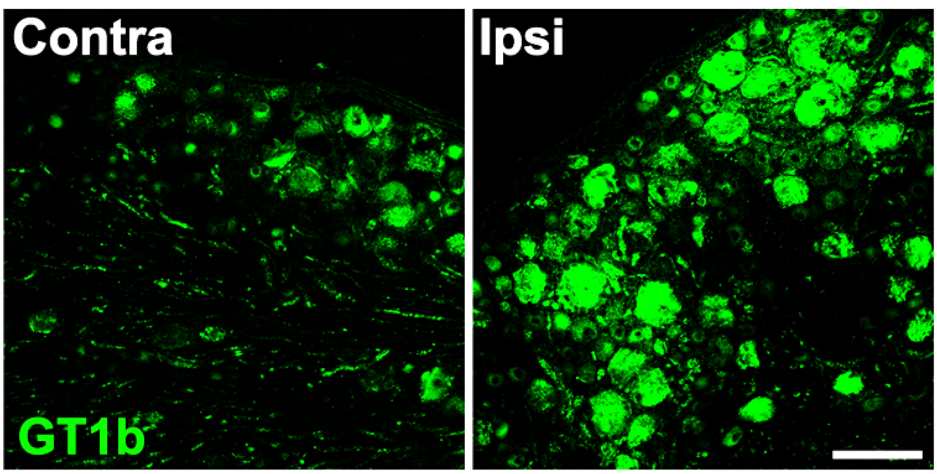

Fig. 39. Nerve injury induces ganglioside GT1b increase in rat DRG neuron. Rat L5 DRG sections with L5 SNL (3 dpi) were immunostained with GT1b antibody and representative images are shown (n = 3; scale bar, 100 μm).

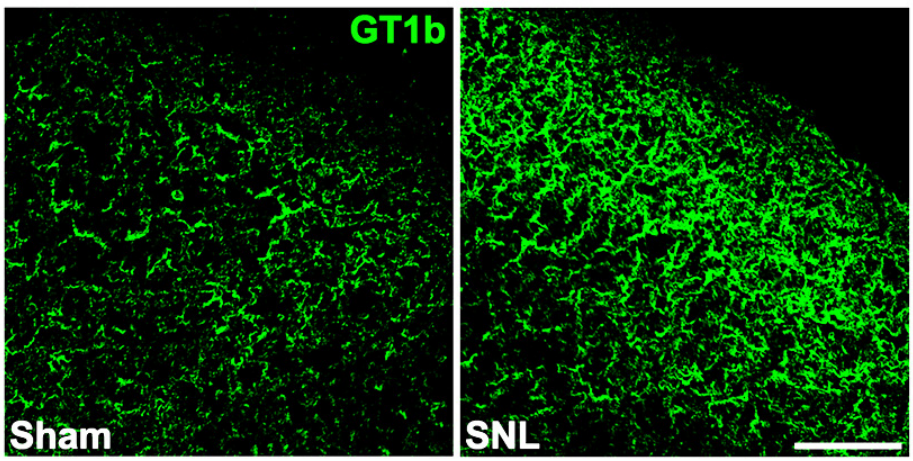

Fig. 40. Nerve injury induces ganglioside GT1b increase in afferent axon in spinal cord dorsal horn. L5 spinal cord sections of rats with L5 SNL (3 dpi) were immunostained with GT1b antibody and representative images are shown (n = 3; scale bar, 100 μm).

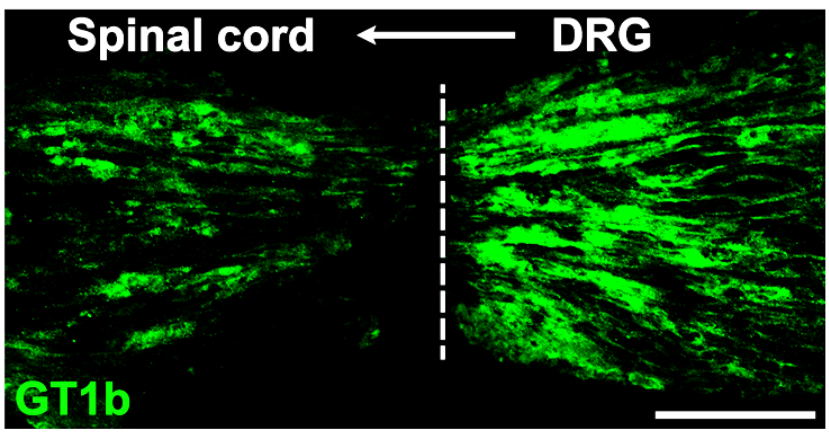

Fig. 41. Ganglioside GT1b is transported from DRG to spinal cord via afferent axon. Rat L5 dorsal root sections with concurrent rhizotomy and L5 SNL (3 dpi) were immunostained with GT1b antibody and representative images are shown (n = 3; scale bar, 100 μm). The dotted line denotes the transection site.

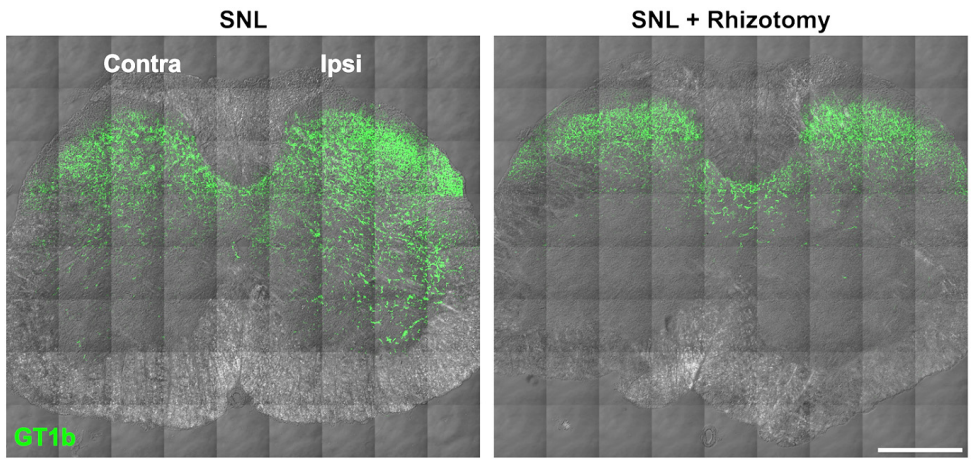

Fig. 42. Rhizotomy totally blocks GT1b upregulation in spinal cord due to nerve injury. L4-5 spinal cord sections from SNL-injured rats with or without rhizotomy (3 dpi) were immunostained with GT1b antibody. Representative images are shown (n = 3; scale bar, 500 μm).

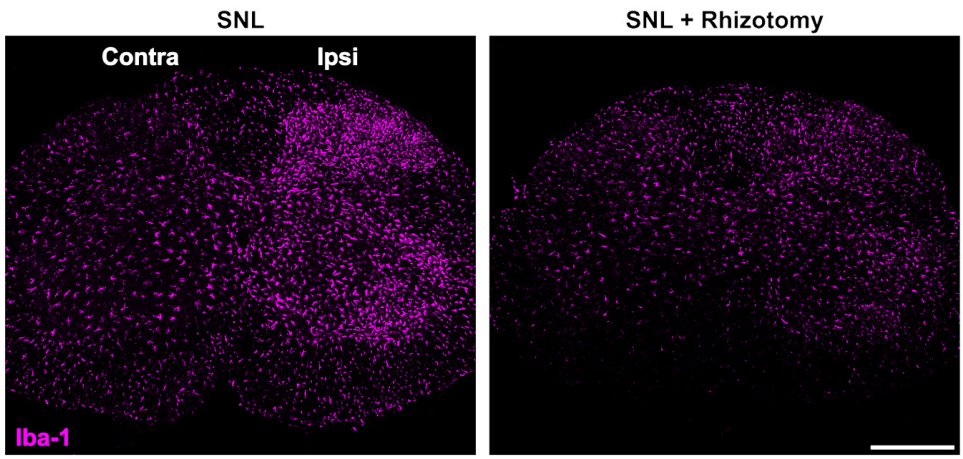

Fig. 43. Rhizotomy completely inhibits nerve injury-induced spinal cord microglia activation. L4-5 spinal cord sections from SNL-injured rats with or without rhizotomy (3 dpi) were immunostained with Iba-1 antibody. Representative images are shown (n = 3; scale bar, 500 μm).

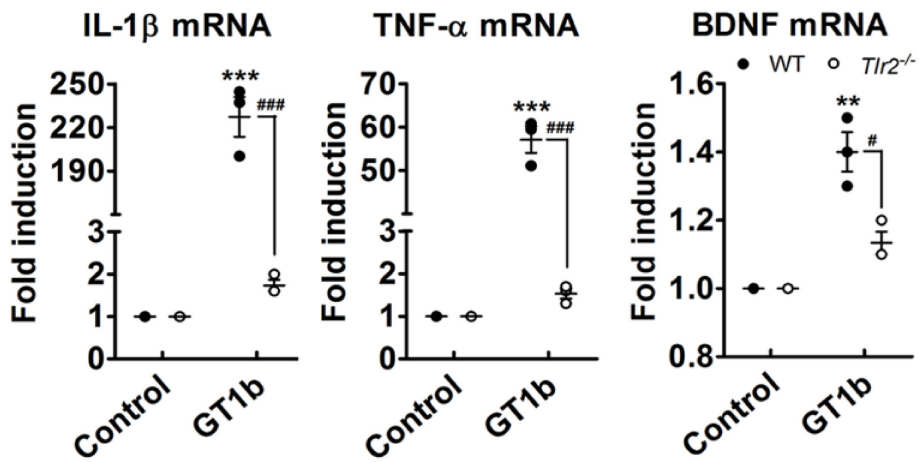

Fig. 44. Ganglioside GT1b induces pain-mediating gene expression in glial cells in a TLR2-dependent manner. Glial cells cultured from WT and *Tlr2*$^{-/-}$ mice were stimulated with 4.5 μM of GT1b for 3 h and IL-1β, TNF-α, and BDNF transcript level were measured by real-time RT-PCR (Student's *t*-test, $^{**}p < 0.01$; $^{***}p < 0.001$, vs. control in WT, $^{\#}p < 0.05$; $^{\#\#\#}p < 0.001$, vs. *Tlr2*$^{-/-}$ mice).

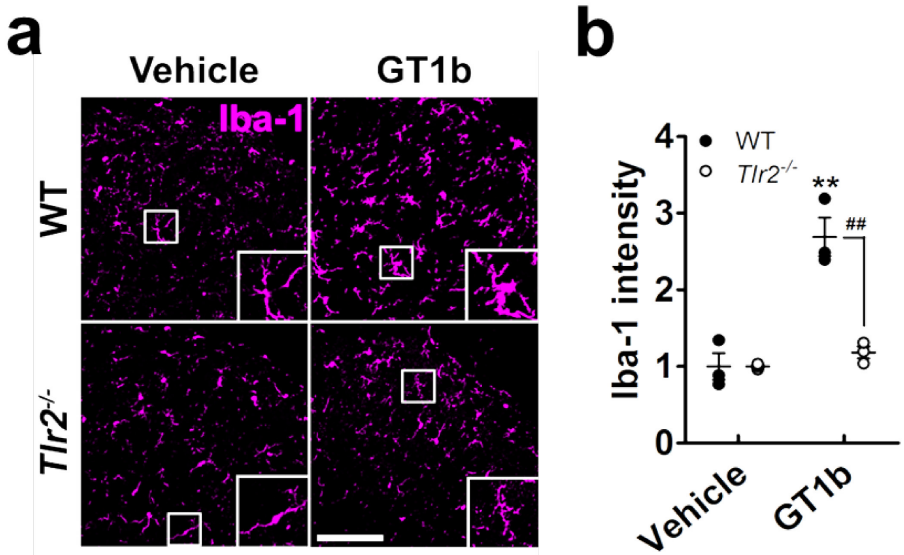

Fig. 45. Spinal cord microglia activation by GT1b injection is completely inhibited in *Tlr2*$^{-/-}$ mice. (a) L4-5 spinal cord sections prepared from WT (n = 3/group) and *Tlr2*$^{-/-}$ mice (n = 3/group) on 1 day after intrathecal injection of GT1b (25 μg/5 μl in saline) were immunostained with Iba-1 antibody and representative images are shown (scale bar, 100 μm). Vehicle-injected mice served as controls. (b) The fluorescent intensity of Iba-1-IR was measured and presented as fold induction compared to the corresponding control (Student's t-test, $^{**}p < 0.01$, vs. control in WT, $^{\#\#}p < 0.01$, vs. *Tlr2*$^{-/-}$ mice).

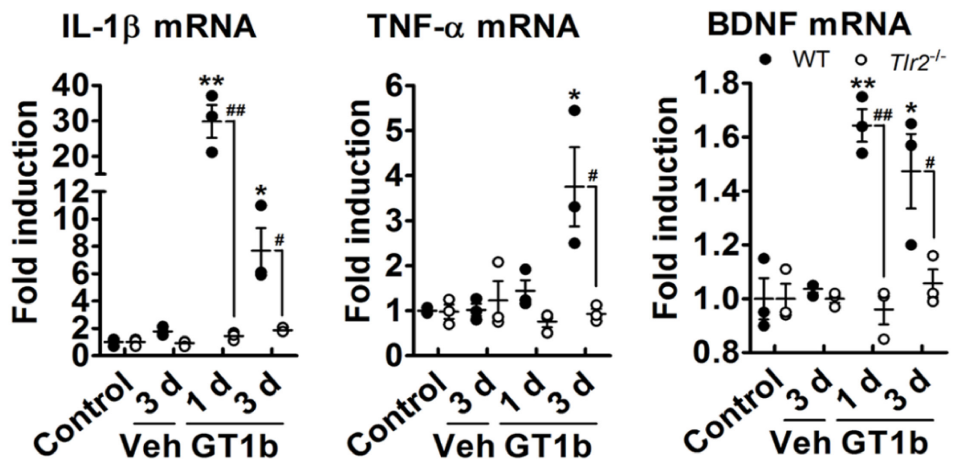

Fig. 46. Pain-mediating gene expression by GT1b injection is blocked in *Tlr2*$^{-/-}$ mice. IL-1β, TNF-α, and BDNF transcript level were measured by real-time RT-PCR in L4-5 spinal cord tissues of WT and *Tlr2*$^{-/-}$ mice after intrathecal injection of GT1b (25 μg/5 μl, n = 3/group) or vehicle (n = 3/group, Student's t-test, *$p < 0.05$; **$p < 0.01$, vs. control in WT, $^{\#}p < 0.05$; $^{\#\#}p < 0.01$, vs. in *Tlr2*$^{-/-}$ mice).

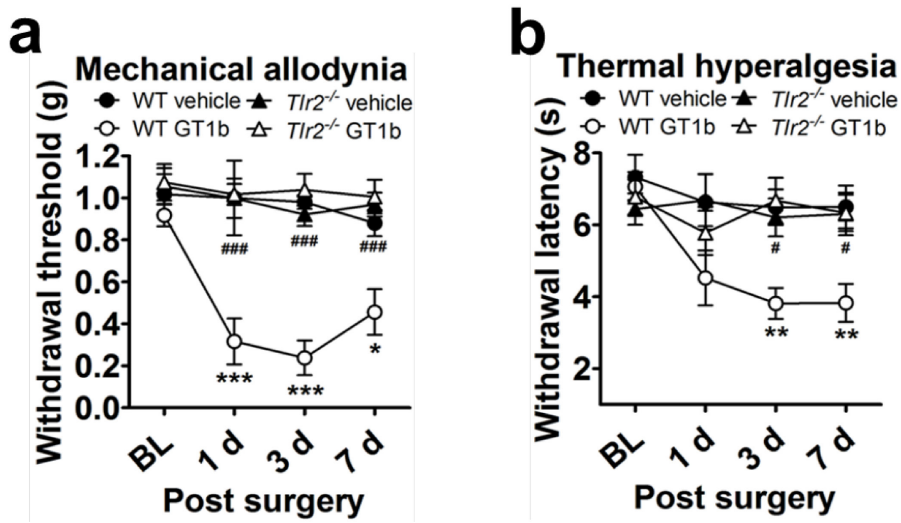

Fig. 47. GT1b injection fails to induce pain hypersensitivity in *Tlr2*$^{-/-}$ mice. Mechanical allodynia (a) and thermal hyperalgesia (b) were assessed in WT (vehicle, $n = 5$; GT1b, $n = 5$) and *Tlr2*$^{-/-}$ mice (vehicle, $n = 6$; GT1b, $n = 7$) after intrathecal injection of GT1b (25 μg/5 μl) or vehicle (one-way ANOVA, $^{*}p < 0.05$; $^{**}p < 0.01$; $^{***}p < 0.001$, vs. vehicle in WT, $^{\#}p < 0.05$; $^{\#\#\#}p < 0.001$, vs. WT GT1b group in each time point).

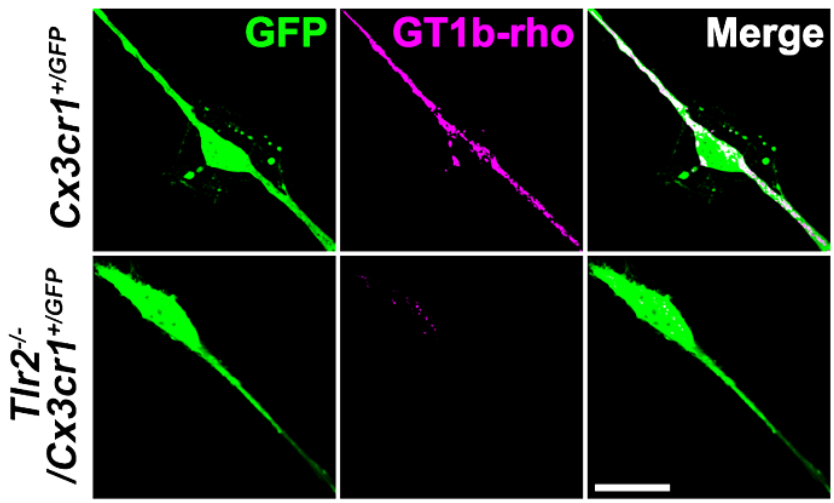

Fig. 48. GT1b-rhodamine directly binds to TLR2 on microglia. Primary microglia cultured from *Cx3cr1*$^{+/GFP}$ and *Tlr2*$^{-/-}$*/Cx3cr1*$^{+/GFP}$ mice were incubated with 5 μg/ml of GT1b-rhodamine and representative images are shown (scale bar, 20 μm).

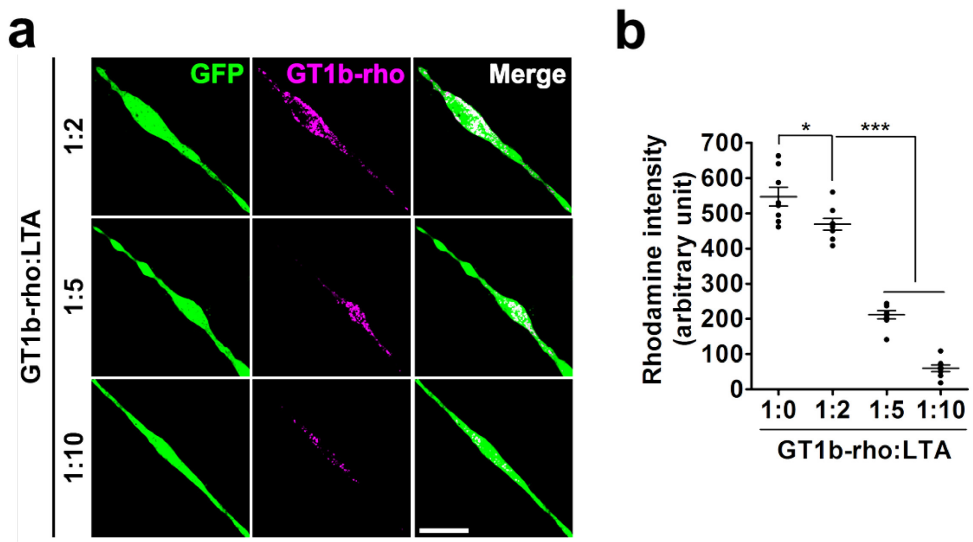

Fig. 49. LTA interrupts interaction between GT1b-rhodamine and TLR2 on microglia. (a) Primary microglia cultured from *Cx3cr1*$^{+/GFP}$ mice were incubated with 5 μg/ml of GT1b-rhodamine in the presence or absence of LTA and representative images are shown (scale bar, 20 μm). (b) The fluorescent intensity of GT1b-rhodamine was measured and presented as mean ± SEM (Student's *t*-test, *$p < 0.05$; ***$p < 0.001$).

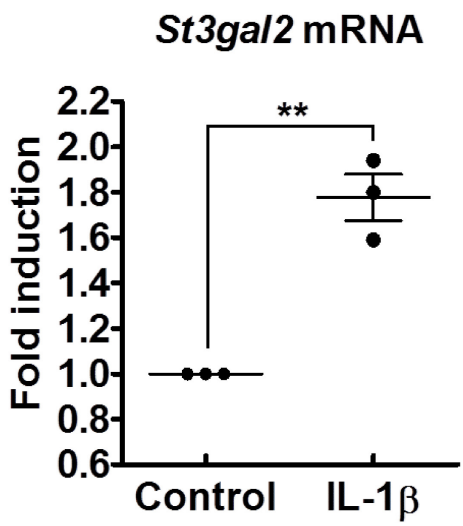

Fig. 50. IL-1β stimulation induces *St3gal2* mRNA expression in primary DRG neuron. Primary DRG neurons cultured from WT mice were stimulated with 10 ng/ml of recombinant IL-1β for 12 h and *St3gal2* transcript level were measured by real-time RT-PCR (Student's *t*-test, $^{**}p < 0.01$).

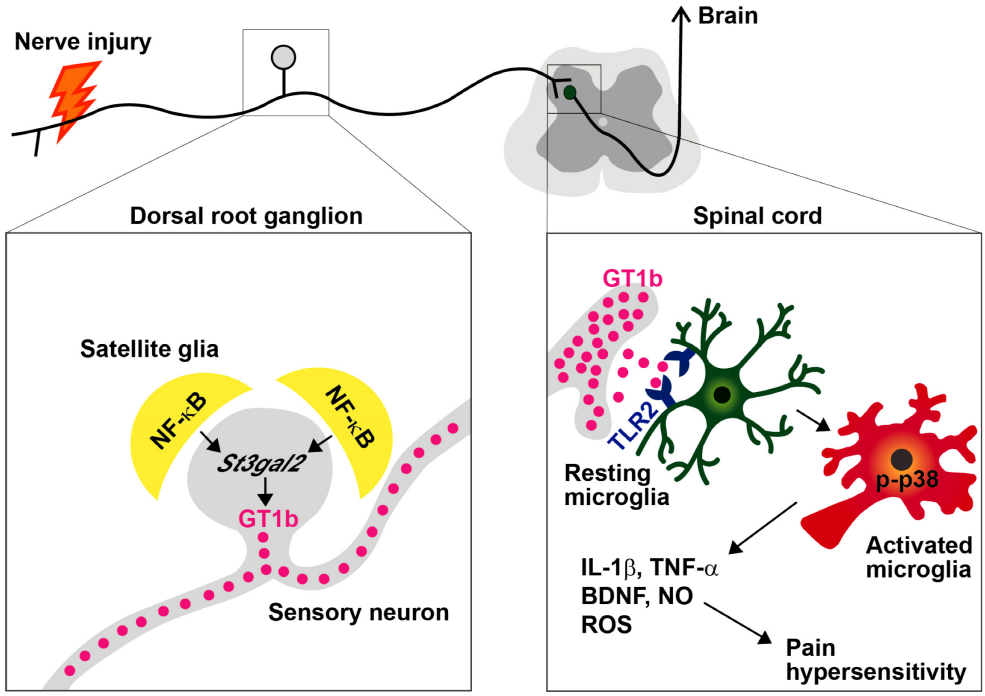

Fig. 51. SGC activation induces spinal cord microglia activation and pain central sensitization through GT1b-TLR2 signaling. Peripheral nerve injury induces IKK/NF-κB-dependent SGC activation in the DRG. Activated SGCs, in turn, induce *St3gal2* expression in sensory neurons and subsequent GT1b increase within 1 d of nerve injury. Then, GT1b is transported to the spinal cord, where it functions as an endogenous agonist of microglial TLR2, leading to pain-mediating gene expression and thereby contributing to pain central sensitization.

References

1. Abram, S.E. (2000). Neural blockade for neuropathic pain. Clin J Pain 16, S56-61.

2. Amir, R., Kocsis, J.D., and Devor, M. (2005). Multiple interacting sites of ectopic spike electrogenesis in primary sensory neurons. J Neurosci 25, 2576-2585.

3. Anderson, C.M., and Swanson, R.A. (2000). Astrocyte glutamate transport: review of properties, regulation, and physiological functions. Glia 32, 1-14.

4. Attal, N. (2012). Neuropathic pain: mechanisms, therapeutic approach, and interpretation of clinical trials. Continuum (Minneap Minn) 18, 161-175.

5. Beach, T.G., Woodhurst, W.B., MacDonald, D.B., and Jones, M.W. (1995). Reactive microglia in hippocampal sclerosis associated with human temporal lobe epilepsy. Neurosci Lett 191, 27-30.

6. Bethea, J.R., Castro, M., Keane, R.W., Lee, T.T., Dietrich, W.D., and Yezierski, R.P. (1998). Traumatic spinal cord injury induces nuclear factor-kappaB activation. J Neurosci 18, 3251-3260.

7. Biber, K., Tsuda, M., Tozaki-Saitoh, H., Tsukamoto, K., Toyomitsu, E., Masuda, T., Boddeke, H., and Inoue, K. (2011). Neuronal CCL21 up-regulates microglia P2X4 expression and initiates neuropathic pain development. EMBO J 30, 1864-1873.

8. Bohren, Y., Tessier, L.H., Megat, S., Petitjean, H., Hugel, S., Daniel, D., Kremer, M., Fournel, S., Hein, L., Schlichter, R., *et al.* (2013). Antidepressants suppress neuropathic pain by a peripheral beta2-adrenoceptor mediated anti-TNFalpha mechanism. Neurobiol Dis 60, 39-50.

9. Braun, P.E., Sandillon, F., Edwards, A., Matthieu, J.M., and Privat, A. (1988). Immunocytochemical localization by electron microscopy of 2'3'-cyclic nucleotide 3'-phosphodiesterase in developing oligodendrocytes of normal and mutant brain. J Neurosci 8, 3057-3066.

10. Burke, N.N., Geoghegan, E., Kerr, D.M., Moriarty, O., Finn, D.P., and Roche, M. (2013). Altered neuropathic pain behaviour in a rat model of depression is associated with changes in inflammatory gene expression in the amygdala. Genes Brain Behav 12, 705-713.

11. Campbell, J.N., and Meyer, R.A. (2006). Mechanisms of neuropathic pain. Neuron 52, 77-92.

12. Carlton, S.M., and Hargett, G.L. (2007). Colocalization of metabotropic glutamate receptors in rat dorsal root ganglion cells. J Comp Neurol 501, 780-789.

13. Chaplan, S.R., Bach, F.W., Pogrel, J.W., Chung, J.M., and Yaksh, T.L. (1994). Quantitative assessment of tactile allodynia in the rat paw. Journal of neuroscience methods 53, 55-63.

14. Cheng, C.F., Cheng, J.K., Chen, C.Y., Lien, C.C., Chu, D.C., Wang, S.Y.,

and Tsaur, M.L. (2014). Mirror-image pain is mediated by nerve growth factor produced from tumor necrosis factor alpha-activated satellite glia after peripheral nerve injury. Pain 155, 906-920.

15. Cook, S.P., Vulchanova, L., Hargreaves, K.M., Elde, R., and McCleskey, E.W. (1997). Distinct ATP receptors on pain-sensing and stretch-sensing neurons. Nature 387, 505-508.

16. Costigan, M., Scholz, J., and Woolf, C.J. (2009). Neuropathic pain: a maladaptive response of the nervous system to damage. Annu Rev Neurosci 32, 1-32.

17. Coull, J.A., Beggs, S., Boudreau, D., Boivin, D., Tsuda, M., Inoue, K., Gravel, C., Salter, M.W., and De Koninck, Y. (2005). BDNF from microglia causes the shift in neuronal anion gradient underlying neuropathic pain. Nature 438, 1017-1021.

18. Dubovy, P., Klusakova, I., Svizenska, I., and Brazda, V. (2010). Satellite glial cells express IL-6 and corresponding signal-transducing receptors in the dorsal root ganglia of rat neuropathic pain model. Neuron Glia Biol 6, 73-83.

19. Dworkin, R.H., O'Connor, A.B., Audette, J., Baron, R., Gourlay, G.K., Haanpaa, M.L., Kent, J.L., Krane, E.J., Lebel, A.A., Levy, R.M.*, et al.* (2010). Recommendations for the pharmacological management of neuropathic pain: an overview and literature update. Mayo Clin Proc 85, S3-14.

20. Eisen, M.B., Spellman, P.T., Brown, P.O., and Botstein, D. (1998). Cluster analysis and display of genome-wide expression patterns. Proc Natl Acad Sci U S A 95, 14863-14868.

21. Ellies, L.G., Sperandio, M., Underhill, G.H., Yousif, J., Smith, M., Priatel, J.J., Kansas, G.S., Ley, K., and Marth, J.D. (2002). Sialyltransferase specificity in selectin ligand formation. Blood 100, 3618-3625.

22. Foster, T.S. (2007). Efficacy and safety of alpha-lipoic acid supplementation in the treatment of symptomatic diabetic neuropathy. Diabetes Educator 33, 111-117.

23. Fu, E.S., Zhang, Y.P., Sagen, J., Candiotti, K.A., Morton, P.D., Liebl, D.J., Bethea, J.R., and Brambilla, R. (2010). Transgenic inhibition of glial NF-kappa B reduces pain behavior and inflammation after peripheral nerve injury. Pain 148, 509-518.

24. Ginhoux, F., Greter, M., Leboeuf, M., Nandi, S., See, P., Gokhan, S., Mehler, M.F., Conway, S.J., Ng, L.G., Stanley, E.R., *et al.* (2010). Fate Mapping Analysis Reveals That Adult Microglia Derive from Primitive Macrophages. Science 330, 841-845.

25. Gould, T.D. (2009). Mood and anxiety related phenotypes in mice : characterization using behavioral tests (New York, NY: Humana Press).

26. Grace, P.M., Hutchinson, M.R., Maier, S.F., and Watkins, L.R. (2014). Pathological pain and the neuroimmune interface. Nat Rev Immunol 14,

217-231.

27. Grotenhermen, F., and Muller-Vahl, K. (2012). The therapeutic potential of cannabis and cannabinoids. Dtsch Arztebl Int 109, 495-501.

28. Guan, Z., Kuhn, J.A., Wang, X., Colquitt, B., Solorzano, C., Vaman, S., Guan, A.K., Evans-Reinsch, Z., Braz, J., Devor, M.*, et al.* (2016). Injured sensory neuron-derived CSF1 induces microglial proliferation and DAP12-dependent pain. Nat Neurosci 19, 94-101.

29. Hanani, M. (2012). Intercellular communication in sensory ganglia by purinergic receptors and gap junctions: implications for chronic pain. Brain Res 1487, 183-191.

30. Harada, K., Kamiya, T., and Tsuboi, T. (2015). Gliotransmitter Release from Astrocytes: Functional, Developmental, and Pathological Implications in the Brain. Front Neurosci 9, 499.

31. Harden, R.N. (2005). Chronic neuropathic pain. Mechanisms, diagnosis, and treatment. Neurologist 11, 111-122.

32. Hargreaves, K., Dubner, R., Brown, F., Flores, C., and Joris, J. (1988). A new and sensitive method for measuring thermal nociception in cutaneous hyperalgesia. Pain 32, 77-88.

33. Haydon, P.G. (2001). GLIA: listening and talking to the synapse. Nat Rev Neurosci 2, 185-193.

34. Henkel, J.S., Beers, D.R., Zhao, W., and Appel, S.H. (2009). Microglia

in ALS: the good, the bad, and the resting. J Neuroimmune Pharmacol 4, 389-398.

35. Hu, P., and McLachlan, E.M. (2002). Macrophage and lymphocyte invasion of dorsal root ganglia after peripheral nerve lesions in the rat. Neuroscience 112, 23-38.

36. Huang, T.Y., Belzer, V., and Hanani, M. (2010). Gap junctions in dorsal root ganglia: possible contribution to visceral pain. Eur J Pain 14, 49 e41-11.

37. Humbertson, A., Jr., Zimmermann, E., and Leedy, M. (1969). A chronological study of mitotic activity in satellite cell hyperplasia associated with chromatolytic neurons. Z Zellforsch Mikrosk Anat 100, 507-515.

38. Hunt, J.L., Winkelstein, B.A., Rutkowski, M.D., Weinstein, J.N., and DeLeo, J.A. (2001). Repeated injury to the lumbar nerve roots produces enhanced mechanical allodynia and persistent spinal neuroinflammation. Spine (Phila Pa 1976) 26, 2073-2079.

39. Hylden, J.L., and Wilcox, G.L. (1980). Intrathecal morphine in mice: a new technique. Eur J Pharmacol 67, 313-316.

40. Imai, Y., Ibata, I., Ito, D., Ohsawa, K., and Kohsaka, S. (1996). A novel gene iba1 in the major histocompatibility complex class III region encoding an EF hand protein expressed in a monocytic lineage. Biochem Biophys Res Commun 224, 855-862.

41. Inoue, A., Ikoma, K., Morioka, N., Kumagai, K., Hashimoto, T., Hide, I.,

and Nakata, Y. (1999). Interleukin-1beta induces substance P release from primary afferent neurons through the cyclooxygenase-2 system. J Neurochem 73, 2206-2213.

42. Jana, M., Palencia, C.A., and Pahan, K. (2008). Fibrillar amyloid-beta peptides activate microglia via TLR2: implications for Alzheimer's disease. J Immunol 181, 7254-7262.

43. Jasmin, L., Vit, J.P., Bhargava, A., and Ohara, P.T. (2010). Can satellite glial cells be therapeutic targets for pain control? Neuron Glia Biol 6, 63-71.

44. Jefferies, K. (2010). Treatment of neuropathic pain. Semin Neurol 30, 425-432.

45. Jensen, T.S., and Finnerup, N.B. (2014). Allodynia and hyperalgesia in neuropathic pain: clinical manifestations and mechanisms. Lancet Neurol 13, 924-935.

46. Ji, R.R., Kawasaki, Y., Zhuang, Z.Y., Wen, Y.R., and Decosterd, I. (2006). Possible role of spinal astrocytes in maintaining chronic pain sensitization: review of current evidence with focus on bFGF/JNK pathway. Neuron Glia Biol 2, 259-269.

47. Ji, R.R., and Suter, M.R. (2007). p38 MAPK, microglial signaling, and neuropathic pain. Mol Pain 3, 33.

48. Kawasaki, Y., Zhang, L., Cheng, J.K., and Ji, R.R. (2008). Cytokine mechanisms of central sensitization: distinct and overlapping role of

interleukin-1beta, interleukin-6, and tumor necrosis factor-alpha in regulating synaptic and neuronal activity in the superficial spinal cord. J Neurosci 28, 5189-5194.

49. Kidd, B.L., and Urban, L.A. (2001). Mechanisms of inflammatory pain. Br J Anaesth 87, 3-11.

50. Kigerl, K.A., Lai, W., Rivest, S., Hart, R.P., Satoskar, A.R., and Popovich, P.G. (2007). Toll-like receptor (TLR)-2 and TLR-4 regulate inflammation, gliosis, and myelin sparing after spinal cord injury. J Neurochem 102, 37-50.

51. Kim, C., Ho, D.H., Suk, J.E., You, S., Michael, S., Kang, J., Joong Lee, S., Masliah, E., Hwang, D., Lee, H.J., and Lee, S.J. (2013). Neuron-released oligomeric alpha-synuclein is an endogenous agonist of TLR2 for paracrine activation of microglia. Nat Commun 4, 1562.

52. Kim, D., Kim, M.A., Cho, I.H., Kim, M.S., Lee, S., Jo, E.K., Choi, S.Y., Park, K., Kim, J.S., Akira, S.*, et al.* (2007). A critical role of toll-like receptor 2 in nerve injury-induced spinal cord glial cell activation and pain hypersensitivity. J Biol Chem 282, 14975-14983.

53. Kim, D., You, B., Jo, E.K., Han, S.K., Simon, M.I., and Lee, S.J. (2010). NADPH oxidase 2-derived reactive oxygen species in spinal cord microglia contribute to peripheral nerve injury-induced neuropathic pain. Proc Natl Acad Sci U S A 107, 14851-14856.

54. Kim, D., You, B., Lim, H., and Lee, S.J. (2011a). Toll-like receptor 2 contributes to chemokine gene expression and macrophage infiltration in the dorsal root ganglia after peripheral nerve injury. Mol Pain 7, 74.

55. Kim, S.H., and Chung, J.M. (1992). An experimental model for peripheral neuropathy produced by segmental spinal nerve ligation in the rat. Pain 50, 355-363.

56. Kim, S.J., Park, G.H., Kim, D., Lee, J., Min, H., Wall, E., Lee, C.J., Simon, M.I., Lee, S.J., and Han, S.K. (2011b). Analysis of cellular and behavioral responses to imiquimod reveals a unique itch pathway in transient receptor potential vanilloid 1 (TRPV1)-expressing neurons. Proc Natl Acad Sci U S A 108, 3371-3376.

57. Kirschning, C.J., and Schumann, R.R. (2002). TLR2: cellular sensor for microbial and endogenous molecular patterns. Curr Top Microbiol Immunol 270, 121-144.

58. Kommers, T., Vinade, L., Pereira, C., Goncalves, C.A., Wofchuk, S., and Rodnight, R. (1998). Regulation of the phosphorylation of glial fibrillary acidic protein (GFAP) by glutamate and calcium ions in slices of immature rat spinal cord: comparison with immature hippocampus. Neurosci Lett 248, 141-143.

59. Kumar, K., Toth, C., and Nath, R.K. (1996). Spinal cord stimulation for chronic pain in peripheral neuropathy. Surg Neurol 46, 363-369.

60. Lappe-Siefke, C., Goebbels, S., Gravel, M., Nicksch, E., Lee, J., Braun, P.E., Griffiths, I.R., and Nave, K.A. (2003). Disruption of Cnp1 uncouples oligodendroglial functions in axonal support and myelination. Nat Genet 33, 366-374.

61. Ledeboer, A., Sloane, E.M., Milligan, E.D., Frank, M.G., Mahony, J.H., Maier, S.F., and Watkins, L.R. (2005). Minocycline attenuates mechanical allodynia and proinflammatory cytokine expression in rat models of pain facilitation. Pain 115, 71-83.

62. Lee, M., McGeer, E.G., and McGeer, P.L. (2011). Mechanisms of GABA release from human astrocytes. Glia 59, 1600-1611.

63. Lefevre, Y., Amadioa, A., Vincent, P., Descheemaeker, A., Oliet, S.H.R., Dallel, R., and Voisin, D.L. (2015). Neuropathic pain depends upon D-serine co-activation of spinal NMDA receptors in rats. Neuroscience Letters 603, 42-47.

64. Lewin, G.R., and Moshourab, R. (2004). Mechanosensation and pain. J Neurobiol 61, 30-44.

65. Li, Z.W., Omori, S.A., Labuda, T., Karin, M., and Rickert, R.C. (2003). IKK beta is required for peripheral B cell survival and proliferation. J Immunol 170, 4630-4637.

66. Lim, H., Kim, D., and Lee, S.J. (2013). Toll-like receptor 2 mediates peripheral nerve injury-induced NADPH oxidase 2 expression in spinal cord

microglia. J Biol Chem 288, 7572-7579.

67. Liu, F.Y., Sun, Y.N., Wang, F.T., Li, Q., Su, L., Zhao, Z.F., Meng, X.L., Zhao, H., Wu, X., Sun, Q.*, et al.* (2012). Activation of satellite glial cells in lumbar dorsal root ganglia contributes to neuropathic pain after spinal nerve ligation. Brain Res 1427, 65-77.

68. Livak, K.J., and Schmittgen, T.D. (2001). Analysis of relative gene expression data using real-time quantitative PCR and the 2(-Delta Delta C(T)) Method. Methods 25, 402-408.

69. Lu, V.B., Biggs, J.E., Stebbing, M.J., Balasubramanyan, S., Todd, K.G., Lai, A.Y., Colmers, W.F., Dawbarn, D., Ballanyi, K., and Smith, P.A. (2009). Brain-derived neurotrophic factor drives the changes in excitatory synaptic transmission in the rat superficial dorsal horn that follow sciatic nerve injury. J Physiol 587, 1013-1032.

70. Luo, J.G., Zhao, X.L., Xu, W.C., Zhao, X.J., Wang, J.N., Lin, X.W., Sun, T., and Fu, Z.J. (2014). Activation of spinal NF-kappaB/p65 contributes to peripheral inflammation and hyperalgesia in rat adjuvant-induced arthritis. Arthritis Rheumatol 66, 896-906.

71. Ma, W., and Quirion, R. (2006a). Increased calcitonin gene-related peptide in neuroma and invading macrophages is involved in the up-regulation of interleukin-6 and thermal. hyperalgesia in a rat model of mononeuropathy. J Neurochem 98, 180-192.

72. Ma, W., and Quirion, R. (2006b). Targeting invading macrophage-derived PGE2, IL-6 and calcitonin gene-related peptide in injured nerve to treat neuropathic pain. Expert Opin Ther Targets 10, 533-546.

73. Maeda, T., Kiguchi, N., Kobayashi, Y., Ikuta, T., Ozaki, M., and Kishioka, S. (2009). Leptin derived from adipocytes in injured peripheral nerves facilitates development of neuropathic pain via macrophage stimulation. Proc Natl Acad Sci U S A 106, 13076-13081.

74. Malarkey, E.B., and Parpura, V. (2008). Mechanisms of glutamate release from astrocytes. Neurochem Int 52, 142-154.

75. Marchand, F., Perretti, M., and McMahon, S.B. (2005). Role of the immune system in chronic pain. Nat Rev Neurosci 6, 521-532.

76. Masuda, T., Iwamoto, S., Yoshinaga, R., Tozaki-Saitoh, H., Nishiyama, A., Mak, T.W., Tamura, T., Tsuda, M., and Inoue, K. (2014). Transcription factor IRF5 drives P2X4R+-reactive microglia gating neuropathic pain. Nat Commun 5, 3771.

77. Masuda, T., Ozono, Y., Mikuriya, S., Kohro, Y., Tozaki-Saitoh, H., Iwatsuki, K., Uneyama, H., Ichikawa, R., Salter, M.W., Tsuda, M., and Inoue, K. (2016). Dorsal horn neurons release extracellular ATP in a VNUT-dependent manner that underlies neuropathic pain. Nat Commun 7, 12529.

78. Masuda, T., Tsuda, M., Yoshinaga, R., Tozaki-Saitoh, H., Ozato, K., Tamura, T., and Inoue, K. (2012). IRF8 is a critical transcription factor for

transforming microglia into a reactive phenotype. Cell Rep 1, 334-340.

79. Milligan, E.D., and Watkins, L.R. (2009). Pathological and protective roles of glia in chronic pain. Nat Rev Neurosci 10, 23-36.

80. Miyagi, M., Ohtori, S., Ishikawa, T., Aoki, Y., Ozawa, T., Doya, H., Saito, T., Moriya, H., and Takahashi, K. (2006). Up-regulation of TNFalpha in DRG satellite cells following lumbar facet joint injury in rats. Eur Spine J 15, 953-958.

81. Moore, R.A., Wiffen, P.J., Derry, S., Toelle, T., and Rice, A.S. (2014). Gabapentin for chronic neuropathic pain and fibromyalgia in adults. Cochrane Database Syst Rev, CD007938.

82. Nimmerjahn, A., Kirchhoff, F., and Helmchen, F. (2005). Resting microglial cells are highly dynamic surveillants of brain parenchyma in vivo. Science 308, 1314-1318.

83. Numazaki, M., and Tominaga, M. (2004). Nociception and TRP Channels. Curr Drug Targets CNS Neurol Disord 3, 479-485.

84. O'Neill, L.A., and Kaltschmidt, C. (1997). NF-kappa B: a crucial transcription factor for glial and neuronal cell function. Trends Neurosci 20, 252-258.

85. Omenn, G.S. (1987). Pain and Disability - Clinical, Behavioral, and Public-Policy Perspectives - Osterweis,M, Kleinman,a, Mechanic,D. Issues Sci Technol 4, 99-100.

86. Palma, C., Minghetti, L., Astolfi, M., Ambrosini, E., Silberstein, F.C., Manzini, S., Levi, 86. G., and Aloisi, F. (1997). Functional characterization of substance P receptors on cultured human spinal cord astrocytes: synergism of substance P with cytokines in inducing interleukin-6 and prostaglandin E2 production. Glia 21, 183-193.

87. Park, J.S., Svetkauskaite, D., He, Q., Kim, J.Y., Strassheim, D., Ishizaka, A., and Abraham, E. (2004). Involvement of toll-like receptors 2 and 4 in cellular activation by high mobility group box 1 protein. J Biol Chem 279, 7370-7377.

88. Pavic, R., Pavic, M.L., Tvrdeic, A., Tot, O.K., and Heffer, M. (2011). Rat sciatic nerve crush injury and recovery tracked by plantar test and immunohistochemistry analysis. Coll Antropol 35 Suppl 1, 93-100.

89. Perea, G., Navarrete, M., and Araque, A. (2009). Tripartite synapses: astrocytes process and control synaptic information. Trends Neurosci 32, 421-431.

90. Raghavendra, V., Tanga, F., and DeLeo, J.A. (2003). Inhibition of microglial activation attenuates the development but not existing hypersensitivity in a rat model of neuropathy. J Pharmacol Exp Ther 306, 624-630.

91. Ramabadran, K., Bansinath, M., Turndorf, H., and Puig, M.M. (1989). Tail immersion test for the evaluation of a nociceptive reaction in mice.

Methodological considerations. Journal of pharmacological methods 21, 21-31.

92. Ranoux, D., Attal, N., Morain, F., and Bouhassira, D. (2008). Botulinum toxin type A induces direct analgesic effects in chronic neuropathic pain. Ann Neurol 64, 274-283.

93. Ro, L.S., Chen, S.T., Tang, L.M., and Jacobs, J.M. (1999). Effect of NGF and anti-NGF on neuropathic pain in rats following chronic constriction injury of the sciatic nerve. Pain 79, 265-274.

94. Rohlmann, A., Laskawi, R., Hofer, A., Dobo, E., Dermietzel, R., and Wolff, J.R. (1993). Facial nerve lesions lead to increased immunostaining of the astrocytic gap junction protein (connexin 43) in the corresponding facial nucleus of rats. Neurosci Lett 154, 206-208.

95. Rutkowski, M.D., Pahl, J.L., Sweitzer, S., van Rooijen, N., and DeLeo, J.A. (2000). Limited role of macrophages in generation of nerve injury-induced mechanical allodynia. Physiol Behav 71, 225-235.

96. Schafers, M., Brinkhoff, J., Neukirchen, S., Marziniak, M., and Sommer, C. (2001). Combined epineurial therapy with neutralizing antibodies to tumor necrosis factor-alpha and interleukin-1 receptor has an additive effect in reducing neuropathic pain in mice. Neurosci Lett 310, 113-116.

97. Scholz, J., and Woolf, C.J. (2007). The neuropathic pain triad: neurons, immune cells and glia. Nat Neurosci 10, 1361-1368.

98. Sheikh, K.A., Sun, J., Liu, Y., Kawai, H., Crawford, T.O., Proia, R.L., Griffin, J.W., and Schnaar, R.L. (1999). Mice lacking complex gangliosides develop Wallerian degeneration and myelination defects. Proc Natl Acad Sci U S A 96, 7532-7537.

99. Shi, M., Qi, W.J., Gao, G., Wang, J.Y., and Luo, F. (2010). Increased thermal and mechanical nociceptive thresholds in rats with depressive-like behaviors. Brain Res 1353, 225-233.

100. Slattery, D.A., and Cryan, J.F. (2012). Using the rat forced swim test to assess antidepressant-like activity in rodents. Nature Protocols 7, 1009-1014.

101. Smith, H.S. (2012). Opioids and neuropathic pain. Pain Physician 15, ES93-110.

102. Sorkin, L.S., Xiao, W.H., Wagner, R., and Myers, R.R. (1997). Tumour necrosis factor-alpha induces ectopic activity in nociceptive primary afferent fibres. Neuroscience 81, 255-262.

103. Spataro, L.E., Sloane, E.M., Milligan, E.D., Wieseler-Frank, J., Schoeniger, D., Jekich, B.M., Barrientos, R.M., Maier, S.F., and Watkins, L.R. (2004). Spinal gap junctions: potential involvement in pain facilitation. J Pain 5, 392-405.

104. Stephenson, J.L., and Byers, M.R. (1995). GFAP immunoreactivity in trigeminal ganglion satellite cells after tooth injury in rats. Exp Neurol 131, 11-22.

105. Sturgill, E.R., Aoki, K., Lopez, P.H., Colacurcio, D., Vajn, K., Lorenzini, I., Majic, S., Yang, W.H., Heffer, M., Tiemeyer, M.*, et al.* (2012). Biosynthesis of the major brain gangliosides GD1a and GT1b. Glycobiology 22, 1289-1301.

106. Sung, B., Lim, G., and Mao, J. (2003). Altered expression and uptake activity of spinal glutamate transporters after nerve injury contribute to the pathogenesis of neuropathic pain in rats. J Neurosci 23, 2899-2910.

107. Takamizawa, K., Iwamori, M., Mutai, M., and Nagai, Y. (1986). Gangliosides of bovine buttermilk. Isolation and characterization of a novel monosialoganglioside with a new branching structure. J Biol Chem 261, 5625-5630.

108. Takeda, M., Takahashi, M., Nasu, M., and Matsumoto, S. (2011). Peripheral inflammation suppresses inward rectifying potassium currents of satellite glial cells in the trigeminal ganglia. Pain 152, 2147-2156.

109. Takeuchi, O., Hoshino, K., Kawai, T., Sanjo, H., Takada, H., Ogawa, T., Takeda, K., and Akira, S. (1999). Differential roles of TLR2 and TLR4 in recognition of gram-negative and gram-positive bacterial cell wall components. Immunity 11, 443-451.

110. Tang, S.C., Arumugam, T.V., Xu, X., Cheng, A., Mughal, M.R., Jo, D.G., Lathia, J.D., Siler, D.A., Chigurupati, S., Ouyang, X.*, et al.* (2007). Pivotal role for neuronal Toll-like receptors in ischemic brain injury and

functional deficits. Proc Natl Acad Sci U S A 104, 13798-13803.

111. Tanga, F.Y., Nutile-McMenemy, N., and DeLeo, J.A. (2005). The CNS role of Toll-like receptor 4 in innate neuroimmunity and painful neuropathy. Proc Natl Acad Sci U S A 102, 5856-5861.

112. Tettamanti, G., Bonali, F., Marchesini, S., and Zambotti, V. (1973). A new procedure for the extraction, purification and fractionation of brain gangliosides. Biochim Biophys Acta 296, 160-170.

113. Todd, A.J. (2010). Neuronal circuitry for pain processing in the dorsal horn. Nat Rev Neurosci 11, 823-836.

114. Toma, J.S., McPhail, L.T., and Ramer, M.S. (2007). Differential RIP antigen (CNPase) expression in peripheral ensheathing glia. Brain Research 1137, 1-10.

115. Torsney, C., and MacDermott, A.B. (2006). Disinhibition opens the gate to pathological pain signaling in superficial neurokinin 1 receptor-expressing neurons in rat spinal cord. J Neurosci 26, 1833-1843.

116. Trang, T., Beggs, S., and Salter, M.W. (2011). Brain-derived neurotrophic factor from microglia: a molecular substrate for neuropathic pain. Neuron Glia Biol 7, 99-108.

117. Trbojevic-Cepe, M., Kracun, I., Jusic, A., and Pavlicek, I. (1991). Gangliosides of human cerebrospinal fluid in various neurologic diseases. J Neurol Sci 105, 192-199.

118. Tsuda, M., Shigemoto-Mogami, Y., Koizumi, S., Mizokoshi, A., Kohsaka, S., Salter, M.W., and Inoue, K. (2003). P2X4 receptors induced in spinal microglia gate tactile allodynia after nerve injury. Nature 424, 778-783.

119. Ulmann, L., Hatcher, J.P., Hughes, J.P., Chaumont, S., Green, P.J., Conquet, F., Buell, G.N., Reeve, A.J., Chessell, I.P., and Rassendren, F. (2008). Up-regulation of P2X4 receptors in spinal microglia after peripheral nerve injury mediates BDNF release and neuropathic pain. J Neurosci 28, 11263-11268.

120. Van Rooijen, N., and Sanders, A. (1994). Liposome mediated depletion of macrophages: mechanism of action, preparation of liposomes and applications. Journal of immunological methods 174, 83-93.

121. Vega-Avelaira, D., Geranton, S.M., and Fitzgerald, M. (2009). Differential regulation of immune responses and macrophage/neuron interactions in the dorsal root ganglion in young and adult rats following nerve injury. Mol Pain 5, 70.

122. Vit, J.P., Ohara, P.T., Bhargava, A., Kelley, K., and Jasmin, L. (2008). Silencing the Kir4.1 potassium channel subunit in satellite glial cells of the rat trigeminal ganglion results in pain-like behavior in the absence of nerve injury. J Neurosci 28, 4161-4171.

123. Vunnam, R.R., and Radin, N.S. (1980). Analogs of Ceramide That

Inhibit Glucocerebroside Synthetase in Mouse-Brain. Chemistry and Physics of Lipids 26, 265-278.

124. Walf, A.A., and Frye, C.A. (2007). The use of the elevated plus maze as an assay of anxiety-related behavior in rodents. Nature Protocols 2, 322-328.

125. Watkins, L.R., Milligan, E.D., and Maier, S.F. (2001). Glial activation: a driving force for pathological pain. Trends Neurosci 24, 450-455.

126. Wei, X.H., Na, X.D., Liao, G.J., Chen, Q.Y., Cui, Y., Chen, F.Y., Li, Y.Y., Zang, Y., and Liu, X.G. (2013). The up-regulation of IL-6 in DRG and spinal dorsal horn contributes to neuropathic pain following L5 ventral root transection. Exp Neurol 241, 159-168.

127. Woodham, P., Anderson, P.N., Nadim, W., and Turmaine, M. (1989). Satellite cells surrounding axotomised rat dorsal root ganglion cells increase expression of a GFAP-like protein. Neurosci Lett 98, 8-12.

128. Woolf, C.J., and Mannion, R.J. (1999). Neuropathic pain: aetiology, symptoms, mechanisms, and management. Lancet 353, 1959-1964.

129. Yang, L.J., Zeller, C.B., Shaper, N.L., Kiso, M., Hasegawa, A., Shapiro, R.E., and Schnaar, R.L. (1996). Gangliosides are neuronal ligands for myelin-associated glycoprotein. Proc Natl Acad Sci U S A 93, 814-818.

130. Yin, Q., Fan, Q., Zhao, Y., Cheng, M.Y., Liu, H., Li, J., Lu, F.F., Jia, J.T., Cheng, W., and Yan, C.D. (2015). Spinal NF-kappaB and chemokine

ligand 5 expression during spinal glial cell activation in a neuropathic pain model. PLoS One 10, e0115120.

131. Yoshino, J.E., Dinneen, M.P., Sprinkle, T.J., and DeVries, G.H. (1985). Localization of 2',3'-cyclic nucleotide 3'-phosphodiesterase on cultured Schwann cells. Brain Res 325, 199-203.

132. Zeng, Q., Wang, S., Lim, G., Yang, L., Mao, J., Sung, B., Chang, Y., Lim, J.A., Guo, G., and Mao, J. (2008). Exacerbated mechanical allodynia in rats with depression-like behavior. Brain Res 1200, 27-38.

133. Zhang, H., Mei, X., Zhang, P., Ma, C., White, F.A., Donnelly, D.F., and Lamotte, R.H. (2009). Altered functional properties of satellite glial cells in compressed spinal ganglia. Glia 57, 1588-1599.

134. Zhang, J.M., and An, J. (2007). Cytokines, inflammation, and pain. Int Anesthesiol Clin 45, 27-37.

국문초록

신경병증성 통증은 신경세포의 손상이나 신경계의 기능이상으로 발생하며, 유해한 자극 또는 환경으로부터 신체를 보호하고 그리고 치유를 돕는 통증의 유익한 기능을 넘어선 병리학적 증상이다. 신경병증성 통증은 통증을 유발하지 않는 무해한 자극에도 통증반응을 나타내는 이질통 (allodynia), 통증을 유발하는 자극에 대해 더욱 민감한 통증반응을 보이는 통각과민 (hyperalgesia), 그리고 외부자극이 없는 상태에서 화끈거리나, 심지어 타는듯한 감각의 임상적 특성 (spontaneous pain)을 나타낸다. 이러한 증상들은 신경병증성 통증 환자에게 극심한 통증을 주고, 사회적, 경제적인 활동을 저해하며, 그리고 우울증과 같은 정신질환의 발병에도 영향을 미친다. 고전적으로, 신경병증성 통증의 발병 기전을 이해하기 위해 감각신경세포의 과흥분성 메커니즘과 통증 신경회로의 중추감작 (central sensitization)에만 초점을 맞추어 많은 연구들이 진행되었다. 이러한 고전적 관점을 바탕으로 신경세포를 대상으로 하는 통증과민화 기전 연구 및 통증억제 약물 개발이 진행되었지만, 신경병증성 통증 발생의 명확한 분자기전에 대한 이해의 부족으로 인해 아직까지 신경병증성 통증을 효과적으로 통제할 수 있는 적절한 치료법이나 약물이 없는 실정이다.

말초신경손상에 의한 신경병증성 통증의 발병 시 척수에 존재하는 소교세포 (microglia)와 척수후근 신경절 (dorsal root ganglion)에

존재하는 위성 교세포 (satellite glia)가 활성화된다는 사실들이 밝혀졌으며, 또한 이 교세포들의 활성화가 통증과민화 발생에 중요하고 그리고 활성 저해제를 이용하여 척수와 신경절에서 각 교세포들의 활성화를 억제하면 신경병증성 통증이 완화된다는 연구결과들이 보고되었다. 하지만 말초신경 손상에 의한 척수 소교세포와 위성 교세포의 분자적 활성화 메커니즘과 그리고 두 교세포들 사이에 어떤 상관관계가 있는지에 대해서는 아직 명확히 규명되지 않았다. 따라서, 본 연구에서는 각 교세포의 활성화 분자기전을 이해하고 그리고 통증 발병 시 소교세포와 위성 교세포 사이의 관계를 규명하기 위해 위성교세포 특이적으로 NF-κB 활성화가 억제되는 조건별 유전자적중 생쥐를 이용하여 연구들을 수행하였다.

조건별 유전자적중 생쥐의 L5 척수신경을 절단하여 신경병증성 통증모델을 만든 후, 통증발병 양상 분석, 조직 면역염색, 그리고 여러 분자적 실험기법들을 이용하여 각 교세포의 활성화 기전과 상관관계를 규명하였다. 조건별 유전자적중 생쥐의 척수후근 신경절에서는 말초신경 손상이 유발한 위성 교세포의 활성화가 억제되고, L5 척수후근 신경절조직으로 침투하는 대식세포의 수가 대조군에 비해 현저하게 줄어들었다. 또한, 척수조직에서 소교세포의 활성화가 뚜렷이 감소되고, 이질통과 통각과민 테스트에서도 그 증상들이 대조군에 비해 완화되었다. 하지만 신경절로 침윤하는 대식세포들이 척수 소교세포의 활성화와

신경병증성 통증 발병에는 기여하지 못하였다. 이는 신경절에서 위성교세포의 활성화가 척수 소교세포의 활성화와 통증발생에 중요하다는 점을 제시한다. 신경절에서 위성교세포의 활성화가 척수 소교세포의 활성화를 유도하는 기전을 밝히기 위해 유전자 적중생쥐와 대조군 생쥐의 신경절 조직에서 달리 발현되는 유전자들을 분석하여 *St3gal2* 유전자를 발견했다. 이 *St3gal2*는 신경세포에서 강글리오시드 GT1b와 GD1a 생산을 담당하는 단백질을 암호화하는 유전자로서, 손상된 감각신경세포에서 그 발현이 증가되지만 유전자적중 생쥐에서는 발현 증가가 억제되었다. 말초신경 손상 후, 감각신경세포에서 *St3gal2* 유전자 발현증가에 따른 강글리오시드 GT1b의 생산이 증가되었으며 그리고 생산된 GT1b는 감각신경세포의 중추 축삭돌기를 따라 척수로 이동되었다. 척수에서 GT1b는 소교세포 특이적으로 발현하는 톨유사수용체 2 (toll-like receptor 2)의 내재성 리간드로 작용하여 소교세포를 활성화시키고, 이로 인해 통증과민화가 유발됨을 확인하였다.

이상의 연구를 통해서 말초신경 손상이 NF-κB 신호전달 경로를 통해 일차적으로 신경절의 위성 교세포를 활성화시키고, 감각신경세포로부터 생산된 GT1b가 이차적으로 척수 소교세포를 활성화시킴으로써 통증과민화를 유발할 수 있다는 사실을 확인하였다. 이는 신경절에서 활성화된 위성 교세포와 감각신경세포 사이의 상호작용이 손상된 신경세포와 척수 소교세포 사이의 상호작용에 의한

중추감작 발생보다 우선하며, 말초신경 손상 시 위성 교세포의 활성화를 억제하거나 또는 손상된 신경세포로부터 강글리오시드 GT1b의 생산, 작용을 억제함으로써 신경병증성 통증 발병을 효과적으로 제어할 수 있음을 보여준다.

주요어: 신경병증성 통증, 소교세포, 위성 교세포, IκB kinase, GT1b, *St3gal2*

학번: 2012-30114